GEOLOGICAL AND STRUCTURAL INTERPRETATION OF THE KONONGO AREA OF THE ASHANTI GOLD BELT USING AIRBORNE MAGNETIC AND RADIOMETRIC DATA

by

BENJAMIN BOADI, BSc Physics (Hons)

A Thesis Submitted to the Department of Physics,

Kwame Nkrumah University of Science and Technology

in partial fulfillment of the requirements for the degree

of

MASTER OF SCIENCE (GEOPHYSICS)

College of Science

Supervisor: Dr. K. Preko

June, 2012

Declaration

I hereby declare that this submission is my own work towards the MSc and that, to the best of my knowledge, it contains no material previously published by another person or material which has been accepted for the award of any other degree of the University, except where due acknowledgement has been made in the text.

....	....	....
Student Name & ID	Signature	Date

Certified by:

....	....	....
Supervisor Name	Signature	Date

Certified by:

....	....	....
Head of Dept. Name	Signature	Date

Abstract

Integrated airborne geophysical methods namely magnetic and radiometric were used to investigate the Konongo mining area located at the north-eastern boundary of the prospective Ashanti Gold Belt in south-eastern Ghana. These datasets provided useful information on the lithology and geological structures within the area. The geophysics data processing approach employed concentrated on enhancing the geophysical data quality and this aided in tracing accurate positioning of geological boundaries, the responses related to mineralization and geological structures that may be of vital economic importance. The magnetic image enhancing technique such as reduction to the pole, analytic signal and first vertical derivative helped delineate folds, fractures, tectonic boundaries and the D_1-NE / D_2-NNW structural deformation events which are potential hydrothermal fluid traps. The Birimian Meta-sedimentary and meta-volcanic rocks noted to host gold mineralization and other metal ores in the Belt were also delineated. The radiometric data provided geochemical information of potassium (K), thorium (Th) and uranium (U) that proved valuable in delineating bedrock lithology of the area such as the Banso Batholith, Birimian meta-volcanics, Tarkwaian Formation and alteration zones within the area and contact zones. High K, Th and U concentration were mapped in the meta-sediments and the Banso Batholith. The high-resolution airborne magnetic and radiometric data of the study area resulted in better definition of both geological structures and lithological boundaries. This

project shows the usefulness of geophysical data in mapping possible geological structures that host hydrothermal gold mineralization.

Contents

List of Tables

List of Figures

List of Symbols and Acronyms

κ	Magnetic susceptibility
F_e	The Earth's magnetic field
Z_e	Vertical component of the Earth's magnetic field
H_e	Horizontal component of the Earth's magnetic field
I	Angle of inclination
D	Angle of declination
M	Intensity of magnetization
H	Applied external field
nT	Nanotesla
c.g.s	centi gram second
J_r	Remanent magnetization
J_i	Induced magnetization
Q	Königsberger's ratio
N_t	Number of atoms present at time t(s)
N_o	Number of atoms present at time t=0
λ	Decay constant
$T_{\frac{1}{2}}$	Half life
U	Uranium
Th	Thorium
K	Potassium

Acknowledgments

My first and foremost appreciation goes to the Almighty God for His unending mercies and grace towards me throughout the duration of this work. I am highly indebted to Mr. D. D. Wemegah for the training he gave me in GIS and the other geophysical softwares used for this project. I sincerely thank my supervisor Dr. K. Preko for his motivation, encouragement and criticism that helped to improve this work. To Dr. L. K. Amekudzi, Dr. M. K. E. Donkor and Mr. E. Manu I say may God favour you for introducing me to the Linux and Latex platform. This work would not have been possible without the supports of Mr. S. Attah (Ghana Geological Survey Department) and Mr. K. Takyi-Kyeremeh (Newmont Ghana Gold Limited) who provided the Airborne geophysical datasets and the Oasis Montaj (Geosoft) respectively. I thank all the lecturers who took me through the geophysics programme and to all my course mates who shared their knowledge on this project I say God bless you. My final thanks go to Mr and Mrs Asante, Mrs M. Octhere and all my family members. I really appreciate your support both physical and spiritual.

CHAPTER 1

INTRODUCTION

There are many geophysical methods (such as gravity, radiometric, magnetic, and seismic) whose operations are based on different physical principles, operational techniques and different physical properties of the Earth (e.g. density, magnetic susceptibility, electrical conductivity and radioactivity). These methods can be employed to provide solutions to geological problems and structural mapping. Although all these methods are ground-based, it is also possible to carry out some of these geophysical methods in airborne surveys.

Airborne geophysics is a powerful means available to the earth scientist for investigating very large areas rapidly. The broad view of the earth that the airborne perspective provides has been well recognized since the early days of balloon photography and military reconnaissance (Dobrin, 1952). Compared with ground-based methods, the advantages of these methods are that very large areas and difficult terrain can be surveyed remotely in short periods of time thus making it very cost effective.

There are three chief airborne geophysical procedures utilizing magnetic, electromagnetic, and radiometric methods while a fourth one, airborne gravity, has also become an acceptable technique from the past decade (Murphy, 2007). Airborne magnetic and radiometric surveys have been used extensively in the mineral exploration industry predominantly for the delineation of metalliferous deposits. Recent advances in technology have substantially increased the accuracy and resolution of these techniques so that they can be used to provide useful information on lithology and geological structures. Additionally, advances in data analysis, processing and image enhancement techniques have improved the resolution of geophysical datasets further so that very subtle variations in the geophysical responses can be identified.

According to Telford et al. (1990) the physical principles of aeromagnetic methods are based on taking measurements of the ambient magnetic susceptibility of the surface geology and using the data to determine the distribution of magnetic minerals and hence changes in lithology. Igneous deposits generally contain a high concentration of magnetic minerals and the aeromagnetic method was originally developed to remotely detect large subsurface deposits of ore minerals.

Wilford et al. (1997) indicate that airborne radiometric survey similarly is used to measure variations in the mineral composition in order to map lateral lithological changes. This method involves the measurement of naturally occurring radioactive elements that exist in rock forming minerals and soil profiles. These elements are uranium (U), thorium (Th) and potassium (K), which can be found as trace elements in all rocks and decay naturally giving off gamma radiation (gamma rays). These gamma rays that are emitted can be measured by a gamma ray spectrometer which can determine the source element by its peak gamma ray energy.

The Geophysical datasets for the Konongo area was extracted from the aeromagnetic and radiometric collected for the Ashanti Belt by the Ghana Geological Survey Department in 1997 was processed and interpreted based on grids and images generated from the datasets.

1.1 Literature Review

The first attempt to prospect for radioactive minerals in Ghana (Kesse, 1985) began in 1952 when D. Ostle, a geologist of the Atomic Energy Division of the United kingdom Geological Survey, P. H. Hale, an Engineer of the Atomic Energy Research Establishment at Harwell, UK and one time geologist of the then Gold Coast (now Ghana) Geological Survey, carried out a radioactive reconnaissance survey using carborne equipment. Three anomalies were encountered namely,

- the Accra-North anomaly in laterites above gneisses of the Dahomeyan system,
- anomaly located above Bongo Granite on the Bolgatanga-Navrongo traverse,
- the Bobikuma anomaly discovered in laterites above the older Basin Granite.

In 1960, Hunting Surveys Limited of the United Kingdom undertook geophysical exploration for minerals in Ghana by the use of airborne magnetic and radiometric surveys in two trial areas, A and B, with a total coverage of 17092 km^2 (Kesse, 1985). Area A total 12430 km^2 and covered the well-know gold and sulphide mineralization zones stretching from the coast west of Takoradi through Tarkwa and Prestea, Dunkwa and Obuasi to Konongo. Area B, 4662 km^2 in area, was located at the southeastern part of the country. It stretched northeastwards covering the Buem and the Togo-Dahomeyan contacts where chromite mineralization in serpentinite and iron ore in shale had been located. The results of these surveys were quite satisfactory in both areas.

- Magnetic maps showing contracts between rock units of high and low magnetic susceptibilities were produced. Dikes, intrusives and fracture zones could clearly be identified on the map.

- Geological interpretations based mostly on these magnetic maps proved useful, particularly in differentiating 'high' from 'low' magnetic bodies, fault and fracture zones within the areas examined.

- One significant result of the surveys was that the well-known (and worked) reefs in the mineralization zones were located at, or very near, the intersection of shear zones and faults.

Airborne geophysical, magnetic and radiometric surveys were conducted over the Bulman leases (Australia) in October 2007 . Sawyer and Gunn (2008) reported the surveys identified several areas that warranted further investigation for fault system related carbonate hosted Mississippi Valley Type Pb-Zn mineralization. The magnetic survey confirmed that the known Pb-Zn mineralization in the Bulman area is underlain by an extensive sill of Derim Derim Dolerite (fine to coarse grained dolerite and gabbro sills). The interpretation highlighted a system of east-west and north-south faults that spatially correlate with known mineralization and Pb-Zn geochemical soil anomalies. The potassium anomaly is coincident with an east-west offset in the Bulman fault, and a north-south trending Pb geochemical soil anomaly. This anomaly could indicate potassic alteration associated with an increased fluid influx.

Aeromagnetic data reflects the distribution of magnetic minerals in bedrock and are unaffected by non-magnetic cover. The interpretation of the aeromagnetic survey over the Faiyum area, Western Desert, Egypt was carried out by El-awady et al. (1984). Qualitative as well as quantitative interpretations of the aeromagnetic data were carried out to obtain more information about the crystalline basement structure and the local structure in the sedimentary section. The analysis of the constructed magnetic maps which include the total intensity map, the vertical map, the regional map, the residual map, the second vertical derivative map and the downward continuation maps serve as basis for revealing the structural pattern of the basement complex, and the shallower structures.

Billings (1998) and Wilford et al. (1997) reviewed the application of airborne gamma ray spectrometry to regolith and soil mapping. The interpretation of aerial photography and satellite imagery has been the traditional means for the rapid mapping of soil types over large areas. The soil properties are inferred from differences in vegetation and from differences in landforms. But these features are easily obscured by the impact of land use by humans, cultural features, and the effect of bush fires. However, the gamma ray spectrometric response is unaffected by these disturbances. Also, the distribution of K, U and Th in the natural environment is controlled by many of the same factors that control the distribution of soil types. The method is thus being increasingly used for soil and regolith mapping.

1.2 Research Problem Definition

The mining industry contributes largely to the economy of Ghana in three important ways. Firstly, it is a foreign exchange earner. Secondly, it is a major source of employment especially in the rural areas and thirdly, it contributes greatly to the internal economy of the country by payment of taxes and duties (Kesse, 1985). The Ashanti Belt in Ghana is a major gold hosting Belt. Lo and Pitcher (1996) indicate the mineralization is hosted in two settings: Birimian metavolcanics and Tarkwaian conglomerate. The Birimain metavolcanics are associated with sericite alteration, with a potassium enrichment signature. The Tarkwaian conglomerate can be mapped through its association with a potassium-rich phyllite marker horizon.

Therefore, identifying the distribution of the geomorphology, certain soils, different rock types as well as geological structures hosting materialization from magnetic and radiometric data has been the interest of the mining industries operating in this Belt since it goes a long way to facilitate mineral exploration. The area under investigation (Konongo) comprises Birimian series and Tarkwaian Formation which host the mineralization zone of the Ashanti Belt (Griffis et al., 2002). This project seeks to correlate radiometric and magnetic data from the study area to help map the geology as well as to identify some possibly existing faults, folds, lineaments and fracture systems, which are the main metal ore hosting structures in the Birimian Formation.

1.3 Objectives of the Research

The area under investigation is characterized by an active mining industry, mainly gold deposits. The major objectives of the study are threefold, namely:

- Map the lithology and geological structures of the study area using airborne radiometric and magnetic datasets.
- Identify possible hydrothermal alteration zones from the radiometric data.
- Deduce an integrated geological structural map indicating potential mineralization zone.

1.4 Structure of Thesis

The Thesis work has six (6) chapters with each chapter addressing a main heading. Chapter one introduces the subject matter, outlining the background of the research, objectives of the research, justification of the objectives of the research as well as literature review.

Chapter two gives the general overview of the geological settings of the study area. It reviews both the regional and local geology of the study area.

Chapter three outlines the main fundamental theory behind airborne radiometric and magnetic survey, taking into account some enhancement techniques applicable to magnetic and radiometric data.

Chapter four gives an overview the location and accessibility of the research area, physiography, climate and occupation of inhabitants. The methods used to acquire the datasets and some available software for enhancing the datasets were introduced in this chapter. This chapter also outlines the processing steps employed in the data processing.

Chapter five analyses the various maps obtained from the radiometric and magnetic datasets. Interpretations to the deduced maps are also given in this chapter. Finally, this chapter correlates the magnetic and radiometric data to produce an integrated mineral potential map that would aid mineral resource exploration in the study area.

Chapter six and seven draws conclusions from the research and makes recommendations for future work.

CHAPTER 2

GEOLOGICAL SETTING

This chapter reviews the regional geology of the study area (the Konongo and Kurofa License) which includes lithological relationships, geological structures, metamorphism and also mineral potential of the area. The importance of geology in this work cannot be over emphasized. According to Cozens (1989), a full understanding of the geology of Ghana should allow the prediction of the location of yet unknown ore bodies.

2.1 Regional Geology

Ghana falls mostly within the West African Craton which stabilized in the early Proterozoic (2000 Ma) during the Eburnean Orogeny. This Orogeny also stabilized the Zaire Craton and affected vast parts of Western Africa and neighbouring regions in South America that were conterminous with the Eburnean tectonothermal province. Outside South Africa, the West African Craton is the second largest region in Africa where lower Proterozoic rocks are extensively preserved. These early Proterozoic rocks comprise extensive belts of metamorphosed volcanic and sedimentary rocks exposed in Ghana, Burkina Faso, Niger and Cote d'Ivoire. On the east and west, the Craton is bounded by late Proterozoic mobile belts (700-500 Ma) referred to as the Pan African mobile belts (Kesse, 1985; Wright, 1985; Leube et al., 1990).

Almost 45% of Ghana's territory belongs to the Shield area. This part consists of Lower Proterozoic volcanics and flyschoid meta-sediments of the Birimian System. The Birimian was deformed, metamorphosed and intruded by syn and post-granitoids during the Eburnean Orogeny. In elongated basins which follow the north-easterly trending Birimian belts, middle Proterozoic molasse type sediments of the Tarkwaian Formation were deposited (Kesse, 1985). The Ghana shield area has therefore two main rocks system, the Birimian Supergroup with its associated granitoid intrusives and the Tarkwaian Formation.

2.1.1 The Birimian System

Rocks of the Birimian System underlie most of southern, western and northern Ghana. They host most of the gold and diamond deposits in the country; hence they have been subjected to considerable study. Ideas on the stratigraphy, structure and age of the Birimian rocks have evolved over the years as a result of work by the Geological Survey Department (GSD), the Soviet Geological Team and the Ghana-German Mineral Prospecting Project (GGMPP) in Ghana and the work of French geologists in Francophone West Africa. Kesse (1985) gives an overview of the ideas about the Birimian up to the early 1980's.

The Birimian consists of metamorphosed volcanic and sedimentary rocks which form five sub-parallel belts of volcanic rocks separated by broad 'basins' of sedimentary rocks. In order to provide a general sub-division of the Birimian System, Asihene and Barning (1975) evaluated various proposals and came up with an 'official' sub-division, which was to be used by Ghana Geological Survey (GGS) personnel in various ongoing mapping projects in southern Ghana. The Birimian Meta-sedimentary Formation was given a five-fold division of arenaceous and argillaceous units. The Birimian Meta-volcanic Formation was divided into three main volcanic suites; this included an upper Basic Volcanic Sub-series, middle Acid Volcanic Sub-series and a lower Sedimentary-Volcanic Sub-series that included tuffaceous greywackes, quartzite, conglomerates and grits (Griffis et al., 2002).

The rock types present in the Meta-sedimentary Belt are greywackes with turbidite features, phyllite, slates, schists, weakly metamorphosed tuffs, sandstones as well as some granitoids. Some of the phyllites contain pyrite, and finely divided carbonaceous matter (Hirdes et al., 1988). The Meta-volcanics or Volcaniclastics succession consists of lava flows and dike rocks of basaltic and andesitic composition (Leube et al., 1990). Most of these rocks have now metamorphosed to hornblende actinolite-schists, calcareous chlorite schists and amphibolites (the greenstones).

Radiometric age-dating of detrital grains from Birimian System in the Ashanti and Sefwi Belts, as well as from the Kumasi Basin, generally fall within the range 2180-2130 Ma (Davis et al., 1994). Similar results were obtained from samples in the southern sector of the Ashanti Belt (Loh and Hirdes, 1996). However, the latter area also yielded a cluster of older dates ($\approx$ 2260 Ma) from detrital zircons, which have been interpreted to represent very early Birimian volcanic activity. These are the oldest Birimian dates so far reported from the Birimian of West Africa (Griffis et al., 2002).

2.1.2 The Tarkwaian Formation System

Rocks of the Tarkwaian Formation are concentrated mainly at the south-western part of Ghana in Tarkwa area where they outcrop in a north-east to south-west trending belt (Kesse, 1985). The Tarkwaian Formation is thought to rest unconformable on the Birimian, though in some places, the Metasediments and the Tarkwaian Formation are inter-folded due to post-Tarkwaian orogenic activity (Junner, 1940). In some localities, no angular unconformity can be observed between the Birimian System and the Tarkwaian Formation. The Tarkwaian Formation is associated with hypabyssal acidic to basic igneous rocks which make up approximately 20% of the total thickness of the system (Kesse, 1985).

The common minerals composition of these rocks are chlorite, sericite, zoisite, calcite, quart, limonite and chloritoid. Locally, biotite, epidote, tourmaline and spessartite may be developed. They are free of limestone or dolomites and organic matter. The sediments must be regarded as integral part of the Eburnean orogenic cycle of which they represent the final molasse stage (Kesse, 1985).

The age of the Tarkwaian Formation has been the subject of recent study by Hirdes and Nunoo (1994) and Davis et al. (1994). The age of deposition of the Tarkwaian Formation can be bracketed by the youngest zircon grain from the lowermost Kawere series and age of the authigenic rutile which formed after deposition. These dates give a time range of 2096 to 2132 Ma.

2.1.3 Birimian Granitoids

Four main types of granitoids are recognized in the Birimian of Ghana. They include Winneba, Cape Coast, Dixcove and Bongo granitoids (Junner, 1940; Kesse, 1985). The latter three have been recently termed 'Basin', 'Belt' and 'K-rich' granitoids (Hirdes et al., 1993). The ages of the granitoids of Ghana have been found to fall into two rather well-defined groups. The granodiorite massives that intrude the Birimian rocks ages about 2100 Ma while the most abundant granites (basin-type) cutting both the Birimian and the Tarkwaian Formation usually give ages of about 1800 Ma (Kesse, 1985).

The High K are porphyritic, hornblende-microcline plutonic granites that are locally found in north-eastern Ghana where the granites intrude Tarkwaian Formation that overlie the Bole-Navrongo Volcanic Belt. This granitoid is peraluminous and lacks a foliation (Leube et al., 1990). They are thought to be younger than the Belt Granite. A granitoid similar in composition to the High K type, the Banso granitoid, crops out within the Ashanti Belt south of Kumasi. Contact metamorphic minerals have been observed in Tarkwaian Formation close to the granitoid (Mauer, 1986). The latter observations plus petrographic and geochemical similarities described by Mauer (1986) suggest that the Banso granitoid intrudes the Tarkwaian Formation and thus occupies a similar tectonic position to that of the Bongo type granitoid.

The Basin-type granitoid complex are at times well foliated, often magmatic, potash-rich granitoids which come in the form of muscovite biotite granite and granodiorite, porphyroblastic biotite gneiss, aplites and pegmatites (Kesse, 1985). These granitoids are characterized by the presence of many enclaves of schists and gneisses. They are generally associated with Birimian meta-sediments and their internal structures are always concordant with those of their host rocks.

Belt-type granitoid complex consists of hornblende granite or granodiorite grading locally into quartz diorite and hornblende diorite, sometimes believed to have been formed from gabbros by magmatic differentiation (Kesse, 1985). This complex forms non-foliated discordant to semi-discordant bodies in the enclosing country rocks which are found within the granite complex.

2.1.4 Associated Intrusives

Mafic dikes and sills represent the youngest volcanic rocks in Ghana. They are mainly gabbro, dolerite, epidiorite and norite. They cut both the Birimian System and Tarkwaian Formation. The dolerites are not metamorphosed and commonly have intruded parallel to bedding. They are porphyritic containing plagioclase phenocrysts in a carbonatized groundmass (Griffis et al., 2002).

2.2 Local Geology

The Konongo area was mapped by the Ghana Geological Survey in 1937 and 1967. The 1967 work included a geological survey that defined broad areas of gold and arsenic mineralization (Moon and Mason, 1971). The Konongo District lies at the north-eastern end of the Ashanti Belt. It extends for 30 km from the base of the prominent Voltaian escarpment south-west to the north end of the Lake Bosumtwi area (Griffis et al., 2002).

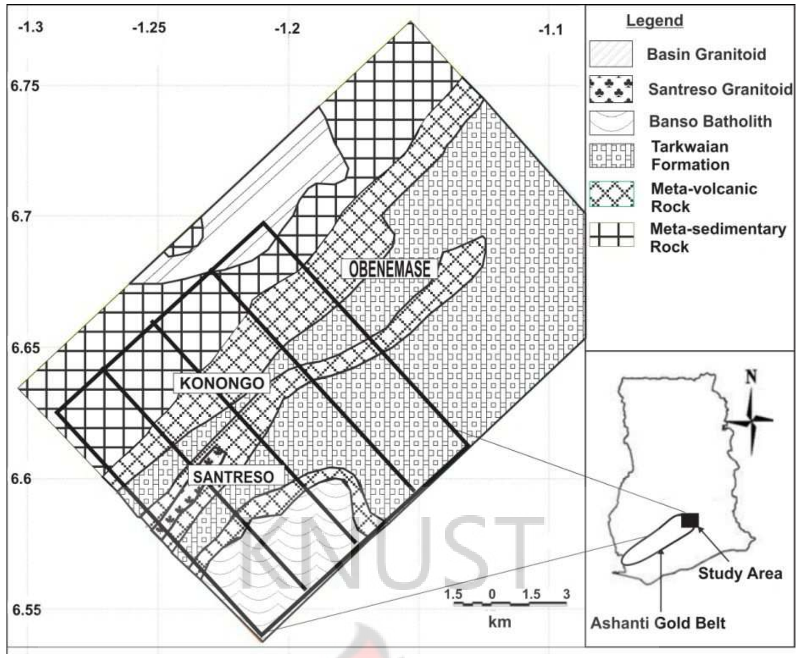

Figure 2.1: Geological map of the Konongo area (Modified From Griffis et al. (2002))

The geology of the area is dominated by NE trending bands of Birimian Meta-sediments/volcanics and the Tarkwaian Clastic Formation. To the east, the Tarkwaian Formation widens out very substantially and to the west of the District, there are mainly Birimian Meta-sedimentary units of the Kumasi Basin. Also within the basin domain are large masses of basin-type granitoids belonging to the Kumasi complex (Griffis et al., 2002).

The south-eastern part of the District is dominated by the large, unusual Banso Batholith, which is rich in radiometric potassium (Griffis, 1998). Early workers in the area (Hirst, 1942) believed this granitoid to be similar to the Winneba intrusions and indicated that it was post-Birimian and pre-Tarkwaian because of the lack of contact metamorphic effects in Tarkwaian Formation close to the Batholith. However, recent work has challenged this view and it appears that the Banso Batholith is a fairly late-stage intrusion that apparently post-dates the Tarkwaian Formation (Griffis et al., 2002).

The area features a major, N-S trending, late-stage dolerite dike system that cuts across the Banso Batholith and splits up into at least three branches that extend through the Konongo District. The structure in the area is certainly complex and features tightly folded and faulted bands of Birimian and Tarkwaian Formation; the trends of the major faults as well as the fold planes, strike to the NE and dip steeply to the NW (Griffis et al., 2002). Gold mineralization is commonly associated with these fault zones (lineaments), which are useful exploration targets (Adjovu, 2006). Structurally the project area covers a segment of the Konongo-Axim Shear System. This shear zone occurs close to the belt margin and hosts a number of deposits and operating mines.

Southern Ghana is endowed with numerous world-class orogenic gold deposits in the Ashanti and Sefwi belts, including Obuasi, Edikan, Konongo, Prestea, Bibiani, Obotan, and Chirano plus Newmont's Ahafo and Akyem deposits. These deposits are hosted by a variety of rock types and commonly are controlled by a network of second-order thrust faults that are splays from regional-scale faults at or near belt-basin margins (Allen, 2011).

The use of the integrated airborne geophysical datasets from Konongo and its surrounding areas showed previously mapped and discovered geological structures. These include regional deep and shallow seated geological structures that can be linked to early Proterozoic orogenic event. The early Proterozoic orogenic event involved the accretion of volcanic arcs accompanied by compressional deformation, metamorphism, granite plutonism, uplift and deposition of molasses collectively referred to as Eburnean (Griffis et al., 2002).

2.3 Metamorphism

Metamorphic grade of the Birimian rocks is that of the greenschist facies, with local amphibolite facies aureoles around granitoid plutons. Recent work in the southern Ashanti region (John et al., 1999) suggests that the greenschist facies is widely retrograde after amphibolite facies conditions. Both belt and basin rocks are highly deformed with widespread isoclinal folding and regional bedding-parallel cleavage attributed to regional NW-SE compression during the peak of the Eburnean Orogeny. The deformation and metamorphism of the entire Birimian Supergroup, Tarkwaian clastic Group and intrusion of the basin granitoid suite occurred between 2116 and 2088 Ma (Griffis et al., 2002).

Regional north-east striking shear zones parallel to the belt margins are also assumed to have developed during the peak Eburnean and appear to be fundamentally important in the development of the Birimian gold deposits for which Ghana is well known such as Ashanti, Prestea-Bogosu, Konongo, and Bibiani. Regional deformation comprises the main compressive tectonic stage that has resulted in folding, reverse faulting and regional foliation dipping about 70^0 to the south-east. Regional metamorphism is characterized by greenschist facies (Adjovu, 2006).

All Birimian and Tarkwaian Formation have been metamorphosed and many of the Eburnean granitoids display metamorphic features (Griffis et al., 2002). It is commonly accepted for the Birimian units of southern Ghana that the regional level of metamorphism is usually lower greenschist facies (Zitzmann et al., 1997; Eisenlohr and Hirdes, 1992) but with local variations although in many areas, higher temperatures and pressures is indicated by amphibolite facies.

Ledru et al. (1994) have identified metamorphic suites north of Tarkwa in some of the phyllitic units that include biotite and muscovite and andalusite and kyanite which are present locally in Konongo. Contact metamorphic minerals possibly to be hosted in the study area include biotite, garnet and staurolite, which indicate minimum temperatures of 400^{o}C; with less commonly, occurrences of kyanite and sillimanite in meta-sedimentary areas found adjacent to the meta-volcanoclastic (Griffis et al., 2002).

2.4 Mineralization

Mineralization in Konongo is associated with a complex array of deformed quartz veins and arsenopyrite-silica-sericite-carbonate alteration (Oliver, 2009). Most of the known gold deposits occur along a 1-2 km wide, NE trending band that can be traced through most of the District. The majority of occurrences are hosted in Birimian Meta-sediments and volcanics, which mainly include volcaniclastics, tuffaceous beds and a few more massive metamorphosed basaltic flows.

The main vein systems or reefs in the southern Konongo-Odumasi area (Akyenase, Odumasi and Awere reefs) occur in a 400 m wide band featuring garnet-biotite hornfels, carbonaceous phyllite, chlorite-carbonate schist and biotite schist. A prominent band of Birimian manganiferous Meta-sediments (gondite, consisting of Mn garnet, rhodochrosite and quartz) can be traced through many parts of the District (Hirst, 1942).

The reefs consist of steeply plunging oreshoots associated with a major regional shear system. The quartz vein systems appear to have multiple fracturing and generations of quartz with the best values commonly associated with gray laminated quartz veins; adjacent shears commonly contain abundant graphitic gouge. The gold occurs in the quartz veins and is intimately associated with sulphides (arsenopyrite, pyrite, pyrrhotite, and minor chalcopyrite), especially the acicular crystals of fine-grained arsenopyrite. The sulphides occur in both the veins and in the host rocks along the margins of the veins (Griffis et al., 2002).

Different theories have been proposed for the Birimian gold mineralization; plutonic/magmatic theory (Junner, 1940), volcanogenic theory (Ntiamoah-Agyakwa, 1979) and metamorphic theory (Hirdes et al., 1988). However, it has been broadly accepted that hydrothermal activity is the principal ore deposition process (Manu, 1993) in the Birimian and the main pathways for hydrothermal fluids are faults and fractures. The understanding of the dynamics of hydrothermal fluids through conduits and the resulting alterations on the surrounding rocks can be used to define favourable zones for blind ore deposits (Amenyoh et al., 2009).

The principal geological structures hosting many of the epithermal and mesothermal gold deposits include faults, fractures and shear zones play the most important role in gold mineralization in the Birimian of Ghana (Allibone et al., 2002). Therefore the delineated structures of the study area likely to be potential hosts of metal ore mineralization. The continuous reactivation of these structures has had profound effect on both the distribution and the mode of gold mineralization throughout the country (Cozens, 1989). The Ashanti gold deposit at Obuasi and other gold deposits at Konongo, Bibiani, Bogoso and Prestea are all located along the Ashanti gold belt and controlled by faults and shear zones which are generally marked by zones of graphitic and mylonitic materials with quartz and carbonate veining.

The gold mineralization at Konongo originated as a hydrothermal mobilization of gold from the basement rocks and/or as a hydrothermal leaching of the Birimian volcanic pile during a third phase folding (F_{a3}) Orogeny. The factors causing the channelling of the migrating mineralizing fluids originated in the sequence and were probably related to a combination or tectonically induced structures and minor petrofabric and chemical differences in the containing Birimian sediments. Once contained in the folded stratigraphic sequence the paths of the migrating hydrothermal fluids were influenced by the changing forms of the folds. Upward migrating fluids became channelled in the hinges of folds especially anticlines (Cozens, 1989).

Most literature reviews about the geological setting (Cozens, 1989; Silva et al., 2003; Kesse, 1985) of the Konongo District have made a clear implication that the study area is under laid by the Birimian geology and fall within the Ashanti belt. Comparable to other Birimian belts in Ghana, the study area consists of early Proterozoic belt and basin rocks including the Tarkwaian (Cozens, 1989). These rocks form the most important rock types that host economic mineral deposits such as gold, diamond, bauxite and manganese in Ghana. From the interpreted composite geological map, over 70% of the study area is mainly underlain by metamorphosed Birimian belt and basin rocks and bounded at the south by granitoids. The area host prominent NE-SW trending structures and few NNW-SSE ones which are similar to those of the Sefwi and Kibi belts.

The transportation and deposition of hydrothermal fluids into host rocks required rock permeability. Along faults and fractures (conduits) local rock permeability is higher at fault bends, fault branches (fault splays), faults intersects or step away from faults average orientation. An increase in local permeability causes transient local reduction in pore fluid pressure, which suck fluid towards the damaged zone, thereby further enhancing fluid flow in the zone. The drop in pressure may lead to precipitation of metals in the zone of maximum fluid flux. Therefore in predictive geology a particular attention to the slightest change in strike, dip or continuity of the fault is important (Allibone et al., 2002; Etheridge et al., 1987).

CHAPTER 3

THEORETICAL BACKGROUND OF GEOPHYSICAL METHODS USED

3.1 Magnetism of the Earth

The Earth's magnetic field is mainly due to the different fields, namely external field and internal field (Herndon, 1996). The internal field is global and has its origin deep in the Earth's interior (referred to as the main field). Geologists believe the Earth's core is largely made up of molten iron. Seismic studies indicate that inner core is solid and the outer core is liquid. The inner core is above the Curie temperature, so it cannot contribute to the Earth's magnetic field. Modern theories suggest the Earth's magnetic field is caused by flow of material in the outer core which generates electricity, which is associated with the flow of electrical current. The flow of these electrical currents effectively creates a huge electromagnet (Clark and Emerson, 1991).

3.1.1 Nature of the Geomagnetic Field

As far as exploration geophysics is concerned, the geomagnetic field of the Earth is composed of three parts (Telford et al., 1990):

- The main field, which varies relatively slowly and is of internal origin.
- The small field (compared to the main field), which varies rather rapidly and originates outside the Earth.
- The spatial variations of the main field which are usually smaller than the main field, are nearly constant in time and place, and are caused by local magnetic anomalies in the near-surface crust of the Earth. These are the targets in magnetic prospecting.

The geomagnetic field (Telford et al., 1990) resembles that of a dipole whose north and south magnetic poles are located approximately at 75^0N, 101^0W and 69^0S, 145^0E. The dipole is displace about 300 km from the Earth's centre toward Indonesia and is inclined some 11.5^0 to the Earth's axis.

3.1.2 The Earth's Magnetic Field

If an unmagnetized steel needle could be hung at its centre of gravity, so that it is free to orient itself in any direction, and if other magnetic fields are absent, it would assume the direction of the Earth's total magnetic field, a direction that is usually neither horizontal nor in-line with the geographic meridian (Telford et al., 1990). The magnitude of this field F_e, the inclination (or dip) of the needle from the horizontal I, and the angle it makes with geographic north (the declination) D, completely define the main magnetic field.

The magnetic elements (Whitham, 1960) are illustrated in Fig. 3.1. The field can also be described in terms of the vertical component, Z_e, reckoned positive downward, and the horizontal component H_e, which is always positive. X_e and Y_e are the components of H_e, which are considered positive to the north and east, respectively (Telford et al., 1990).

Furthermore the vertical component of the magnetic intensity of the Earth's magnetic field varies with latitude, from a minimum of around 30000 nT at the magnetic equator to 60000 nT at the magnetic poles. These elements are related as follows:

$$
\begin{aligned}
F_e^2 = H_e^2 + Z_e^2 &= X_e^2 + Y_e^2 + Z_e^2 \\
H_e = F_e \cos I \qquad & Z_e = F_e \sin I \\
X_e = H_e \cos D \qquad & Y_e = H_e \sin D \\
\tan D = \frac{Y_e}{H_e} \qquad & \tan I = \frac{Z_e}{H_e} \\
\mathbf{F_e} = F_e \mathbf{f_1} = F_e(\cos D \cos I \mathrm{i} &+ \sin D \cos I \mathrm{j} + \sin I \mathrm{k})
\end{aligned}
\tag{3.1}
$$

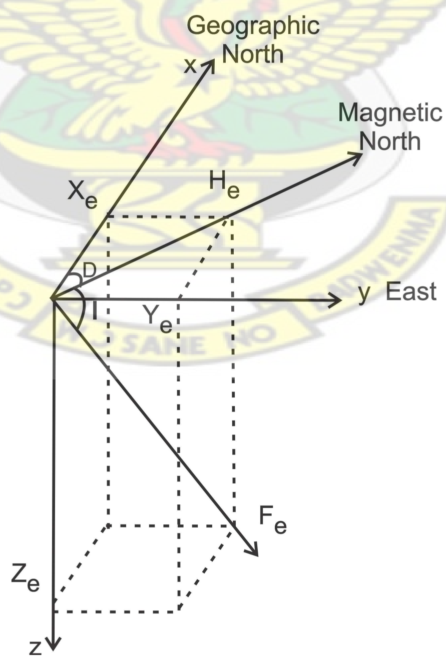

Figure 3.1: Elements of the Earth's magnetic field (Whitham, 1960)

3.2 Magnetism of Rocks and Minerals

Many rocks that contain iron-bearing minerals act as tiny magnets. As magma or lava cool, these minerals begin to form. At this point the molten rocks have not completely solidified, so the magnetic minerals floating in the molten mass become aligned to the magnetic field. When the rock finally solidifies, these minerals 'lock in' the magnetic field. Sedimentary rocks also have a magnetic record. As iron bearing sedimentary minerals is deposited from the water column, they also become aligned with the exiting magnetic field. The magnetism remains locked in the rock unless the rock is subsequently heated above the Curie point, the temperature at which all magnets lose their magnetism. When the heated rock again cools below the Curie point, it will record the magnetic field at this later time, and the old magnetic field will be lost. It is important, therefore, to establish that a rock's magnetism is primary and has not been re-set at a later time (Reeves, 1989; Petersen, 1990).

Local changes in the main field result from variations in the magnetic mineral content of near surface rocks. The sources of local magnetic anomalies cannot be very deep, because temperatures below ~40 km should be above the Curie point, the temperature (~550^{0}C) at which rocks lose their magnetic property (Telford et al., 1990).

Magnetic anomalies are caused by magnetic minerals (mainly magnetite and pyrrhotite) contained in the rocks (Rajagopalan, 2003). Magnetically important minerals are surprisingly few in number. Substances can be divided on the basis of their behaviour when placed in an eternal field (Telford et al., 1990). In a diamagnetic material, such as halite, all the electron shells are complete and so there are no unpaired electrons. When an external magnetic field is applied, a magnetization is induced. The electrons orbit in such a way so as to produce a magnetic field which opposes the applied field, giving rise to a weak, negative susceptibility (Reynolds, 1997). The most common diamagnetic earth materials are graphite, marble, quartz and salt.

Unpaired electrons of incomplete electron shells produce unbalanced spin magnetic moments and weak magnetic interactions between atoms in paramagnetic materials such as fayerite, amphiboles, pyroxenes, olivine, garnets and biotite. Paramagnetic materials have weak positive susceptibility but one which decreases inversely with the absolute temperature according to the Curie-Weiss Law (Reynolds, 1997).

Ferromagnetism decreases with increasing temperature and disappears entirely at the Curie temperature. Truly ferromagnetic materials occur only rarely in nature but include substances such as cobalt, nickel and iron, all of which have parallel alignment of moments (Nagata, 1961). In anti-ferromagnetic materials, for example hematite, the moments are aligned in and anti-parallel manner (Nagata, 1961). Although the magnetic fields of the oppositely orientated dipoles cancel each other out, crystal lattice defects result in a net residual moment or parasitic (anti)-ferromagnetism (Reynolds, 1997).

In ferrimagnetic materials, of which magnetite, titanomagnetite and ilmentite are prime examples, the sub-lattices are unequal and anti-parallel. Spontaneous magnetization and large susceptibility are characteristics of ferrimagnetic materials, such as in the case pyrrhotite (Reynolds, 1997; Telford et al., 1990). The majority of naturally occurring magnetic minerals exhibit either ferrimagnetic or imperfectly anti-ferromagnetic characteristics.

3.2.1 Magnetic Susceptibility

Magnetic susceptibility is a measure of the ease with which particular sediments are magnetized when subjected to a magnetic field. The ease of magnetization is ultimately related to the concentration and composition (size, shape and mineralogy) of magnetizable material contained within the sample (Wemegah et al., 2009). Magnetizable minerals include the ferromagnetic minerals (strongly magnetizable) and any of the paramagnetic (moderately magnetizable) minerals and other substances (Wemegah et al., 2009; Reynolds, 1997).

The ratio between the induced magnetization and the inducing field if expressed per unit volume, volume susceptibility (κ) is defined as $\kappa = M/H$, or $\kappa = J/H$ where M or J (also referred to as the intensity of magnetization) is the volume magnetization induced in a material of susceptibility κ, by the applied external field H (Clark, 1997). Although susceptibility has no units, to rationalize its numerical value to be compatible with the SI or rationalized system of units, the value in c.g.s. equivalent units should be multiplied by 4π.

Telford et al. (1990) indicates that although there is great variation, even for a particular rock, and wide overlap between different types, sedimentary rocks have the lowest average susceptibility and basic igneous rocks have the highest. In every case, the susceptibility depends only on the amount of ferrimagnetic minerals present, mainly magnetite, sometimes titanomagnetite or pyrrhotite. The values of chalcopyrite and pyrite are typical of many sulfide minerals that are basically nonmagnetic.

3.2.2 Remanent Magnetization

When a magnetic material is placed in a magnetic field, the material becomes magnetized and the external magnetizing field is reinforced by the magnetic field induced in the material itself. This is known as induced magnetization. If the external field is removed, the induced magnetization disappears at once, but some materials are able to retain a permanent or remnant magnetization and its direction will be fixed within the specimen in the direction of the (now disappeared) inducing field. Rocks containing magnetic minerals may have these two kinds of magnetization: induced and remnant (Clark and Emerson, 1991).

Induced magnetization exists only in the presence of an external magnetic field. Remnant magnetization, however, is frozen within the rock, and the rock remains magnetized in a field-free area. Sometimes the direction of the Earth's field at the time of rock formation or alteration is preserved. The study of rock paleo-magnetism is based on this property and, in some places, can be used to show rock movement through time (Strangway, 1970).

Primary remnant magnetization is acquired by the cooling and solidification of an igneous rock from above the Curie temperature (of the constituent magnetic minerals) to normal surface temperature (TRM) or by detrital remnant magnetization (DRM). Secondary remnant magnetization, such as chemical, viscous or post-depositional remnant magnetization, may be acquired later on in the rock's history (Reynolds, 1997). This is especially true of igneous rocks which have later undergone one or more periods of metamorphism, particularly thermal metamorphism (Sharma, 1986). The intensity of the remnant magnetization J_r may swamp that of the induced magnetization J_i, particularly in igneous and thermally metamorphosed rocks. The ratio of the two intensities (J_r/J_i) is called the Königsberger's ratio Q (Reynolds, 1997).

3.2.3 Magnetization at Low Magnetic Latitudes

Beard and Goitom (2000) express that, near the earth's magnetic equator, the ambient magnetic field is almost horizontal, is oriented approximately north-south, and has a field intensity of between 25000 and 40000 nT, about one-half the intensity at the magnetic poles. The magnetic equator lies within 10^0 of the Earth's geographic equator. The decreased equatorial field intensity causes local magnetic anomalies at low latitudes to have smaller magnitudes than those produced by similar structures at high latitudes.

The north-south orientation of the horizontal inducing field means that a long north-south striking magnetic structure may show no anomaly at all, except at the north and south termination of the structure. However, the general result can be summarized this way: Magnetic readings are high along and near a line that goes through a magnetic object in the direction of the Earth's Field; magnetic readings are low in all other locations.

Furthermore, at very low latitudes, typically between 10^0 inclination, the amplitude correction for north-south trending features unreasonably amplifies noise and distorts magnetic anomalies from sources magnetized in directions different from the inducing field. Due to the dipolar nature of the geomagnetic field, magnetic anomalies observed anywhere rather than magnetic poles are asymmetric even when the causative body distribution is symmetric. This property complicates the interpretation of magnetic data (Rajagopalan, 2003).

3.3 Rock Alteration

Rock alteration is the reaction of hydrothermal fluids with enclosing rocks, causing changes in mineralogy that are most marked adjacent to point of entering of invading fluid (vein) and become less distinct further away (Appiah, 1991). The alteration of magnetic minerals is important to remember when it comes to the interpretation of magnetic anomalies. Rocks which should display large susceptibilities and greatest intensities of magnetization may exhibit much weaker magnetic properties owing to geochemical alteration of the magnetic minerals (Reynolds, 1997).

Alteration of wall rock adjacent to hydrothermal veins by the fluid is responsible for formation of the mineral deposit. Wall rock alteration occurs in the form of pyritization, arsenopyritization, sericitization, chloritization, silicification, and carbonatization. The most abundant ore minerals are pyrite and arsenopyrite, each making up 20-30% of all ore minerals. Gold is commonly associated within bournonite and bonanza ores are associated with mariposite (Appiah, 1991).

Studemeister (1983) pointed out that the redox state of iron in rocks is a useful indicator of hydrothermal alteration. Large volumes of fluid or high concentrations of exotic reactants such as hydrogen or oxygen are required to shift Fe^{3+}/Fe^{2+}. When reactions associated with large water/rock rations occur, the change in redox state of the rocks produces large changes in magnetic properties owing to the creation or destruction of ferromagnetic minerals.

The potassic alteration zone associated with oxidized, magnetic felsic intrusions is often magnetite-rich. This is commonly observed for Au-rich porphyry copper systems (Sillitoe, 1979). However contact metamorphism of hydrothermally altered, demagnetized igneous rocks for instance by dike injection may produce secondary magnetite (Hall and Fisher, 1987). Carbonate alteration of serpentinized ultramafic initially distributes magnetite, without destroying it, and has little effect on susceptibility. Intense talc-carbonate alteration, however, consumes the magnetite and demagnetizes the rock (Clark, 1983).

3.4 Lithology, Structure and Magnetism

Structures may be conveniently subdivided into two groups (Plummer et al., 2001):

- Brittle structures - recording the brittle-elastic failure of rocks in the past. Faults and joints fall in this broad category.
- Ductile structures - preserving the permanent viscoplastic deformation of rock throughout geologic time. Folds and metamorphic foliations are the expression of this type of structure.

Isolated magnetic anomalies, generally circular or oval in plan and several hundred meters across, and with amplitude of tens to hundred of nanoteslas, may arise from accumulation of magnetite and pyrrhotite, which may be associated with economic grades of copper, lead, zinc, silver, gold deposits (Plummer et al., 2001). For example, the Abra deposit in the Bangemall Basin of Australia, which precipitated from mineral bearing solutions are frequently located within the rocks adjacent to major faults.

Sedimentary rocks are usually non-magnetic. The interpretation of survey data assumes that magnetic sources must lie below the base of the sedimentary sequence (Grant, 1985). This allows rapid identification of hidden sedimentary basins in petroleum exploration. The thickness of the sedimentary sequence may be mapped by systematically determining the depths of the magnetic sources (the 'magnetic basement') over the survey area.

Metamorphic rocks probably make up the largest part of the Earth's crust and have wide range of magnetic susceptibility. These often combine, in practice, to give complex patterns of magnetic anomalies over areas of exposed metamorphic terrain. Itabiritic rocks tend to produce the largest anomalies, followed by meta-basic bodies, whereas felsic areas of granitic/gneissic terrain often shows a plethora of low amplitude anomalies imposed on a relatively smooth background (Grant, 1985).

Igneous and plutonic rocks show a wide range of magnetic properties (Plummer et al., 2001). Homogeneous granitic plutons can be weakly magnetic; often conspicuously featureless in comparison with the magnetic signature of their surrounding rocks but this is by no means universal. Banded iron formation (itabirites) can be so highly magnetic that they can be unequivocally identified on aeromagnetic maps. Grant (1985) indicates that, in an area where the Earth's total field is only 23000 nT, less magnetic examples may be confused with mafic or ultramafic complexes.

Also, ore bodies can be significantly magnetic, even though the magnetic carriers are entirely amongst the gangue minerals. In such a case the association with magnetic minerals may be used as a path-finder for the ore through magnetic survey. In general, however, the direct detection of magnetic ores is only to be expected in the most detailed aeromagnetic surveys since magnetic ore bodies form such a very small part of the rocks to be expected in a survey area.

3.5 Enhancement Techniques

Generally, the original total magnetic intensity grid is visually difficult to observe and interpret the various structures. A range of imaging routines can be specified to visually enhance the effects of selected geologic sources using mathematical enhancement techniques. Derived products, such as pole-reduced, residual and vertical derivative fields are useful to enhance near-surface magnetic sources, but their limitations depend on the quality of the data and additional factors such as magnetic inclination and declination. It is not uncommon to see the magnetic data reflecting basement rocks that may have little in common with the geology and structure of the overlying units mapped by the radiometric data (Nicolet and Erdi-Krausz, 2003).

3.5.1 Fourier Transform Filter

Fourier transforms are particularly useful in magnetics for (Telford et al., 1990):

- Resolution of specific anomalies by downward or upward continuation,
- Changing the effective field inclination (reduction to the pole) or conversion of total-field data to vertical-component data,
- Calculation of derivatives and
- General filtering-separating anomalies caused by sources of different size and depth, and modelling.

A much faster algorithm developed by Cooley and Tukey (1965) called the Fast Fourier Transform (FFT) is an efficient algorithm to compute the discrete Fourier transform (DFT) and its inverse.

3.5.2 Reduction to the Pole (RTP)

An observed anomaly has asymmetric shape, when magnetization occurs anywhere other than magnetic poles (Mendonça and Silva, 1993). This makes a dipolar nature on magnetic field which causes a horizontal displacement between measured anomaly and exact body location. Reduction-to-the-pole (RTP) is a useful and effective operation designed to transform a total magnetic intensity (TMI) anomaly caused by an arbitrary source into the anomaly that this same source would produce if it were located at the pole and magnetized by induction only (Li, 2008).

3.5.3 Analytic Signal

The analytic signal or total gradient is formed through the combination of the horizontal and vertical gradients of the magnetic anomaly. The analytic signal has a form over causative body that depends on the locations of the body (horizontal coordinate and depth) but not on its magnetization direction (Ansari and Alamdar, 2009). Analytic signal is a quantity that includes this property and has been used to edge detection and depth estimation of magnetic bodies by several authors.

3.5.4 Vertical Derivative Filter

Keating (1995) indicates that computation of the first vertical derivative removes long wavelength features of the magnetic field and significantly improves the resolution of closely spaced and superposed anomalies. The values for the first vertical derivative of the magnetic field can be computed directly from the gridded residual magnetic intensity data using a fast Fourier transform, combining the transfer functions of the first vertical derivative and a low-pass filter. The low-pass filter is aimed at attenuating unwanted high frequencies enhanced by the derivative operator.

3.5.5 Total Horizontal Derivative

After the reduction-to-pole correction, a magnetic body is spatially more directly associated with the related magnetic response. The maximum horizontal gradient (more properly the maxima of the total horizontal gradient) of the anomaly slope is then located near or over the body edge. That is, the horizontal gradient operator in map form produces maximum ridges over edges of magnetic basement blocks and faults or other magnetic bodies. In addition, the horizontal gradient highlights linear features, related to contacts, in the data set (Milligan and Gunn, 1997).

3.5.6 Upward and Downward Continuation

Upward continuation smoothens out high-frequency anomalies relative to low-frequency anomalies. The process can be useful for suppressing the effects of shallow anomalies when details on deeper anomalies are required. Downward continuation sharpens the effects of anomalies (enhance high frequencies) by bringing them closer to the plane of observation - it simulates flying the survey closer to the ground (Milligan and Gunn, 1997). In this way anomalies will have less spatial overlap and thus be more easily distinguished one from the other. This process not only reduces the overlap between adjacent anomalies but also increases the amplitude of the anomalies (Gunn, 1975).

3.6 Principles of Radioactivity

The applications of radioactivity in geosciences are based on knowledge of the physical properties of radiation sources, and the ability to detect these sources through the analysis of remotely sensed data. This chapter reviews the principles of radioactivity and its detection.

3.6.1 Basic Radioactivity

Atoms of an element having the same atomic number but different numbers of neutrons (i.e. different mass numbers) are called isotopes. Some isotopes are unstable and change to more stable nuclei by the emission of energetic ionizing radiation. These isotopes are called radioactive isotopes or radioisotopes. Nuclides with this feature are called radionuclide, and the process is called nuclear decay or disintegration (Nicolet and Erdi-Krausz, 2003).

Each radioisotope has a characteristic probability associated with the radioactive disintegration of its nuclei. This is called the 'half-life' of the isotope and is the time taken for half the nuclei to decay. Thus, after one half-life, half the original radioactive isotopes remain, and after two half-lives, one quarter of the original radioactive isotopes remain, and so on (Minty, 1996).

The radioactivity decay law expresses the decrease in the number of atoms of a radionuclide with time (Nicolet and Erdi-Krausz, 2003):

$$N_t = N_o \exp^{-\lambda t} \tag{3.2}$$

where N_t is the number of atoms present after time $t(s)$; N_o is the number of atoms present at time $t = 0$; λ is the decay constant of a radionuclide (s^{-1}). A related constant, the half-life $T_{1/2}(s)$, is the time taken for half the radionuclides to decay:

$$T_{\frac{1}{2}} = \frac{0.693}{\lambda} \tag{3.3}$$

The product λN gives the activity (Bq) of the radionuclide.

Radioactive decay also often occurs in a series (or chain) with a number of daughter products, which are also radioactive, and terminates in a stable isotope. In a closed system, and starting with a specified amount of a mother element, the number of atoms of daughter elements and their activity grows gradually until radioactive equilibrium of the disintegration series is reached (Minty, 1996). At this point, the activities of all the radionuclides of the series are identical. Thus the measurement of the concentration of any daughter element can be used to estimate the concentration of any other element in the decay series.

3.6.2 Disequilibrium

Disequilibrium occurs when one or more decay products in a decay series are completely or partially removed or added to the system (Minty, 1996). Thorium rarely occurs out of equilibrium in nature, and there are no disequilibrium problems with potassium. However, in the uranium decay series disequilibrium is common, and can occur at several positions in the ^{238}U decay series: ^{238}U can be selectively leached relative to ^{234}U; ^{234}U can be selectively leached relative to ^{238}U; ^{230}Th and ^{226}Ra can be selectively removed from the decay chain; and finally ^{222}Rn (radon gas) is mobile and can escape from soils and rocks into the atmosphere (Nicolet and Erdi-Krausz, 2003).

Estimates of uranium concentration are therefore usually reported as equivalent uranium (eU) as these estimates are based on the assumption of equilibrium conditions. Thorium is also usually reported as equivalent thorium (eTh), although the thorium decay series is almost always in equilibrium (Milsom, 2003).

3.6.3 Source-Detector Geometry

Source thickness has a significant effect on the shape of observed spectra. Gregory and Horwood (1961) showed that with increasing source thickness there is build-up of the Compton continuum due to scattering in the sources. The photo-peaks are thus reduced relative to the Compton background. Since low-energy photons are more easily attenuated than high-energy photons, this effect is more pronounced at lower energies.

Terrestrial radiation is attenuated in the source and by material between the source and the detector. The shape of the observed spectrum depends on the amount of attenuating material between the source and the detector. For increasing attenuation, the photo-peaks are reduced relative to the energy continuum. Measured spectra are thus functions of the concentration and geometry of the source, the height of the detector above the ground, the thickness of any non-radioactive overburden, and the response function of the detector (Nicolet and Erdi-Krausz, 2003).

3.7 Measurement of Gamma Radiation

Modern gamma ray spectrometers typically record 256 (or 512) channels of information in the energy range 0-3.0 MeV (Nicolet and Erdi-Krausz, 2003). Each channel thus records all gamma rays absorbed by the detector that have energy within 11.7 keV range; count rates are usually low. An airborne gamma ray spectrometer with 32 litres of NaI detectors will record perhaps one or even zero counts in some high energy channels during a one-second counting period. A typical airborne gamma ray spectrum is shown in Fig. 3.2.

The K energy window monitors the 1.46 MeV gamma rays emitted by ^{40}K. The U and Th energy windows monitor gamma ray emissions of decay products in the U and Th decay series. Thorium is characterized by the strong 2.62 MeV peak of ^{208}Tl. The uranium spectrum is most complex, although the peak at 1.76 MeV is reasonably distinctive (Nicolet and Erdi-Krausz, 2003).

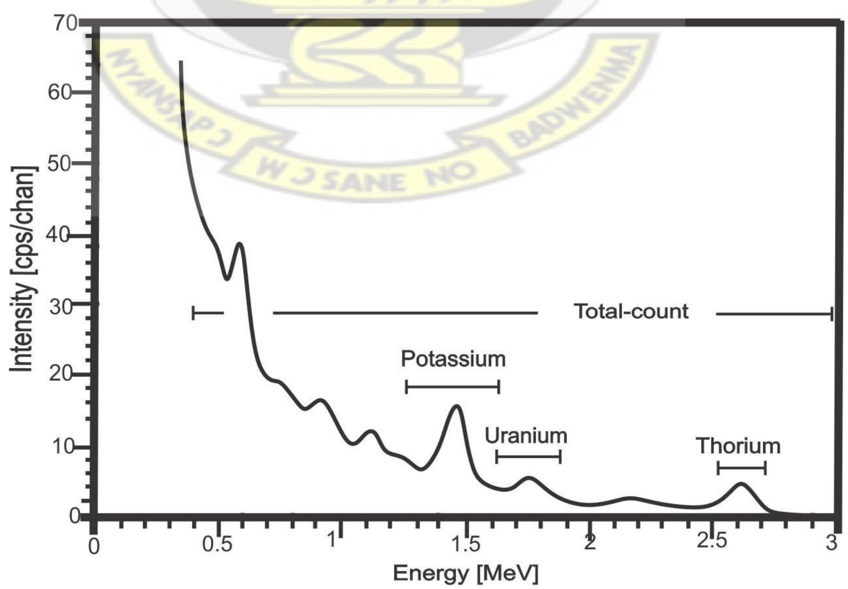

Figure 3.2: Typical airborne gamma ray spectrum showing the positions of the conventional energy windows (Nicolet and Erdi-Krausz, 2003)

Potassium and thorium are clearly evident in granitic gneiss, as well as a smaller fraction of uranium. These windows are generally accepted as the most suitable for the measurement of K, U and Th. The total-count window gives a measure of total radioactivity (Telford et al., 1990). In geology and nuclear geophysics, radioelement concentrations in rocks, air and water are expressed in the following units (ICRU, 1994):

- Mass concentration of K: % K (percent potassium)
- Mass concentration of U: ppm U (parts per million of uranium)
- Mass concentration of Th: ppm Th (parts per million of thorium).

3.8 Mapping Natural Sources of Radiation

The sources of natural gamma-radiation can be conveniently divided into three (3) groups, according to their origin (Minty, 1996). The first group includes ^{40}K, ^{238}U, ^{235}U and ^{232}Th, which are believed to have been synthesized during the creation of the universe and have half-lives of the same order as the age of the Earth (~4.5 Ga). The second group comprises radioactive isotopes that are daughter products from the decay of isotopes in the first group. These have half-lives ranging from small fraction of a second to 104 to 105 years. The third group would include isotopes created by external causes such as the interaction of cosmic rays with the Earth and its atmosphere (Minty, 1996).

3.8.1 Geochemistry of Radioelements

3.8.1.1 Potassium

Potassium (K) is a volatile lithophile element and monovalent under natural conditions (Nicolet and Erdi-Krausz, 2003). Potassium is a major component of the Earth's crust (2.35%). It is an alkali element and shows a simple chemistry. The major hosts of K in rocks are potassic feldspars (principally orthoclase and microcline with ~13% K) and micas (biotite and muscovite with typically 8% K). Potassium is absent from mafic minerals (Dickson and Scott, 1997). Consequently K is relatively high in felsic rocks (granites), but low in mafic basalts and very low in dunites and peridotites (Fertl, 1983).

During weathering, the major K hosts will be destroyed in the order biotite-K-feldspar-muscovite. Potassium released during weathering can be taken up in the formation of K-bearing minerals such as illite or adsorbed in minor amounts into other clays (montmorillonite) under suitable conditions. The feldspar mineral series, the feldspathoids leucite and nepheline, and the micas biotite and muscovite, together contain virtually all the potassium in metamorphic and magmatic rocks (Dickson and Scott, 1997).

3.8.1.2 Thorium

Thorium (Th) is an actinide element with a valence state of Th^{4+} in solution with evidence for lower valence states in solid state. It forms with the anions fluoride, oxalate, iodate and phosphate insoluble precipitates (Krishnaswami, 1999). Thorium can be dissolved in acid solutions and its solubility is enhanced by humic acids (Chopin, 1988).

Thorium is a constituent of the accessory minerals zircon, monazite, allanite and xenotime, apatite and sphene at levels greater than 1000 ppm or as trace amount in other rock-forming minerals. Major Th-bearing minerals (monazite and zircon) are stable during weathering and may accumulate in heavy mineral sand deposits. Th freed by the breakdown of minerals during weathering may be retained in Fe or Ti oxides-hydroxides and with clays (Dickson and Scott, 1997).

3.8.1.3 Uranium

Uranium (U) is a reactive metal with an average abundance of about 3 ppm in the Earth's crust (Langmuir and Hermans, 1980). Uraninite is common as minute inclusions in the rock forming minerals in granites or as large grains in mineralized granites and pegmatites. Uraninite also occurs in hydrothermal veins and sedimentary rocks. The accessory minerals zircon, monazite, apatite, allanite and sphene are common in igneous and metamorphic rocks, of which zircon and monazite are the most resistant to weathering (Nicolet and Erdi-Krausz, 2003).

Uranium freed by the breakdown of minerals during weathering may be retained in authigenic iron oxides and clay minerals or precipitated under reducing conditions forming uranium deposits in favourable circumstances (Dickson and Scott, 1997). Uranium itself does not emit gamma-rays during its decay but the most energetic gamma-rays emitted by its daughter isotopes come from ^{214}Bi which occurs late in the decay series (Dickson and Scott, 1997).

3.8.2 Distribution of the Radioelements in Rocks and Soils

Potassium is also highly incompatible during crystallization of magma. Earlier studies by the Geological Survey of Canada (Killeen, 1979) concentrated mainly on igneous rocks. For example, a rock type by radioelement content of 2.5% K, 3 ppm U and 15 ppm Th could be granite, felsic intrusive/extrusive, intermediate extrusive or shale. A rock with low radioelement content (i.e. $< 1\%$ K, < 1 ppm U, and < 5 ppm Th) could be anything except felsic intrusive or shale. Nevertheless, within small regions, different rock types can often be identified on the basis of the relative concentration of radioelements (Dickson and Scott, 1997).

Available data for metamorphic rocks (e.g. gneissic rocks derived from granite and amphibolites derived from dolerite) suggest that metamorphism does not affect radioelement content. Sedimentary rocks generally have radioelement content reflecting the parent source rock. Thus, immature sediments derived from granitic sources may be expected to have quite high radioelement content, but more mature sediments, composed primarily of quartz should have very low values when specific rock types (such as pegmatite, aplites, quartz-feldspar porphyrites and mafic intrusives) occur as narrow intrusions or in small areas, or are subject to faster weathering and erosion than the host country rock, it is difficult to find in-situ soils (Dickson and Scott, 1997).

Granite shows a wide range of weathering behaviour, depending on its mineralogy and the weathering regime, climate etc. Soils derived from granitoids generally lose around 20% of their radioelements contents during pedogenesis. Soils over radioelement-poor arenite, as over other poor radioelement-poor rocks; can show the effects of contamination by transported materials (Darnley, 1996).

Processes other than in-situ weathering can affect the radioelement content of soils. They include clay eluviation, colluvial and aeolian transport, and soil movement. All can affect the concentration of radioelements in the thin 30 cm layer measured during aerial surveying (Wilford et al., 1997).

3.8.3 Direct Detection of Mineralization

The most direct application of gamma ray spectrometry surveys during the 1970's and 1980's was the search for U and Th deposits (Dickson and Scott, 1997). U and Th anomalies may be identified on profile and grid presentations of the data. Ratio and statistical image processing techniques can enhance subtle anomalies. Geochemical analysis and microscopic studies of samples from rock or sediments are needed to fully identify the mineral phases that constitute the radioelements (Charbonneau, 1991).

Due to relatively low penetration of gamma rays through rock and soil, the probability of discovery of uranium mineralization is dependent on the U concentration in the source, its surface dimensions, and the positions of the measured profiles. A small outcrop of high-grade U mineralization is a more difficult target for U exploration than low-grade mineralization with extensive surface outcrop (Nicolet and Erdi-Krausz, 2003).

Dickson and Scott (1997) provide an up-to-date review of the effect of hydrothermal processes, alteration and weathering on radioelement distribution. These processes do not only have implications for the direct detection of U and Th from gamma ray spectrometry surveys, but also for detecting a number of metal deposits. These include granophile deposits of Tin (Sn), Tungsten (W) and Molybdenum (Mo), porphyry Copper-Gold (Cu-Au) mineralization, gold mineralization and stratabound polymetallic mineralization.

Hydrothermal processes can result in changes to the radioelement content of the host rocks. Among the three radioelements, K is mostly affected by such processes, Th less often and U very infrequently. Potassium is often increased during alteration signature but weathering generally decreases the intensity of alteration signature (Dickson and Scott, 1997). Many studies have described the variation of elevated K associated with alteration in porphyry Cu deposits. Moxham et al. (1965) found that the K increase during alteration in porphyry Cu deposits in the south-west U.S.A was of the other of 1.5% K and this was accompanied by an erratic increase, but no Th increase.

Potassium is commonly added to host rocks by mineralizing hydrothermal solutions. It may be hosted by K-feldspar or muscovite and potential outcropping or sub-cropping mineralization can be recognized by increase in K counts during radiometric surveying (Dickson and Scott, 1997). This could reflect the greater mobility of U compared to Th during hydrothermal alteration processes and because Th is generally unaffected by alteration processes, the K/Th ratio gives a better indication of alteration than simply K. Thorium may be mobilized during mineralization processes for example, being partly depleted in areas of K-alteration or intense silicification, but concentrated in Th-rich materials such as laterite.

The relationships between radioelement distribution and each of these deposit types are varied and complex. A thorough understanding of the effects of silicification, K-alteration, weathering processes and local lithological variations is required to evaluate the mineralization potential associated with radioelement anomalies.

CHAPTER 4

MATERIALS AND METHODS

4.1 Project Site Description

The study area is one of the significant areas on the major Prestea-Ashanti Goldfields gold belt though several prospects occur within the 20 km between Konongo and the point at which the gold belt plunges beneath the late Proterozoic Voltaian sediments. The project area is stratigraphically within the volcanic sequence of the Birimian though only minor tuffs and no lavas occur in the area. The rocks of the area are variable grained, sheared, metamorphosed quartzite containing a constant level of mafic and carbonaceous minerals, presumable derived from syngenetic volcanic activity (Cozens, 1984).

4.1.1 Location and Accessibility

Konongo is the district capital of the Asante Akim North District. It is 50 km from Kumasi the Ashanti regional capital and about 220 km from Accra, the capital of Ghana. The sealed highway linking Ghana's capital city Accra, to its second city of Kumasi runs 1 km north and parallel to the project's northern boundary. About 7 km west of Konongo, a sealed road can be located that runs to the south from the main Accra to Kumasi highway. Access to the northern and central portions of the study area is possible by the well maintained road which runs from the market place southwards to the town of Praso. Second class roads link towns like Agogo, Konongo, Odumasi, Petriensa, Domeabra, Juansa, Dwease, Praso, Hwidiem, Kyekyebiase and Wiaso. Access to more remote portions of Konongo is restricted to footpaths, cut-lines which become difficult to access during the peak of the monsoonal seasons (May to July and September to November).

The study area in the Konongo District has the following projection coordinates referenced to the World Geographic System (WGS) 84 and Longitude-Latitude categories with units in degrees: (-1.3227^{0}, 6.7297^{0}) representing upper left corner, (-1.0563^{0}, 6.7297^{0}) as upper right corner, (-1.3227^{0}, 6.4845^{0}) and (-1.0563^{0}, 6.4845^{0}) representing lower left and lower right corners respectively.

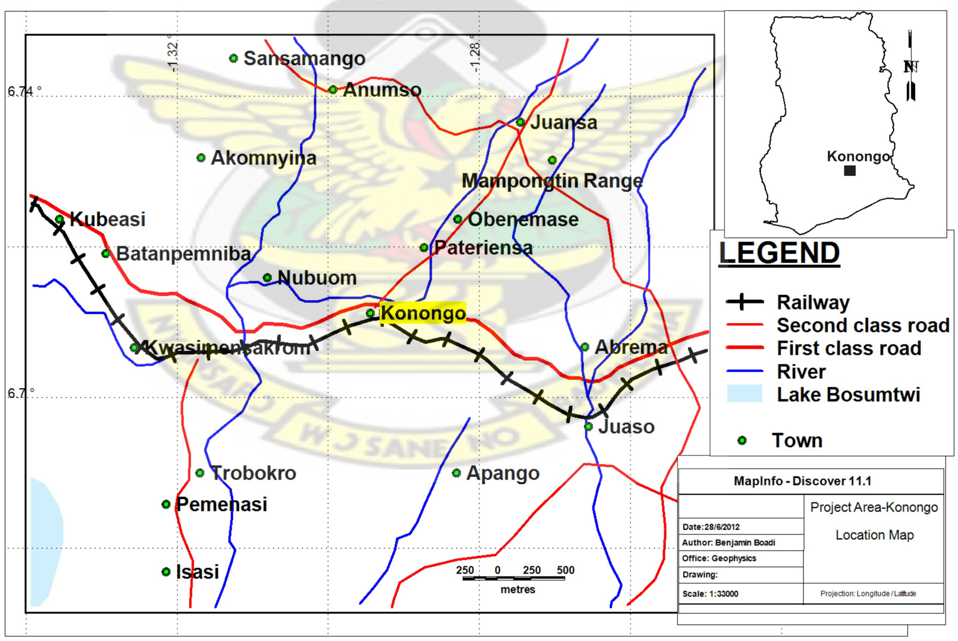

Figure 4.1: Location and accessibility of the study area (modified from Microsoft Student Encarta, 2009)

4.1.2 Physiography and Drainage

The topography of Konongo is that of an undulating land, with the northern sector sloping gently into the Voltaian Formation. The topography of the area is quite variable. To the north of the district is the prominent Kwahu escarpment, where elevations are about 550-600 m above sea level (ASL) near Agogo. The escarpment stands well above the low rolling hills in much of the district, where elevations are mainly in the range 180-260 m ASL. In the SE corner of the district is the very large Banso intermediate granitoid (high radiometric K and low magnetics) with a peak elevation of about 580 m ASL in the central area of the batholith. There are a series of narrow, NE trending ridges running parallel to the strike of the major structures within the immediate district. These hills are underlain by Birimian and Tarkwaian Formations; the ridges have elevations up to about 260 m ASL and a relief of 50-80 m above the surrounding valleys where the lowest areas are around 180 m ASL. The southern portion of the district may be considered to extend just east of Lake Bosumtwi. Konongo is drained by some rivers such as Anum, Owerri and other small seasonal streams which serve as major source of water in the area.

4.1.3 Vegetation

The vegetation is mostly semi-deciduous forest comprising open forest which covers the highlands (575 km^2) and closed forest covering the range (230 km^2). However, most of the original forest has degenerated into secondary forest and grassland due to indiscriminate felling of trees, bush-fire and poor farming practices, such as shifting cultivation and bush fallowing.

4.1.4 Climatic Conditions and Occupation of Inhabitants

The annual rainfall of the district averages between 150-170 mm and the pattern is found to be erratic as well as bimodal with major season. Two rainy seasons occur, one between May and July averages 160 mm per month and the other between September to October averages 186 mm per month. The driest period of the year is from January to March when the dry and dusty Hamattan wind blows southwards off the Sahara desert. During the dry season rainfall averages 54 mm per month. There is a short dry season in August, which at times stretches into September. The minimum monthly temperature is about 26^{0}C and the maximum temperature of 30^{0}C is recorded in March and April. Daily temperatures range from 22^{0}C to 30^{0}C, with humidity averaging 80%.

The District has about 70-80% of the population as farmers and it is a potential area for the cultivation of a variety of agricultural produce. Agriculture in the district is fundamentally rain fed and depends highly on the vagaries of the weather. Most of the local population is engaged in small-scale farming but the district community has also depended on the mining activities in the area, including rather extensive small-scale mining.

The Konongo District is also endowed with gold deposits and has made mining an important economic activity in notable towns like Konongo, Odumasi, Atunsu, Obenimase and Kwakokor. The informal sector handles a few processing activities such as ’gari’ (processed cassava), palm oil, and ’akpeteshi’ (locally distilled gin) and soap which are scattered throughout the district. By far, wholesale and retail trading are important economic activities especially in Konongo, which is fast becoming an important commercial centre for both agriculture and manufactured products. Human labour immigration among the illiterate youth to Konongo is a high feature in the district.

4.2 Data Acquisition

The Geological Survey of Finland (GKT) in collaboration with the Geological Survey of Ghana and the Ghana Minerals Commission in the years 1997-98 carried out systematic airborne geophysical survey in southern Ghana, which the Ashanti belt was part. The survey produced high resolution airborne geophysical information for geological mapping and mineral exploration purposes. Among the airborne geophysical datasets collected include magnetic, radiometric and electromagnetic data (Griffis et al., 2002).

4.2.1 Metadata

These geophysical informations were collected with the following aircraft equipment (Table 4.1) and survey parameters (Table 4.2).

Table 4.1: Airborne Geophysical Survey Equipment (Geological Survey of Ghana, 1998)

Survey Equipment	**Aircraft (Fixed wing)**	**Magnetometer**	**Spectrometer**	**Dual Frequency EM**
Equipment Types	Cessna Titan 404 (C-FYAU)	Scintrex Cesium SC-2	Exploranium GR 820-256 with 2048 in^3 NAI (TI) downward looking crystal and 256 in^3 upward looking crystal	GKT vertical coplanar, dual 3125 and 14368 Hz, coil separation 21.36 m

Table 4.2: Airborne Geophysical Survey Parameters (Geological Survey of Ghana, 1998)

Survey Parameter	Parameter Specification
Period	1997-1998
Travel line spacing	400 m
Travel line direction	NW - SE
Tie-line spacing	5000 m
Tie-line direction	NE - SW
Nominal terrain clearance	70 m
Navigation	Global Positioning System (GPS)
Sampling time	0.1 sec Magnetic, 0.125 sec EM, 1.0 sec. Radiometric
Air speed (nominal)	250 - 290 km/h (70 - 80 m/s)
Measurement spacing	8 m (magnetic), 6 - 7 m (EM), 80 m (Rad)

4.3 Data Processing

The major GIS software used to process and enhance the airborne geophysical data was the Geosoft (Oasis Montaj) and the other geophysical softwares that were used to enhance the data in a variety of formats were MapInfo 10.5 - Discover 11.1, Golden Software Surfer 10 and Model VisionPro 8. The Airborne geophysical datasets namely magnetic and radiometric were obtained from the Ghana Geological Survey Department (Accra) by the Physics Department (Kwame Nkrumah University of Science and Technology-Kumasi) on the 17th November, 2011.

The methodology applied involved the acquisition of two different Geophysical Airborne data sets (magnetic and radiometric), building of databases (projects), data processing and interpretation. Two databases were generated to process the acquired datasets; using Geosoft software for processing the radiometric and magnetic data. This section gives an overview of the processing of the airborne data. The processing of airborne data involved the sequential processes of editing, the application of a gridding routine, and removal of the Earth's background magnetic field.

Some corrections like removing diurnal variation of the Earth's magnetic field, aircraft heading, instrument variation, lag error between aircraft and the sensor and inconsistencies between flight lines and tie lines were made by the Geological survey of Finland (GKT). The geophysical datasets from the Konongo project area were registered and projected in the longitude-latitude coordinate system with Geosoft software constituted the pre-processing phase. The second phase comprised four steps: a) gridding; b) calculating the definitive geomagnetic reference field (DGRF) to be subtracted from the observed magnetic data, c) micro-levelling the entire data set to remove any apparent residual errors and d) merging the different blocks for each different data type.

Airborne geophysical data can be enhanced by a range of linear and non-linear filtering algorithms. A range of imaging routines can be specified to visually enhance the effects of selected geologic sources using mathematical enhancement techniques (Milligan and Gunn, 1997). The following discussion describes some enhancement techniques and their results.

4.3.1 Aeromagnetic Data

Although the magnetic method has been widely used in mineral exploration for decades, recent improvements in magnetic data acquisition, processing and presentation have increased the importance of magnetic surveys; particularly the high resolution aeromagnetic surveys (Clark, 1997).

The original data, after having been projected into longitude and latitude coordinate system (using Geosoft software), the geographical coordinates of the study area (also in longitude and latitude) was superimposed to extract the database for this project. The minimum curvature technique was applied using the GRID AND IMAGE tool in gridding the extracted database for both the radiometric and magnetic data. The MAGMAP tool offering a number of utilities was implemented to help magnetic-anomaly grid (total field intensity minus the definitive international geomagnetic reference field) to be calculated for the appropriate time of year and elevation of the original survey and apply the following filters.

Magnetic anomalies in the Earth's magnetic field are caused by magnetic minerals in the rocks, and maps and images of these anomalies can be interpreted in terms of geology (Silva et al., 2003). Once a grid was produced and the necessary filters applied it was displayed as an image using the GRID AND IMAGE tool.

In order to facilitate interpretation, analytic signal amplitude and two-dimensional fast fourier transformation (2D-FFT) filters were applied to enhance the quality of the data. The 2D-FFT filters used included: reduction to the pole, first vertical and horizontal derivatives, downward and upward continuations, and analytic signal.

4.3.1.1 Reduction to the Pole (RTP)

A reduction to pole (RTP) filter for low geomagnetic latitudes was applied to the magnetic anomaly data (Total Magnetic Intensity: TMI). The approach utilizes an azimuthal filter in the frequency domain to minimize the directional noise caused by the low geomagnetic latitude (Phillips, 1997). The calculation of inclination and declination were made using the central coordinates of the area (longitude: -1.22^0 and latitude: 6.61^0), inclination and declination of -12.34^0 and -5.73^0 respectively to an average total field of 31886.55 nT.

4.3.1.2 First Vertical and Horizontal Derivatives

The RTP grid data was subjected to first vertical derivative (1VD) filter. This filter allows small and large amplitude responses to be more equally represented. The 1VD grid in gray-scale helped enhance linear features in the area. The RTP grid is also enhanced by the application of first horizontal gradient or derivative (1HD) which is critical when trying to map linear features such as fault and/or dikes from the magnetic data. The filter provides higher resolution and better accuracy at wider spacing. The horizontal derivative aided in identifying geologic boundaries of formations in the study area.

Higher derivative images with different filter such as 2VD and 2HD produced interesting results but several distortions were noted to occur in the images due to the enhancement in the noise level introduced in the data by this process. These images were therefore not used in the interpretation but were only used as a guide in the interpretation from the first derivative images.

4.3.1.3 Downward and Upward Continuation (DC and UC)

The appropriation of the magnetic intensities from deeper structures, led to applying the UC filter to suppress the effects of shallow anomalies. DC and UC filter; 50 to 100 m was applied to each grid from the 1VD and 1HD. By so doing high frequency anomalies relative to low frequency anomalies is smooth out. The DC filters enhanced responses from shallow depth sources by effectively bringing the plane of measurement closer to the source (Geosoft User guide, 2005). However, the data contain short wavelength noises that appear as signals coming from very shallow sources in the continuation.

4.3.1.4 Analytic Signal Amplitude

The analytic signal amplitude was calculated from the residual magnetic field. The analytic signal amplitude is independent of the direction of the magnetization of the source, and is related to amplitude of magnetization. The most significant concentrations of mineral deposits in this area are correlated with high analytical signal amplitudes (Silva et al., 2003).

4.3.2 Airborne Radiometric Data

Airborne radiometric data are used as an aid to lithological mapping. For most times, there is a good correlation between patterns in the radiometric data and unweathered rocks. This information compliments magnetic, electromagnetic and geochemical data normally acquired during mineral exploration programs (Gunn et al., 1997; Shives et al., 2000). This is one of the most cost-effective and rapid techniques for geochemical mapping of the radioactive elements: potassium, uranium and thorium. This section describes briefly some enhancing techniques of the radiometric data such as composite image, ratio maps, potassium, thorium and uranium maps for the study area. The goal is to recognize and understand radiometric signatures associated with the host rocks important to mineralization.

4.3.2.1 Total Count (TC), Potassium (K), Thorium (Th) and Uranium (U) Channels

By employing the GRID AND IMAGE tool in Geosoft software, the total count image was created after micro-levelling the entire data set to remove any apparent residual errors. These images were generated by employing mini-curvature gridding since the data were collected in grid window with the grid depending on the instrumentation, cost of exploration and the type of plane used in the survey. The images were then correlated with the pattern and trend of the geological units. The idea is that from literature, mafic and ultramafic rocks units for example, have low radiometric response.

To help identify zones or units that have high concentrations of potassium, the potassium image map was developed. Thorium is generally considered very immobile. However, some gold deposits show increases in K and Th, which suggest that Th was mobilized in hydrothermally altered systems (Silva et al., 2003). Ostrovskiy (1975) refers to a decrease in Th and an increase in K for the alteration environment in variety of ore deposits. It is for this and many more reasons that led to the developing of the Th image map. The uranium image especially ratio map of uranium and potassium (U/K) shows good definition in mapping the granitoid rocks which show low uranium but high potassium concentration. Boyle (1979) suggests that removing of uranium in such a process leaving negative aureoles is as a result of pervasive hydrothermal alteration.

4.3.2.2 Composite Images and Ratio Maps

A composite RGB colour model was created using Geosoft software for which potassium, thorium and uranium were assigned to the red, green and blue respectively because the blue tends to reduce the poorest signal-to-noise ratio of uranium channel. The resulting images to be discussed later on comprise colours generated from the relative intensities of the three components and represents subtle variations in the ratios of the three bands. A histogram equalization to give the best colour variation was used to enhance the contrast of the individual histograms of K, Th and U before combining to composite image. However, for this work, the composite image presented showed a better result.

The ratio images were also created with the motive to remove lithological differences and effects in the data caused by variations in the soil moisture, non-planar source geometry, and errors associated with altitude correction. According to Silva et al. (2003) lithological differences tend to be removed because radioelement concentrations frequently vary as lithology change. For example U/Th and U/K ratios were created for determining the areas where relative concentrations of uranium are high.

4.4 Analysis of Lineaments Using Rose Diagram

Lineaments are evaluated in order to extract further information on the distribution and nature of the lineaments for this purpose a conventional technique called rose diagram was applied. A rose diagram was used to display graphically different tendencies for structures like joints or fault planes representing the angular relationships of the geologic map data. The purpose of this study is to analyse the spatial distribution of lineaments extracted from aeromagnetic images according to their length and orientation in order to contribute to the understanding of the faults of the study area.

CHAPTER 5

RESULTS AND DISCUSSIONS

Airborne magnetic and radiometric datasets were used to delineate the geology, structure and alteration zones in the study area. These datasets generated high resolution maps that show major lithology and structural features present in the Konongo area. These maps helped to identify visually, the individual lithology and delineate geological structures. Elevated radiometric element patterns, anomalous conductive zones and low magnetic susceptible areas which might have resulted from rock alterations or possible mineral deposits were delineated as potential targets for ore deposits.

5.1 Interpretation of Magnetic Data

Magnetic anomalies in the Earth's magnetic field are caused by magnetic minerals in the rocks, and maps of these anomalies can be interpreted in terms of geology (Silva et al., 2003). The central goal for the use of the magnetic data is to delineate geology and structures. Geological structures normally serve as conduits for hydrothermal fluid deposition and are important features in mineral exploration programmes (Amenyoh et al., 2009). Linear features in the granitoid (Banso Batholith), metamorphosed belt and basin rocks are observed as high magnetic anomalies. The concentration of magnetic minerals or their excessive destruction by alteration especially along tectonic structures allows the detection of geological structures (Plumlee et al., 1992).

5.1.1 Total Magnetic Intensity (TMI) Map

The total magnetic field intensity data (Fig. 5.1) was gridded with minimum curvature method and displayed with pseudocolours. This map shows different magnetic anomalies corresponding to different lithological units and geological structures in the study area.

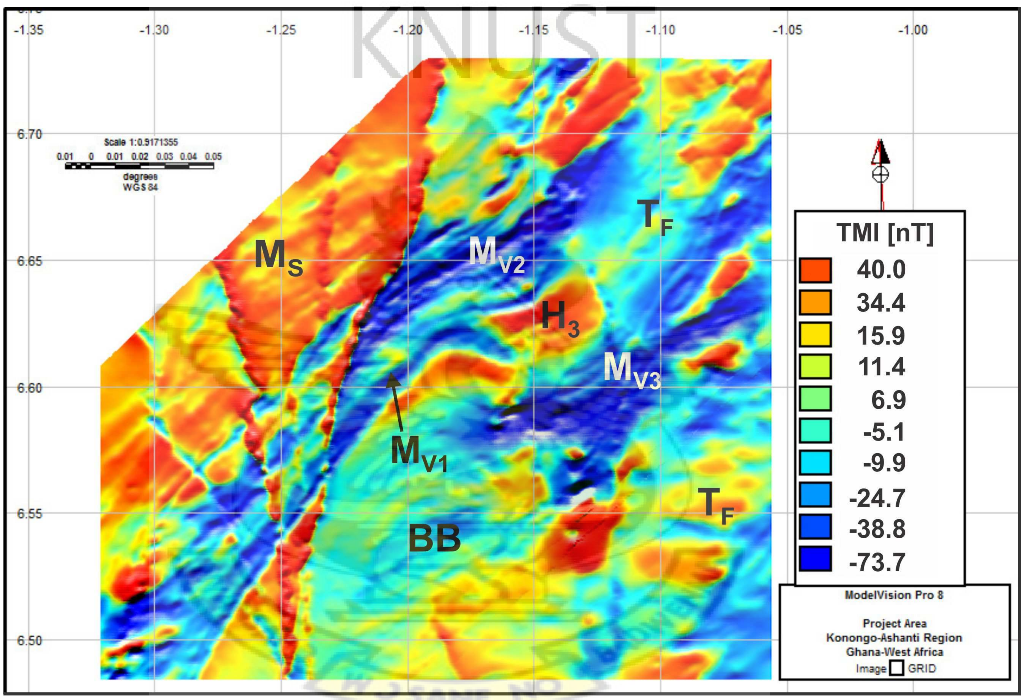

Figure 5.1: Total magnetic intensity grid map.

The amplitude of a magnetic anomaly is directly proportional to magnetization which in-turn depends on magnetic susceptibility of the rocks at specific geographical locations. Close to the Earth's equator (points of low magnetic indication) high susceptible magnetic features appear as low magnetic anomalies and vice versa. The total field magnetic map and its derivatives show high magnetic susceptible areas in low magnetic values while less magnetic susceptible areas are depicted as high magnetic values except for the analytical signal map where high magnetic susceptible areas are shown as high anomalies.

The long stretch low magnetic susceptible pattern M_S, at the top left corner striking NE corresponds with the Meta-sedimentary rock (Argillite and Siltstone) (Fig. 5.1). A well known granitoid position is reflected at the bottom and corresponds to the Banso Batholith (BB). The broad NE-SW high magnetic susceptible patterns M_{V1}, M_{V2} and M_{V3} at the central-part of Fig. 5.1, represent the Meta-volcanic rocks (volcanoclastics) separated by the Tarkwaian Formation (T_F). Some lithologic contacts, faults and fractures are shown as magnetic low although not continuous in some places. The folding of T_F, M_{V1} and M_{V2} at the central part of the area is as a result of the intrusion of this Banso Batholith. At the top-right corner there are some high elevations which also record high magnetic anomaly in the TMI map.

Fig. 5.2 is contour map of the TMI map. The polygons in the map indicate areas that are tectonically disturbed. The contour map indicates that M_{V1}, M_{V2} and M_{V3} were a long NE-SW striking continuous geological unit but after a long period of denudation, they have been folded, fractured and faulted by a splay of faults thus introducing a structural corridor (area of the blue polygon) at the northwest of the Banso Batholith. These structures also extend into the Meta-sedimentary rock. The discontinuity of M_{V1} at the north of the BB is as a result of shearing and faulting.

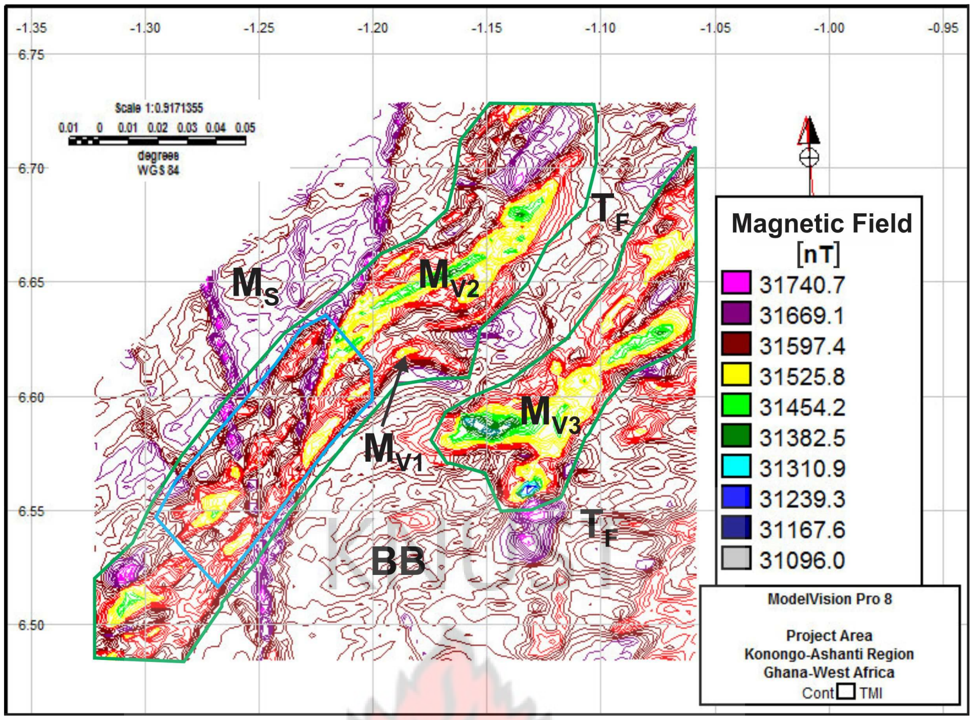

Figure 5.2: Contour map of the TMI map.

The regions marked by the green polygon represent major Birimian meta-volcanic trending in the NE direction in the study area. The meta-volcanics north-west of the Banso Batholith is more tectonically disturbed (faulted, fractured and sheared by the intruding dike system) thus has the potential to host hydrothermal fluids as compared to the meta-volcanic at the north-east of the Banso Batholith which is less sheared and faulted. M_{V1} and M_{V2} are the two Birimian meta-volcanics occupying the same tectonic region but separated by the same Tarkwaian Formation that lies between M_{V2} and M_{V3}.

5.1.2 Reduction to the Pole (RTP) Map

Asymmetric anomalies (caused by the non-vertical inducing field) are difficult to relate to the source bodies or geometry causing the anomalies in magnetic survey (Murphy, 2007). In order to locate the observed magnetic anomalies directly over the magnetic source bodies that caused these anomalies, the TMI grid was transformed into reduction to the pole (RTP) grid using the 2D-FFT filter in Geosoft software to facilitate the interpretation of the magnetic data set. This map of RTP sharpens the contacts between the magnetic high and low patterns and also highlighted on anomalously magnetic susceptible zones probably coming from deeper sources.

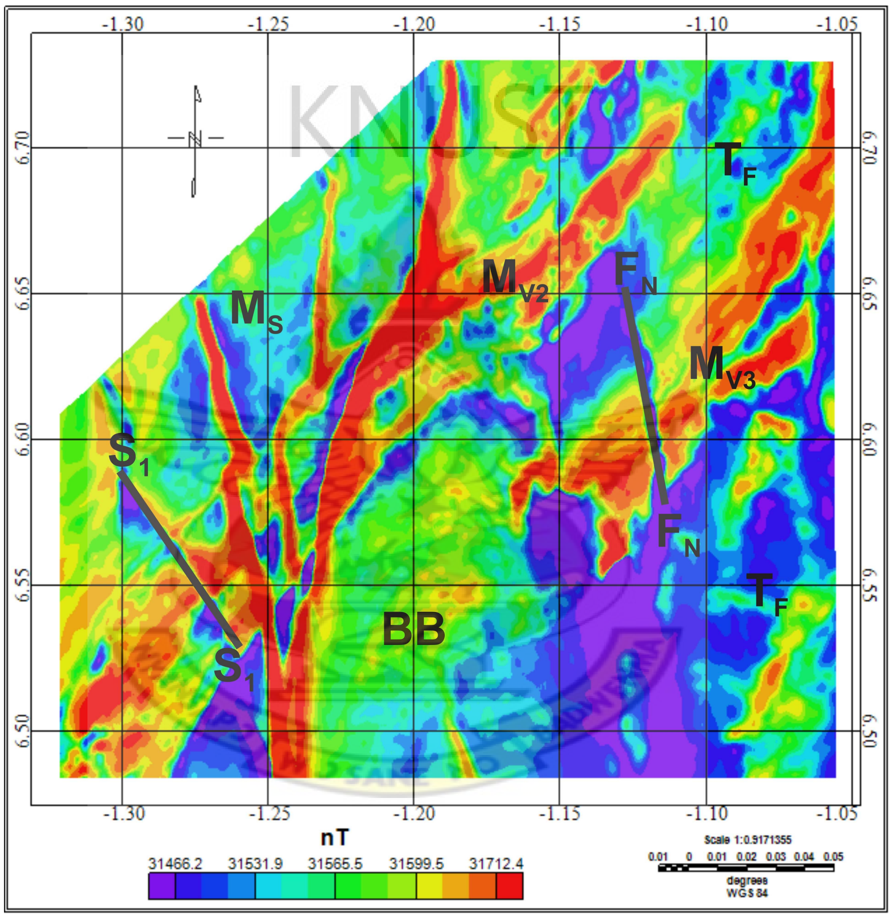

Figure 5.3: TMI grid (I = -12.34^0, D = -5.73^0) reduced to the pole.

The reduced-to-pole magnetic anomaly map (Fig. 5.3) shows that both low and high frequencies characterize the magnetic field in the area. The high frequency anomalies map magnetite-rich formation and meta-volcanoclastic rocks. A rough idea about the shape of the BB is noted in this RTP map which is dome shaped. The folding of the meta-volcanics M_{V1} and M_{V2} by the intrusive high K granitoid (BB) is well pronounced.

The structures S_1-S_1 and F_N-F_N representing faults were not clearly noticed in the TMI grid but were well exposed in the RPT grid. It is seen that the contact zone of structures and metamorphosed geological units is being delineated and will be enhanced by subsequent filtered grids.

5.1.3 Analytic Signal Grid

The Fig. 5.4 indicates three high magnetic anomalous zones (M_{V1}, M_{V2} and M_{V3}) trending in the NE-SW direction which are associated with meta-volcanics.

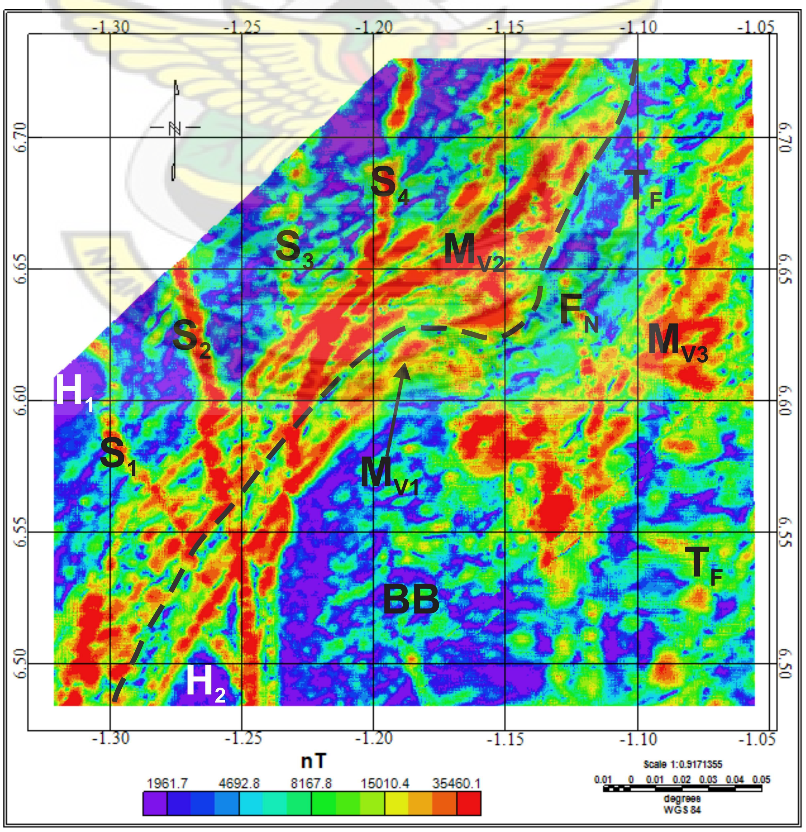

Figure 5.4: Map showing the analytical signal amplitude: Blue low and red high.

The Tarkwaian Formation (T_F), Birimian Meta-sediment (M_S) and the Banso Batholith (BB) registered a low magnetic anomaly. The thick black dotted line is a major synclinal axis. An important characteristic of the analytical signal is its independence of the direction of the magnetization of the source. The amplitude of the analytical signal is related to amplitude of magnetization.

The analytic signal amplitude is independent of the direction of the magnetization of the source and is related to the amplitude of magnetization (Nabighian, 1972; Roest and Pilkington, 1993). The most significant concentrations of mineral deposits in this area are correlated with high analytical signal amplitudes.

In the map above, it is possible to associate the gradients of the analytic signal amplitude and the known gold mineralization. Analytical maps are useful as a type of reduction to pole when applied to magnetic data collected from low magnetic latitude. The features S_1, S_2, S_3 and S_4 with high magnetic anomalies are intrusions that traverse M_S, M_{V1}, M_{V2} and the BB. Another linear feature F_N in the N-S direction cuts across the M_{V3} and the Tarkwaian Formation (T_F).

The fairly magnetic anomaly that forms the oval shape around the high potassium granitoid BB (Fig. 5.12) is probably as a result of contact metamorphism. The domed-shaped magnetic feature H_1 within the meta-sedimentary at the extreme west, represent a possible granitoid intrusion. H_2 is suggested as been part of the Banso Batholith that has been cut off by the mafic intrusions S_1, S_2 and S_3 which happens to the branches of a dike system.

5.1.4 Digitize Elevation Map (DEM)

The Fig. 5.5 is a digitized elevation map that reflects the highlands and lowlands in the study area. The lowlands are at the east and west of the highlands in the study area. The highland at the northern part of the area is partly associated with the M_S, M_{V2} and T_F (Fig. 5.4) in this region.

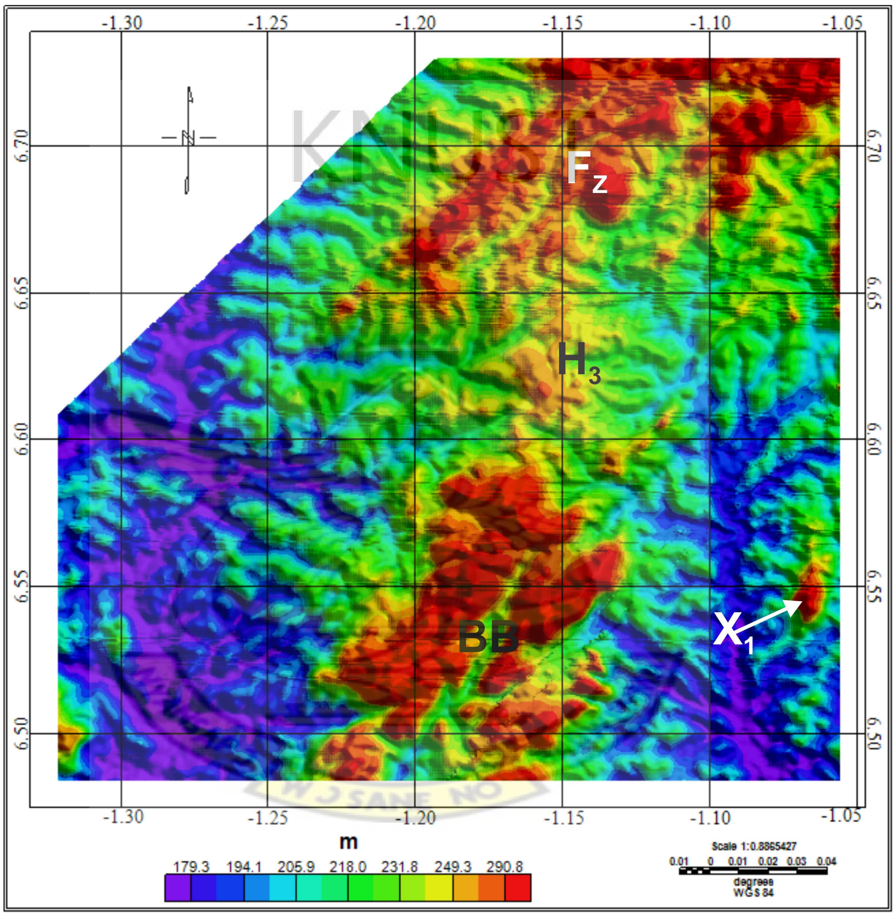

Figure 5.5: Colour shaded digitized elevation map of the study area.

There is another highland at the southern part coinciding with the region hosting the Banso Batholith (Fig. 5.1). The Tarkwaian Formation (T_F) at the east and northeast of the batholith (Fig. 5.1) occupy a lowland and highland respectively in the DEM map. Comparing Fig. 5.5 to Fig. 5.3 it is seen that the geological structures S_1, S_2 and F_N lie in a lowland. At the extreme east of the area is a high elevated geological formation X_1 which recorded a low magnetic anomaly in Fig. 5.3 and Fig 5.4.

5.1.5 First Vertical Derivative (1VD) Map

The Fig. 5.6 is a gray-scale of the first vertical derivative continued upward to 100 m displaying near surface source magnetic features that are associated with geological structures. The 1VD and upward continuation operators have helped attenuate broad, more regional anomalies and enhanced local, more subtle magnetic responses because of their sensitive to shallow magnetic source bodies and contacts.

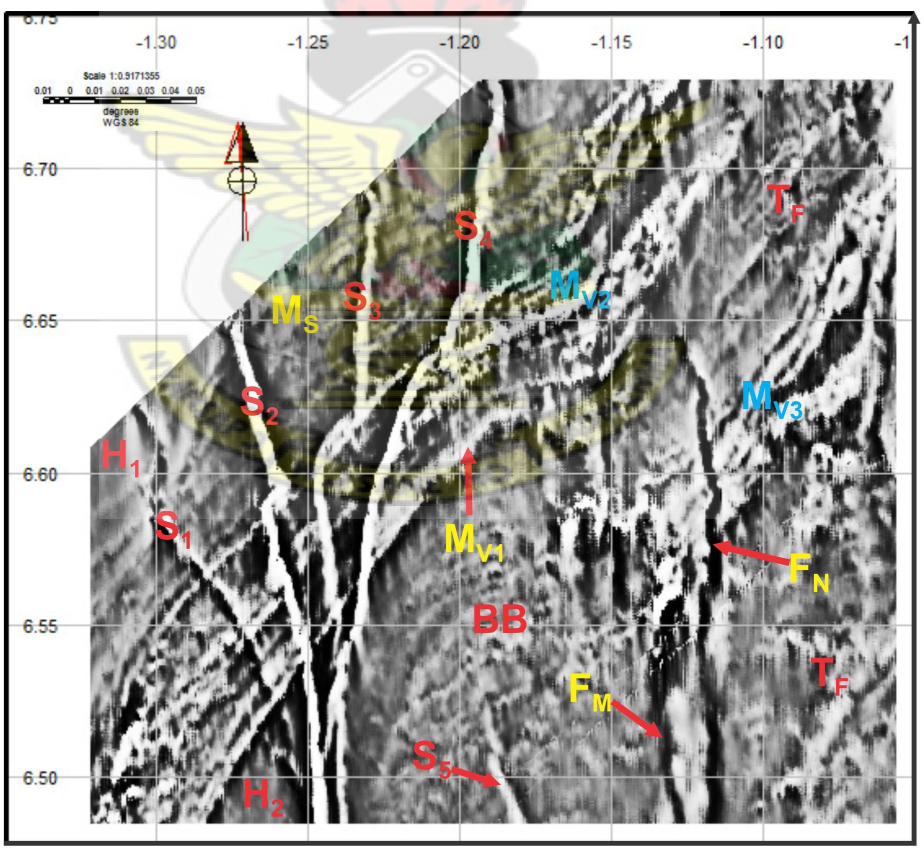

Figure 5.6: First order vertical derivative map and upward continued to 100 m in grey-scale showing magnetic structures: White is high and black is low.

The elongated folded meta-volcanic unit M_{V2} seen in the TMI and RTP maps is rather exposed in the 1VD map as a collection of faulted structures trending in the NE-SW direction (the main direction of the Birimian stru) with the boundary well defined. The high magnetic anomalous structure F_M is found to cut along the contact between BB and the Tarkwaian Formation. The granitoid intrusions BB and H_2 also have their boundaries well enhanced by the low magnetic anomaly forming an oval shape.

The area also features a major, N-S trending, late-stage dolerite dike system (Griffis et al., 2002) that cuts across the Banso Batholith and splits up into at least three structures S_2, S_3 and S_4 in Fig. 5.6 that extend through the Konongo District. The fault S_1 as well as F_N that trends N-S cutting across T_F and M_{V3} in Fig. 5.4 are enhanced in the 1VD map.

5.1.6 First Horizontal Derivative (1HD) Map

After the reduction-to-pole correction, a magnetic body is spatially more directly associated with the related magnetic response. The maximum horizontal gradient produces maximum ridges over edges of magnetic basement blocks and faults or other magnetic bodies.

In addition, the horizontal gradient highlighted linear features, related to contacts in the data set. The collections of faulted discontinuous structures M-M, which are associated with the M_{V2}, were not enhanced due to their non-linear nature but the S_1 to S_4 structures have their boundaries well enhanced.

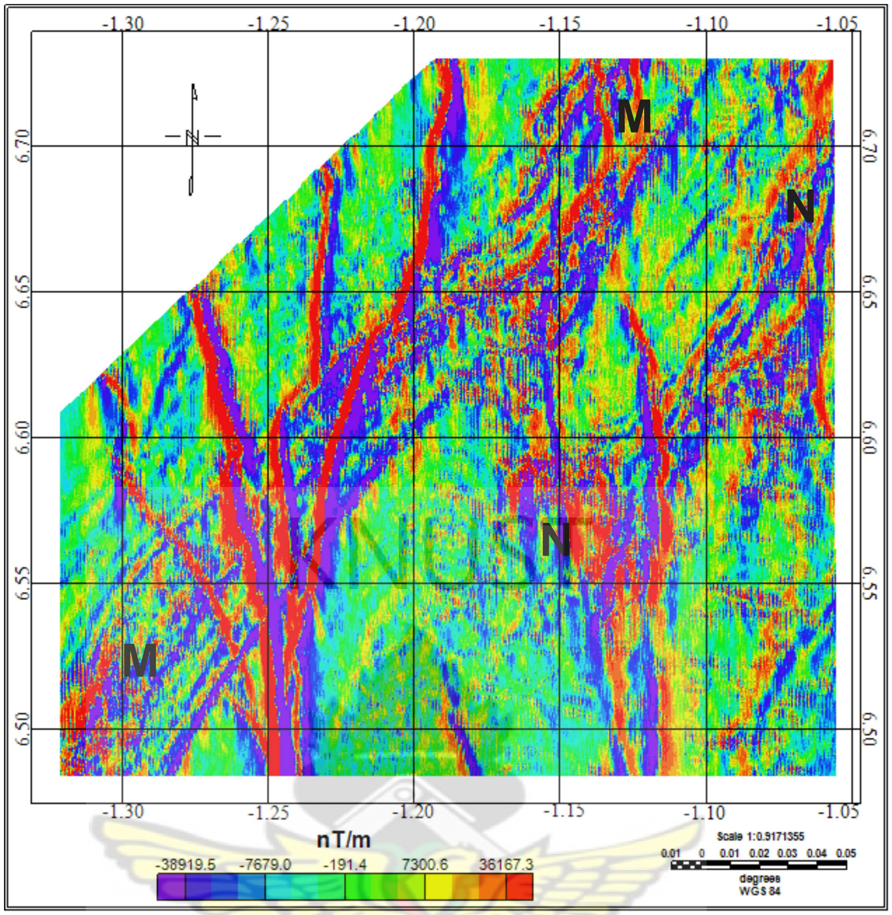

Figure 5.7: First horizontal derivative map upward continued to 100 m.

5.1.7 Magnetic Tilt Derivative (TDR) Map

The magnetic map Fig. 5.8 which is tilt derivative of the TMI map (Fig. 5.1) also helped to deduce the subtle geological boundaries of the various structures enhanced by the other filtered grids. The S_1, F_M and F_N structures seen in the analytic map (Fig. 5.4) as high magnetic anomalies are now identified in the magnetic TDR map (Fig. 5.8) as low magnetic anomalies cutting across the collection of the structures related to meta-volcanics, M_{V1}, M_{V2}, M_{V3} and the Tarkwaian Formation (T_F). The structures F_M, F_N and S_1 are noted as faults with the magnetite and pyrrhotite contents destroyed by sericitisation, biotitisation and carbonate alterations (Airo and Karell, 2001), hence, registering a low magnetic signature.

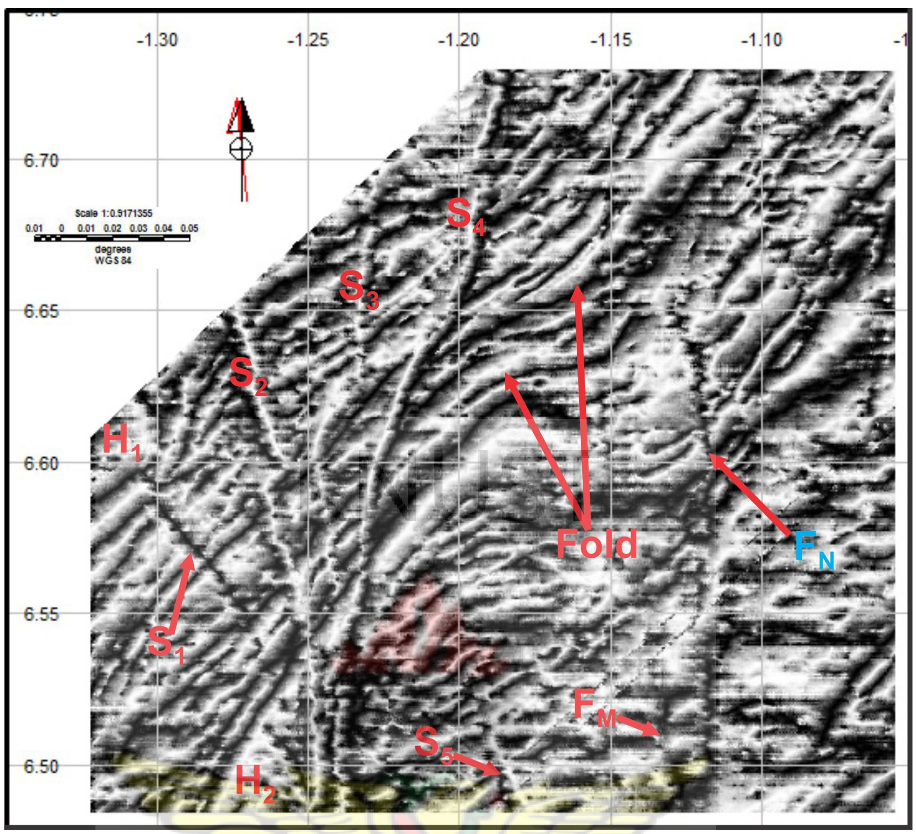

Figure 5.8: A magnetic TDR map in grey-scale.

5.1.8 Delineated Geological Structures

Interpretation of aeromagnetic (or any geophysical) data basically involves two exercises. Firstly, the behaviour of the geophysical data and the physical nature of delineated anomalies are to be ascertained. Secondly, the geological significance of the geophysical indications has to be interpreted (Murphy, 2007).

Fig. 5.9 is a representation of the delineated geological structures superimposed on the RTP map (Fig. 5.3). This map gives an idea about the time-sequence of formation of the lithological units and some geological structures in the Konongo area. At the upper right corner of Fig. 5.9, F_N which was onces a continuous structure has been traverse by M_{V2} creating F_{N1}. Also S_1, S_2, S_3 and S_4 are seen to traverse M_{V1}, M_{V2} and BB while F_N traverse M_{V3} and the Tarkwaian Formation. Thus it can be inferred that M_3 is the oldest among the meta-volcanic rocks while M_3, M_1 and BB are younger than F_N but older than S_1, S_2, S_3 and S_4. The folding and shearing of M_{V1} and M_{V3} respectively by the Banso Batholith suggests that the Banso Batholith is the youngest among the lithological units.

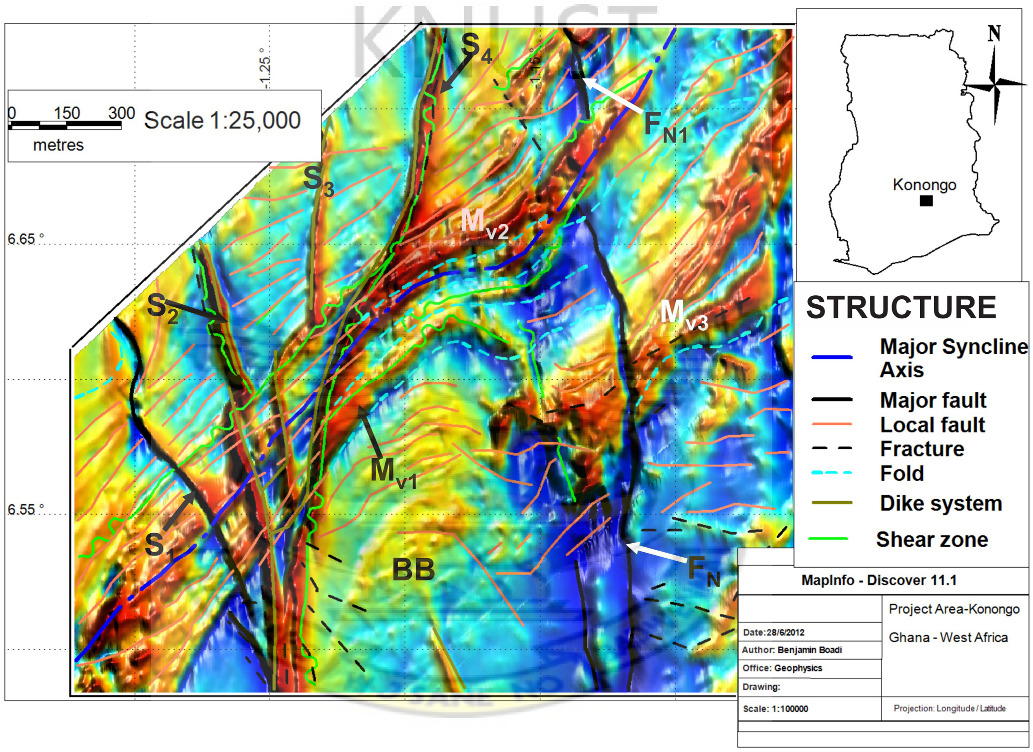

Figure 5.9: The interpreted geological structure map superimposed on the RTP data.

The interpreted magnetic structural map Fig. 5.10 is integrated information from the first vertical derivative map (Fig. 5.6), the total magnetic intensity map (Fig. 5.1) and TDR map (Fig. 5.8). Fig. 5.10 reveals enhanced structural features that include shear zones, faults, shear and fault intersections and fracture systems as magnetic anomalies that mainly trend NE-SW.

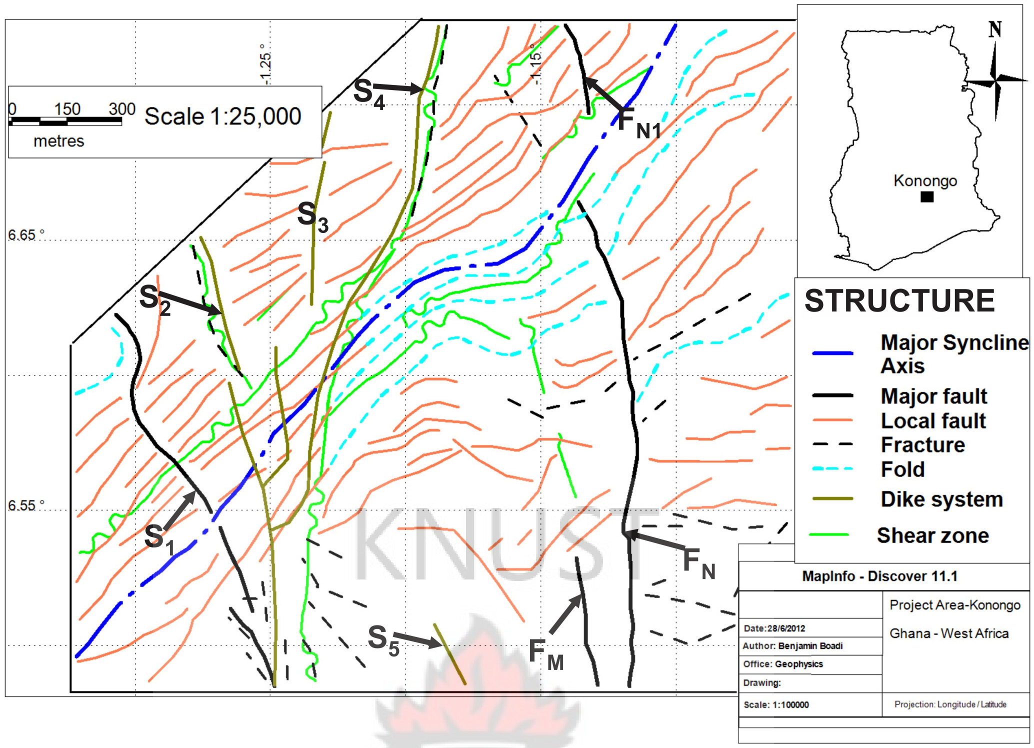

Figure 5.10: Interpreted structural map from the aeromagnetic dataset.

In the attempt to indentify the structures and geology of the area, the first step involved identifying various recognizable patterns directly from the TMI and mathematically enhanced maps of the observed data and relating them to possible physical causes relevant to the distribution of the particular property of the source. Secondly the geophysical interpretation will be properly correlated with the geological data to derive maximum benefit from the geophysical survey.

The aeromagnetic maps of the Konongo area reveal high magnetic resolution and good contrast between geological structures and their host lithologies providing information useful for structural delineation. Rock deformations such as fracturing, faulting and shearing are not uniformly distributed in their host rocks. Often these structures are associated with peculiar uncharacteristic magnetic signatures of the host rocks. Aeromagnetic data record these magnetic signatures which are used to identify these structures and their sequence of occurrence (Amenyoh et al., 2009).

Folds, linear structures such as F_N, S_1, S_4 (Fig. 5.8), shear zones (existing between contact zones of lithological units), semicircular and circular shapes such as H_1 and H_2 (Fig. 5.4) are some of the anomalous features observed from the magnetic maps. The observed linear magnetic features are interpreted as faults, fractures, joints and dikes. Some geological features such as X_1 in Fig. 5.3 were not enhanced in the magnetic data but were noted throughout the radiometric maps.

The TMI map (Fig. 5.1) regardless of the degree of magnetization, shows the skeletal system of the structures dominating in the area. Compressional deformation feature including folding of the meta-volcanic rock units M_{V1}, M_{V2} and Tarkwaian Formation (T_F) between them, trending in the NE direction, caused by the intruding Banso Batholith (BB) are seen in the central part of Fig. 5.1. A circular shaped geological unit H_3 (Fig. 5.1 and Fig. 5.4) within the Tarkwaian Formation is found to lie between M_{V1}, M_{V2} and M_{V3}.

The Fault S_1 also happens to experience some degree of folding at its upper end in the TMI, Analytic and 1VD maps. The semicircular geological body H_1 (Fig. 5.6) causing this folding is of a similar magnetic intensity as H_2 (Fig. 5.4) which is part of the Banso Batholith and can be inferred as a granitoid intruding the Paleoproterozoic meta-sedimentary unit. Folded and the sheared geological structures are noted for their ability to host hydrothermal fluids and hydrocarbons.

The structural features throughout southwestern Ghana are believed to have resulted from one major, progressive NW-SE deformational event (Eisenlohr and Hirdes, 1992) which is thus responsible for the folding of the discontinuous structures of M_{V2} and M_{V3}. The area (Fig. 5.8) also features a major, N-S trending, late-stage dolerite dike system that cuts across the Banso Batholith and splits up into at least three (3) structures (Griffis et al., 2002) that extend through the study area. The structures S_2, S_3, S_4 represent the branches of this dike system and are also considered as dikes intruding the meta-sediments M_S, Tarkwaian Formation (T_F) and meta-volcanics (M_{V1} and M_{V2}).

The deformation of S_2, S_3 and S_4 structures are of a later deformational event trending in the ENE-SWS direction. Isoclinal folding is evident within the basin meta-sediments whereas the folding of the Tarkwaian Formation to the east develops many more open structures. The transitional zone between the basin and belt units displays extensive faulting with a complicated and prolonged history of deformation and reactivation.

Faults that evolved through linkage are commonly associated with sets of splays that break off the main faults. Each splay accommodates a portion of the deformation transferred from the main faults and has its own termination point. Structures are interpreted from the aeromagnetic data where they terminate as a series breaks in smooth magnetic signature serve as marker units within the stratigraphy (Murphy, 2007). This is quite obvious and simple where there are a large number of magnetic markers striking perpendicular to the structures S_1, S_2, S_3, S_4, F_M and F_N (Fig. 5.8).

Intensively faulted and fractured zones associated with folded magnetic signatures are described as shear zone. The area records a series of NE trending shears (Fig. 5.10) which are interpreted as high angle reverse structures formed during regional NW-SE directed compression. These define the lithological pattern in the area with all units striking parallel to these structures. Several further NE structures are present including the same sheared zone that hosts the Konongo deposit to the north (Cozens, 1989).

The Fig. 5.11 is a deduced geological map from the aeromagnetic data showing the Birimian meta-sediments, meta-volcanic, the Tarkwaian formation and dolerite dike system. F_2 and F_3 are foot-walls trending in the SW direction while S_1 and S_2 are hanging walls trending in the NE direction.

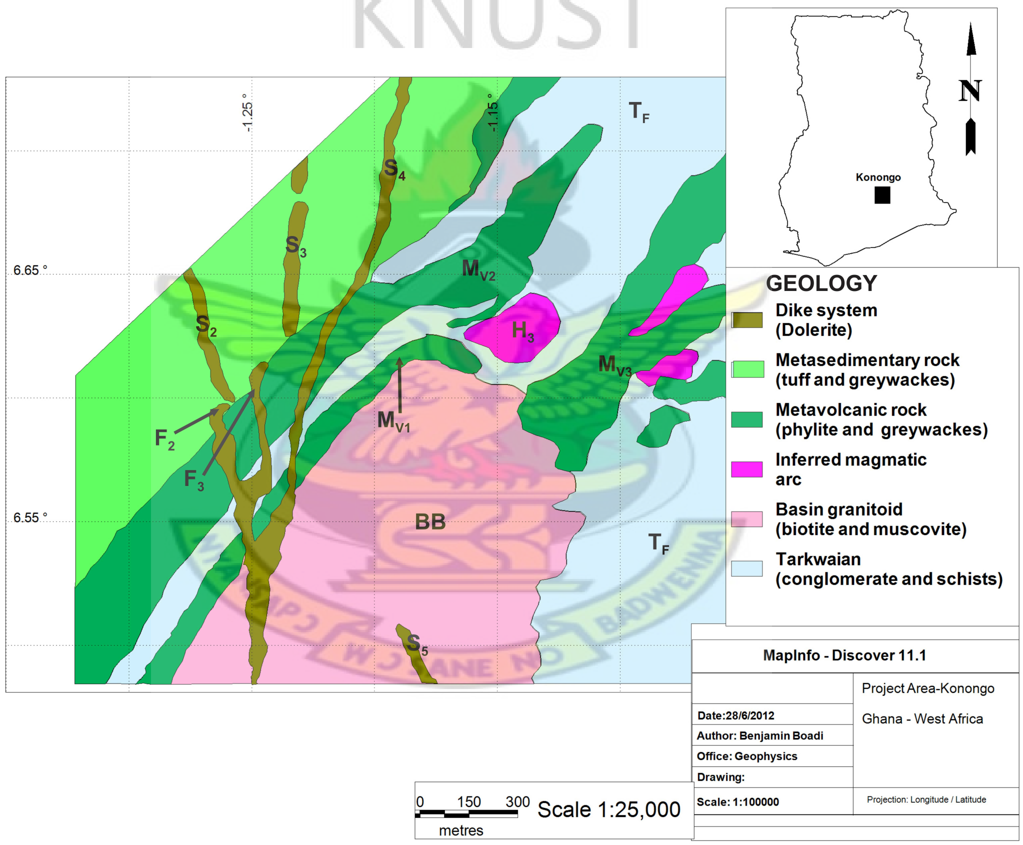

Figure 5.11: Preliminary interpreted geology from aeromagnetic data.

5.2 Interpretation of Radiometric Data

Airborne radiometric surveys are used to measure variations in the mineral composition of surface geology and to map lateral lithological changes. This method involves the measurement of naturally occurring radioactive elements that exist in rock forming minerals and soil profiles (Telford et al., 1990). These elements are uranium (U), thorium (Th) and potassium (K), which can be found as trace elements in all rocks and decay naturally giving off gamma radiation (gamma rays). These gamma rays that are emitted can be measured by a gamma ray spectrometer which determines the source element by its peak gamma ray energy. These data were used as an aid to lithological mapping by determining if a spatial correlation exists between the radiometric data and lithological rocks.

5.2.1 Potassium (K), Thorium (Th) and Uranium (U) Channels

A number of potassium anomalies are evident in the radiometric survey image Fig. 5.12. A particular strong anomaly occurs in the central-south and this coincides with the Banso Batholith (BB) which Griffis et al. (2002) described to be an intrusive high K granitoid. Potassium radiation essentially comes from K feldspar, predominantly microcline and orthoclase or micas such as muscovite and biotite which are common in felsic igneous rocks (e.g. granite) and are low in mafic rocks (e.g. basalts and andesite) but virtually absent from dunite and peridotites (Manu, 1993).

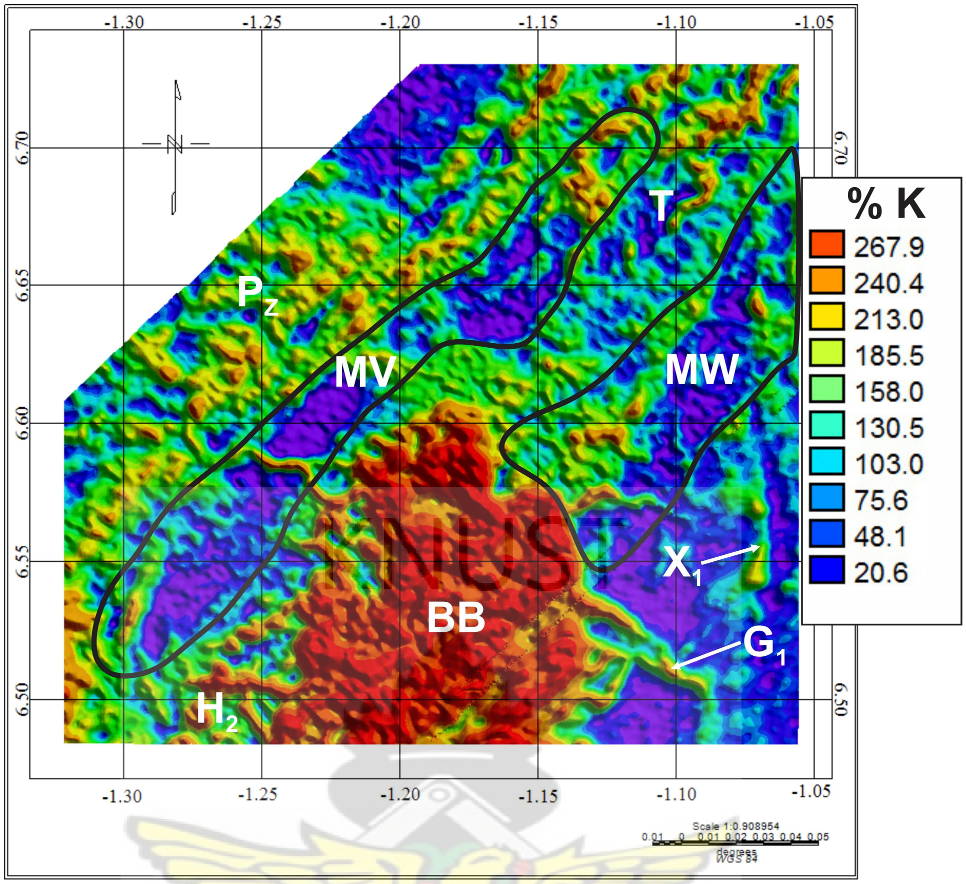

Figure 5.12: Gamma spectrometric image for potassium (K) concentration.

Comparing Fig. 5.12 to the TMI map (Fig. 5.1) the elongated high radiometric anomalous zone P_Z, hosting K concentrations linearly distributed in the NE-SW direction represent the coarse-grained meta-sediment unit M_S. The Meta-volcanic units M_{V2} and M_{V3} have low K concentration (MV and MW) but M_{V1} and the Tarkwaian formation (noted as T in Fig. 5.12) have moderate K concentration.

Anomalies in the thorium data in Fig. 5.13 helped map the boundaries of the granitoids (for H_2 and BB) and the Paleoproterozoic meta-sediments. The highest thorium concentrations are in the northern and eastern parts of the area and are associated partly with Birimian meta-sediments, meta-volcanics and the Tarkwaian Formation.

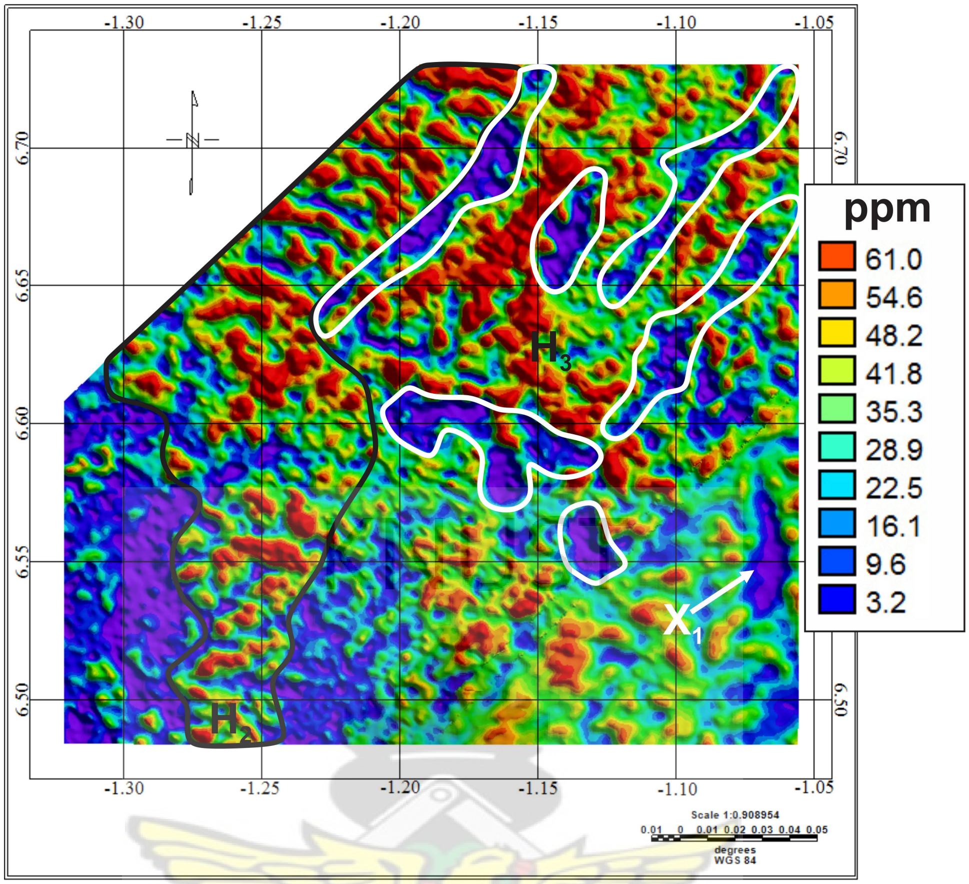

Figure 5.13: Gamma spectrometric image for thorium (Th) concentration.

The Banso granitoid registered relatively low Th concentration. Thorium is generally considered very immobile (Silva et al., 2003) thus the regions with low thorium concentration suggest Th was mobilized in hydrothermally altered systems. The high elevation features F_Z and H_3 in the DEM map (Fig. 5.5) registered high Th concentration in the northern and central part of Fig 5.12. The region marked by the black polygon registering high Th concentration is as a result of highly weathered colluvial deposits from the high elevated geological units in the DEM map.

The low Th patterns (white thick polygons in Th image (Fig. 5.12)) between the Tarkwaian Formation, meta-volcanics, granitoid and meta-sediment represent alteration patterns in the different rocks and along lithologic boundaries. Along these regions are also faults and shears (Fig. 5.8) hosting hydrothermal fluid which leach Th concentration.

Unlike the K and the Th maps, the U map could not clearly indicate distinct boundary between the Meta-sediment and Meta-volcanics. The Tarkwaian Formation, meta-sediment and meta-volcanic rocks are broadly represented by moderate U concentration (Fig. 5.14).

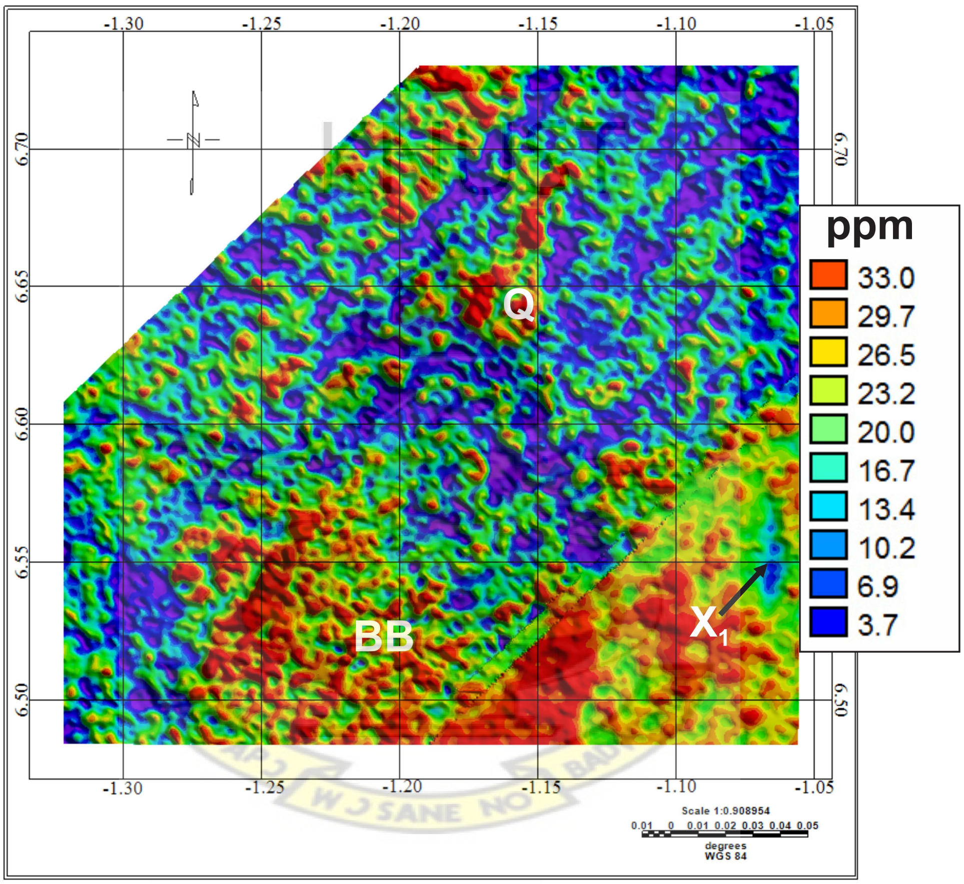

Figure 5.14: Gamma spectrometric image for uranium (U) concentration.

The uranium image shows good definition in mapping the granitoid BB and certain geological formations such as Q and X_1 which have high elevations in the DEM map (Fig. 5.5). The feature Q which is associated with F_Z in the DEM map registered high Th and U concentration but had low K concentration. The south-east of Fig. 5.14 (which lies in a lowland in Fig. 5.5), the region north-west of Q (recording high Th) and portions of the Banso Batholith registered high U concentration. The areas marked by white polygons in Fig. 5.13 also recorded low U concentration.

The image shows short wavelength anomalies corresponding to noise caused by the variations in atmospheric radon concentrations during the course of the survey resulting in significant streaking in the image. This is a typical feature found in uranium images (Minty, 1996), in spite of the micro-levelling.

5.2.2 Ratio Maps of K/U, K/Th and Th/U

Histogram stretching and band rationing of the channels were used to maximize contrast and highlight subtle features in the data. The Th channel and ratio channels (Th/K and Th/U) were used to assess the degree to which the source materials of regolith are weathered or leached since K response is associated with easily weathered minerals, whereas Th and U are typically associated with residual clay, oxides and accessory minerals (Wilford et al., 1997).

Fig. 5.15 represents Th/K concentrations which map some lithologic contrast and enhanced alteration signatures. The increase in K content and decrease in Th/K ratio observed for the mafic meta-volcanic rocks (MV and MW) is indicative of hydrothermal alterations. This is because mafic volcanic rocks generally lack K-bearing minerals and K enrichments are not accompanied by Th during hydrothermal alteration processes (Dickson and Scott, 1997). This information led to the detection of hydrothermal alteration zones within the area (Fig. 5.19). Generally, only K and other metal constituents are added to the host rock by hydrothermal solutions, and it is easily observed in mafic units or along lithologic contacts where the hydrothermal alteration is intensive.

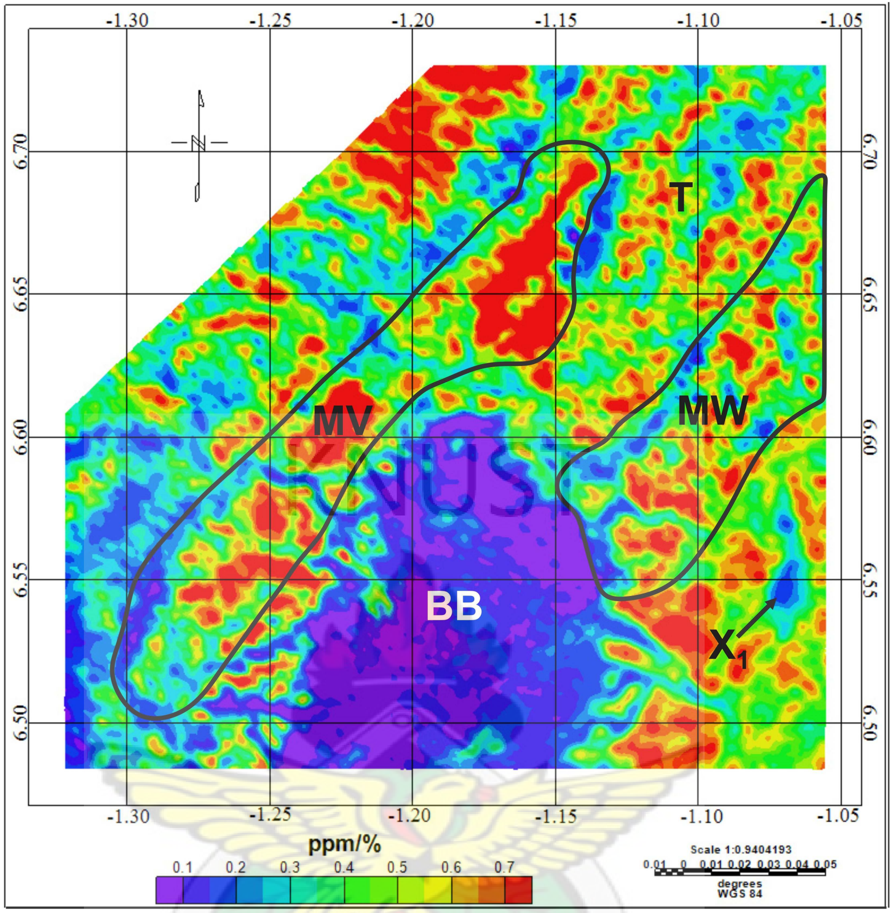

Figure 5.15: A ratio map of thorium and potassium - Th/K.

The U/K (reverse of K/U) ratio was used to determine areas where concentrations of uranium are relatively high. Some of the uranium anomalies are related to zones of gold mineralization mapped in contact with and within the volcanoclastics. The Meta-volcanic lithologic units (M_{V2}, M_{V3} noted as MV and MW respectively in Fig. 5.15) and the Tarkwaian Formation (T_F) at the bottom right of Fig. 5.4 recorded high U concentration (but low K) and the Banso Batholith still revealled it high K concentration (low U).

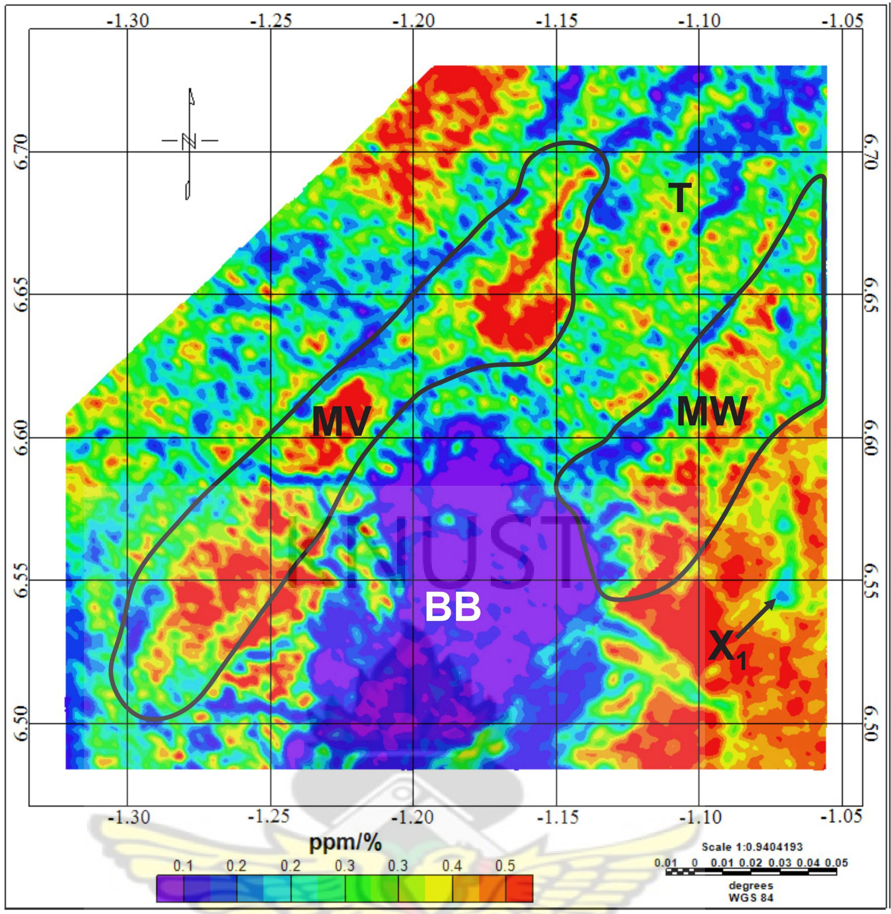

Figure 5.16: A ratio map of uranium and potassium - U/K.

High K/Th (Fig. 5.15) and low K/U (Fig. 5.16) over potassic rocks in the study area are likely to be associated with slightly weathered and highly leached soils respectively.

The ratio images of Th/U (Fig. 5.17) shows that two-thirds (2/3) of the area is dominated by high Th concentration which corresponds to high elevations in the DEM map (Fig. 5.5). The Th/U map highlights Th alteration zone, reflecting coincidentally increased Th and lowered U or K. The Tarkwaian Formation (at the bottom right of Fig. 5.4) which registered high U concentration in Fig. 5.16 is seen to record low Th concentration in Fig. 5. 16.

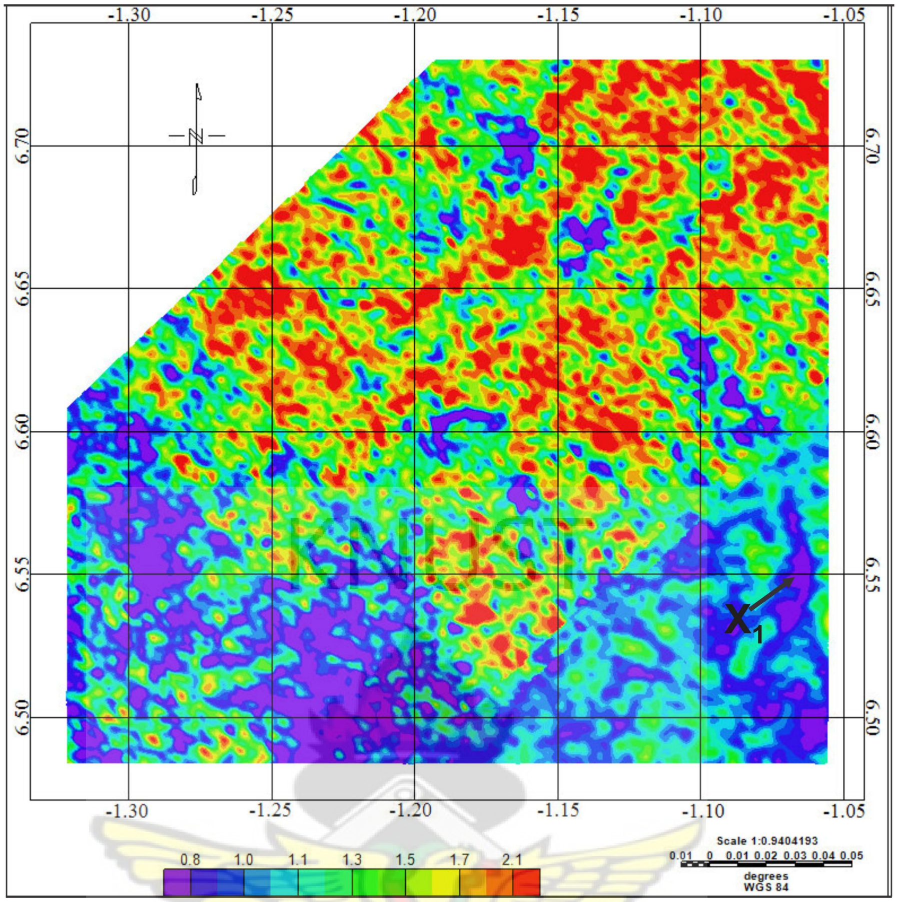

Figure 5.17: A ratio map of thorium and uranium - Th/U.

5.2.3 Composite Images (Ternary map)

The Ternary image Fig. 5.18 comprises of colours generated from the relative intensities of the three components and represents subtle variations in the ratios of the three bands. The mafic and ultramafic, as well as magnetite-rich formations are in black, the granitoids rocks and meta-sediments with high potassium has a magenta colour. Potassium was assigned to red, uranium to blue and thorium to green. The composite image presents strong spatial correlations with the known geologic units. The mafic, ultramafic and the probable Paleoproterozoic magnetite rich formation appear darker than the surrounding units, indicating lower concentrations in K, U, and Th.

These dark regions can be attributed to the low Th pattern marked white polygon in the Th image (Fig. 5.13). The white areas in the ternary image are indication of high concentration of potassium, thorium and uranium. The magenta shows areas of high K and U but low Th concentrations whilst the yellow indicates areas of high K and Th but low U concentrations.

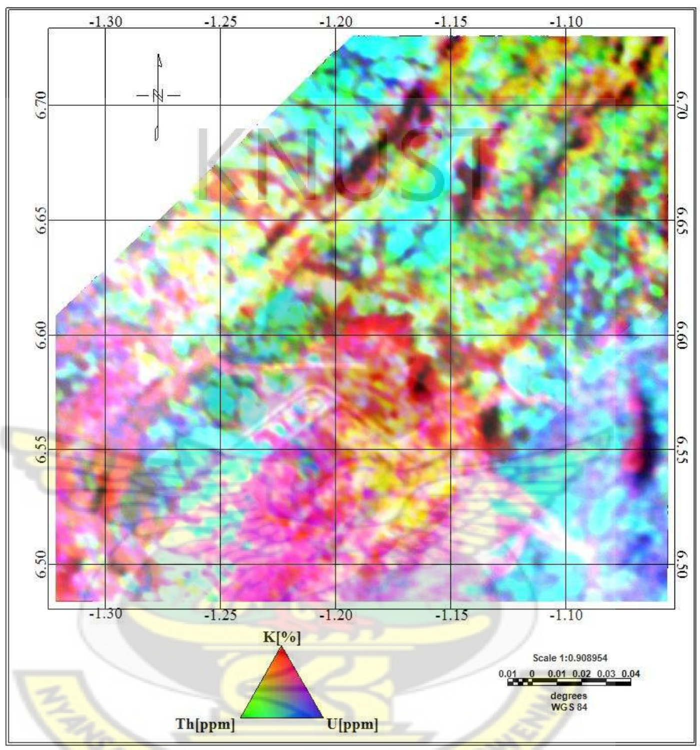

Figure 5.18: Composite Image (RGB=KThU) of the Konongo Area.

The ternary map shows high thorium concentration in the north-east while the Banso Batholith and the south-western corner of the image record high K. The dark regions trending in NE direction are linked with the structures of the meta-volcanic geological units M_{V1} and M_{V3} in the region. The X_1 formation has its boundary enhanced and the constituent radiometric elements are K and U.

Hoover and Pierce (1990) showed that aerial gamma-ray surveying signatures of Au deposits were variable with K being the most reliable pathfinder. Even where Au is within quartz veins, hydrothermal alteration of host rocks can give detectable haloes. This deduction seems valid in the study area, where potassium is associated with many of the favourable host rock structures. Although there is not a particular radiometric signature for gold deposits, studies summarized by Hoover and Pierce (1990) show that changes in the all three radioelements can occur and may be detected in aerial gamma-ray surveys.

5.2.4 The Composite Lithological Map from the Radiometric Datasets

Potassium (K), uranium (U) and thorium (Th) are the three (3) most abundant, naturally occurring radioactive elements. Potassium is a major constituent of most rocks and is a common alteration element in certain types of mineral deposits. Uranium and thorium are present in trace amounts, as mobile and relatively immobile elements, respectively (Dickson and Scott, 1997). As the concentrations of these different radioactive elements vary between different rock types, the information provided by a gamma-ray spectrometer aids in mapping the rocks.

The most significant radiometric response in both the potassium and uranium maps (Fig. 5.12 and Fig. 5.14) recording high concentration of K and U respectively is associated with the Banso batholith within the region. This strong correlation is based on the fact that the intruded Cape Coast granitoid complex (Banso batholith) (Kesse, 1985) is well foliated, often magmatic, potash-rich (have high K concentration) granitoid which come in the form of muscovite, biotite, granite and granodiorite, porphyroblastic biotite gneiss, aplite and pegmatite.

The Basin type granitoid complex (Banso Batholith) is quoted to be enriched in such lithophile elements as Li, Be, Sn and Th (Kesse, 1985). This explains the high Th print highlighting the shape of the Banso Batholith (BB and H_2) at the bottom of Fig. 5.13 as indicated by the magnetic data. Despite extensive surveys carried out by Ostle and Hale and by Uranerzbetgbau-Gmbh, no anomaly was found within the Birimian rocks (Kesse, 1985) but the radiometric technique used in this survey has been able to trace some amount of uranium concentration within the meta-sediments and meta-volcanics (Birimian groups).

In Fig. 5.14 the findings of Kesse (1985) are quite appreciated though after a long period of denudation (three decades) the region hosting the Birimian meta-volcanic units now have some small amount of disseminated U. The high U concentration Q of Fig. 5.14 is found in the upper limb of the magnetic anomaly M_{V2} which corresponds to a meta-volcanic unit. This meta-volcanic unit is more of Th enriched than U with respect to the ratio map of Th/U (Fig. 5.17)

The Tarkwaian Formation was identified by the significant Th signature at the north-east and south-east of Fig. 5.14. The meta-volcanic rocks (M_{V1}, M_{V2} and M_{V3} in Fig. 5.1) have high magnetic anomalies, but possess very low K and Th concentrations and the K normalized map of Fig. 5.12 (low K concentration) showed their distinct boundaries. The meta-sedimentary unit M_S did not show unique radiometric signature. However, it displayed distinct radiometric boundaries that correspond much well with magnetized lineaments, (Fig. 5.13). The low Th patterns (white thick polygons in Th image, Fig. 5.13) between the Tarkwaian Formation, Meta-volcanics, Granitoid and Meta-sediment correspond with the alteration patterns along lithologic boundaries and with the Tarkwaian Formation. The areas which reflect mobilization of immobile Th concentration also indicated hydrothermally altered zones.

Silva et al. (2003) made some remarks, indicating that radiometric data is an excellent tool which helped in mapping and tracing of individual lithological units in areas of outcrop. The mafic, ultramafic and Paleoproterozoic units are distinctive in potassium, total count (composite map of K, Th and U) and RBG maps, because of their low radiometric signature (Fig. 5.18). The granites and dacitic rocks have a high total count radiometric response, appearing as white or blue (high uranium) in the ternary image (Fig. 5.18).

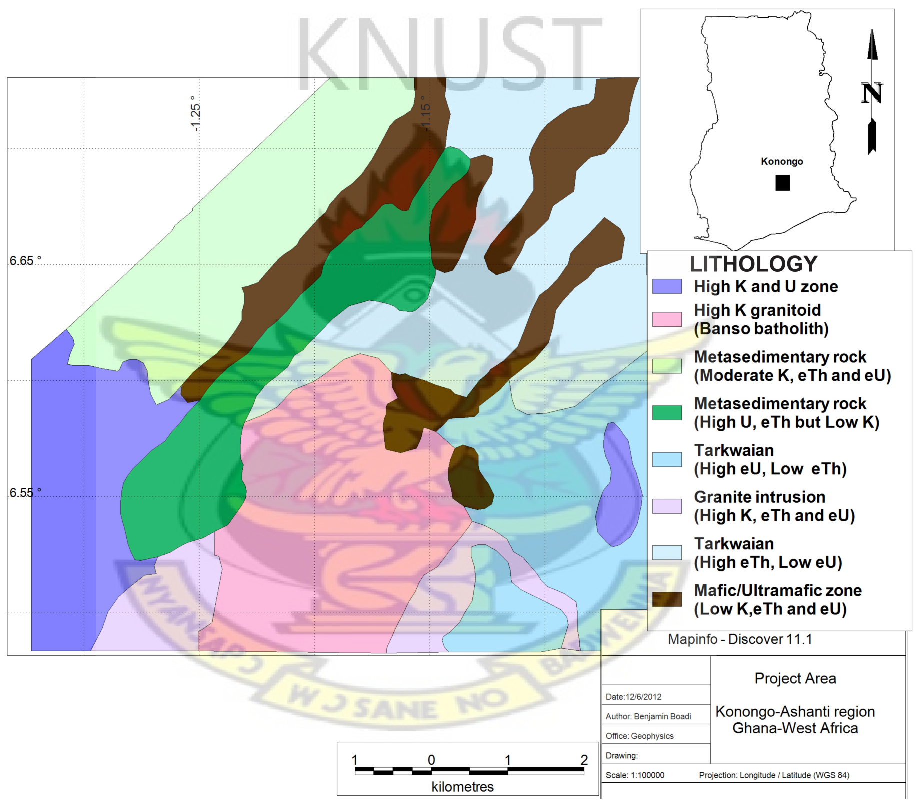

Figure 5.19: Preliminary interpreted geology from airborne radiometric data.

The gamma-ray spectrometric response indicated in the ternary image can be classified as follows: Red (K): regions associated with exposed granitic bedrock. Green (Th): various ferruginous materials at the surface. Blue (U): calcrete, calcareous sediments and soils. Black to brown: (Low in K, Th and U): dry insitu soil and exposed bedrock. These areas correspond to greenstones and some sand plains. White to yellowish (High K, Th, and U): geomorphic active areas with exposed weathered granite and sediments derived from granite.

The geological features X_1 whose radiometric signature is a combination of U and K as observed in the radiometric data (ternary and ratio maps) though a high elevation in Fig. 5.5 is not enhanced in the magnetic data (Fig. 5.1, Fig. 5.3 and Fig. 5.4).

5.3 Relating Geophysical Datasets to Geology

Geochemical properties associated with mining and mineral processing in the Konongo area have resulted in elevated concentrations of ^{238}U and ^{232}Th. Even though the concentrations of these radionuclides are widely distributed, the levels have been found to depend on the local geological conditions, and as a result vary from place to place. The specific levels in soil are related to the types of rock from which the soil originates.

5.3.1 Deformation and Geological Structures

Geological structures delineated from the airborne radiometric and magnetic datasets of the study area include sheared zones, faults, fractures, folds, dikes and lithological boundaries. In spite of the intense weathering of the volcanic belt in the study area, the sequence of deformation is well preserved in these geological structures and the geometry of the granitoid complexes. Evidence from the datasets especially the magnetic data shows that the structures were emplaced as a result of multiple deformations.

Structures in the area are certainly complex and feature tightly folded and faulted bands of

Birimian series and Tarkwaian Formation; the trends of the major faults as well as the fold planes, strike to the NE and dip steeply to the NW. The area also features a major, N-S trending, late-stage dolerite dike system that cuts across the Banso Batholith and splits up into at least three branches that extend through the Konongo District (Griffis et al., 2002). These splay of dikes are noted as S_2, S_3 and S_4 which in the 1VD map and Fig. 5.8 creating the small granitoid H_2 which was once part of the Banso Batholith.

A variety of mafic intrusives occur in most of the volcanic belts of Ghana but they are particularly abundant in the Ashanti Belt and to a lesser degree in the Sefwi Belt. To date, very little attention has been paid to these intrusions and they are generally grouped under a common label. (Griffis et al., 2002) noted that within areas dominated by mafic flows, there are abundant sills and feeder dikes with a common affinity to the tholeiitic basalts.

In a study of airborne geophysical data in the southern Ashanti Belt, Perrouty et al. (2009) suggest the presence of five (5) deformation events, corresponding to the Eburnean Orogeny and associated with magmatism between 2200 and 2000 Ma. The first phase of shortening (D_1), prior to the deposition of the Tarkwaian Formation, is followed by the main tectonic sequence (D_2-D_3), at around 2.1 Ga, characterized by large folds oriented NE-SW in the Birimian and in the Tarkwaian formation. After D_3, two other deformation events occurred: D_4 with sub-horizontal cleavage and recumbent folds and then, D_5 with a NE-SW shortening. Allen (2011) suggested gold mineralization and associated sulphides could be correlated with D_1, D_2 and D_3 deformations.

From the interpreted composite structural map (Fig. 5.10) three episodes of deformation D_1-NE, D_2-NNW and D_3-NNE were observed. The early deformational event D_1 produced sets of NE-SW striking local and regional faults and fractures. This is represented by a weakly developed bedding parallel cleavage as well as by minor folds related to early northwest-southeast compression, and thrust faulting in the meta-sedimentary and meta-volcanic units. D_2 deformational event produced mainly NNW-SSE and NW-SE faults and fractures some of which intersected the earlier D_1 structures. The major thrust faults (black lines) in Fig. 5.10 are attributed to a second phase of deformation (D_2) that formed gently plunging, tight to isoclinal, doubly plunging folds and a second cleavage. At the northern and the eastern parts of the study area D_1/D_2 intersections are observed. The D_3 event produced NNE-SSW set of faults and fractures produced by splay of dikes (S_2, S_3, and S_4) which are more associated with the Banso Batholith, and reactivated some D_1 and D_2 faults and fractures which are observed in the locality of S_5. D_3 deformation was partitioned into local strain domains, but it did not substantially modify the gross structural architecture of the Birimian Supergroup.

The Fig. 5.20 is a Rose Diagram representation of the regional strike of the delineated lineament from aeromagnetic data by using a polar plot where the distance from the center of the plot is proportional to the sum of the line lengths in that orientation.

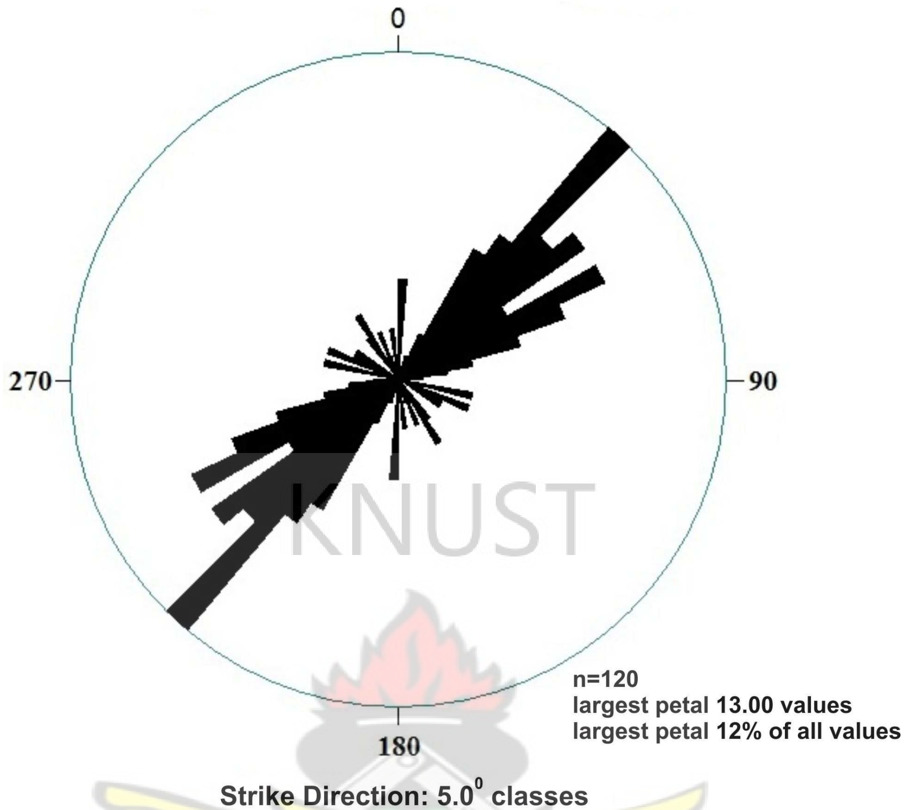

Figure 5.20: Equal area projection rose diagram for lineaments delineated from aeromagnetic maps showing frequency of observed faults strike direction, in 5^0 classes.

Rose (azimuth-frequency) diagram of the lineaments delineated on the imagery shows trends in the NE-SW, NNE-SSW, E-W, NNW-SSE and N-S directions. According to Griffis et al. (2002), the structure in the area is certainly complex and features tightly folded and faulted bands of Birimian and Tarkwaian units; the trends of the major faults as well as the fold planes, strike to the NE and dip steeply to the NW . Therefore the rose petals in the NE-SW and NNE-SSW represent the main strike directions in the Birimian formation.

The Fig. 5.20 indicates that out of 120 azimuths values plotted 12% represented the largest petal which strike between 40^0-50^0 (NE-SW) which correspond to the D_1 structures. About 60% of the total azimuth values range between 30^0 and 70^0 (NE and NNE) strike which represents the regional strike of the lineaments within the Birimian supergroup. (Griffis et al., 2002) and corresponding to the D_1 and D_2 structures. A little over 8% of the azimuths have values approximately at 40^0 and almost 20% have strike values between 100^0 and 180^0 (NW-SE).

The area is dominated by a series of NE trending shears (green lines in Fig. 5.10) which are interpreted as high angle fault structures formed during regional NW-SE compression. These define the lithological pattern in the area with all units striking parallel to these structures. However, there are a few N-S trending sheared zones in the area. Several further NE structures are present including the same shear zone that hosts the Konongo deposit to the north and the main syncline (blue line in Fig. 5.10) in the centre of the area is parallel to these features.

The mafic intrusions appear to be related to fairly late-stage dilational tectonics associated with regional transgressive shear systems that produced narrow basins filled with Tarkwaian molassic sediments (Strogen, 1991; Ledru et al., 1994). The dilational zones within the complex shear systems probably tapped deep-seated zones of mantle-derived mafic magma (Griffis et al., 2002).

More recent work (Kiessling, 1997) which may well apply to most of the region, confirms that the Tarkwaian Formation/Birimian contacts are almost invariably sheared. A higher degree of shearing and faulting have caused the 'breaking' and shifting of the limbs of S_2 and S_3 dikes towards NE direction at the meta-sedimentary and meta-volcanic contact (Fig. 5.22). The high displacement of S_3 compared to that of S_2 is an indication of high level of shearing within the region (unlike vertical shear zone adjacent to the S_2 dike) thus developing a foot-wall (F_2 and F_3 in the SW direction) and hanging-wall (S_2 and S_3 in the NE direction) environment (Fig. 5.11). S_4 is more sheared in the NE direction than faulted due to a shear zone traverse along the upper limb in the NNE direction thus preserving the linear nature.

5.3.2 Alteration

The Konongo area is situated in the Ashanti Gold Belt, which hosts the world class Obuasi Gold Deposit, operated by Anglogold Ashanti Limited, and the Prestea/Bogosu deposits which are currently being mined by Golden Star Resources Limited. Both the Obuasi and Prestea/Bogosu deposits are similar in terms of geological setting and mineralization styles to the deposits found within the Konongo District (Griffis et al., 2002). The gold ores which are localized within the Ashanti structural belt are suggested to be a conduit for deep-seated fluids during uplift and dilatancy. Evidence of alteration that preceded gold mineralization is best preserved in spatially associated altered mafic dikes and alteration of country rocks occurred under rock-dominant, greenschist facies conditions (Mumin et al., 1996). Tay and Momade (2009) believed that the ore-bodies together with the ore constituents represent an end-product of a through-going magmatic hydrothermal solutions, which originated from a sub-apexing granitic pluton at depth.

Changes that occurred in rocks after their formation (alterations) may be due to metamorphism, post-metamorphic structural deformation or low temperature chemical reactions (weathering) (Amenyoh et al., 2009). According to Leube et al. (1990) and Milesi et al. (1992) the Birimian mineralization is associated with events that promoted rock alterations. Studies in some gold belts in Ghana (e.g. Ashanti belt) have shown that metamorphism, post-metamorphic structural deformation and hydrothermal activities are events related to gold mineralization in the Birimian (Manu, 1993).

Most Birimian metamorphic rock alterations are associated with hydrothermal activities. Hydrothermal activities result from the actions of hot aqueous solutions (hydrothermal solutions) on rocks that leave footprints which are often targets for mineral exploration programmes. Hydrothermal solutions are capable of dissolving and transporting wide range of metals and salts and consequently play important role in ore deposition processes (Boamah, 1993; Manu, 1993). Usually hydrothermal solutions assess conduits in rocks where it transports its loads and deposited them as ore whenever the physio chemical conditions for ore deposit formation are favoured. The sources of the hydrothermal fluid could be magmatic, marine, connate metamorphic or meteoric water or combination of any of these (Evans, 1993).

5.3.3 Effects of Metamorphism and Hydrothermal Alteration

Pervasive alteration have destroyed the primary textures of most rock types at the study area and the effects is clearly obvious in both datasets (magnetic and radiometric), but particularly in the radiometric dataset. The decrease in K content and increase in Th (Fig. 5.12 and Fig. 5.15 respectively) indicated as M_V, observed for the meta-volcanic rock is indicative of hydrothermal alterations. According to Griffis et al. (2002), mafic volcanic rocks generally lack K-bearing minerals and K enrichments are not accompanied by Th during hydrothermal alteration processes. Generally, only K and other metal constituents are added to the host rock by hydrothermal solutions, and it is easily observed in mafic units or along lithologic contacts (such as the dark regions in the ternary map) where the hydrothermal alteration is intensive.

In the magnetic data such as the TMI and Analytic maps, the contacts between the meta-volcanic rock (M_{V2}) and the meta-sedimentary rock (M_S) are bounded by shear zones, faults and fractures high magnetic anomalies (Fig. 5.1 and Fig. 5.4). The intensity of these magnetic anomalous features including the sheared contacts, declined swiftly from the meta-volcanic rocks into the meta-sedimentary rocks. This is due to the hydrothermal activities that accompanied the rock deformations and metamorphism especially within brittle shear zones. The incursion of hydrothermal fluid through faults, fractures and rock contacts as indicated by cause rock alteration. Rocks alterations which are normally initiated along zones of rock weakness may or may not be mineralized but often coincide with economic mineral deposits in metallogenic provinces.

The Fig. 5.21 has some allocated regions which are interpreted as alteration zones from the airborne magnetic and radiometric datasets. The altered region marked X_2 which is associated with the Banso Batholith has high potassium and thorium concentration and the regions G_1, G_2 and G_3 mark areas with high K, Th and U concentration. High K and Th concentration but low U is mark by X_1.

The ternary map (Fig. 5.18) reflects NE-SW trending dark region at the extreme northeast and at the contact zone between the Banso batholith and meta-volcanics M_{V1} and M_{V3}. Comparing these regions to Fig. 5.12 and Fig. 5.13, areas of low thorium and potassium concentration were identified respectively. These regions correspond to the hydrothermal altered zones A_1, A_2, A_3 and A_4 in Fig. 5.21. Thorium is generally considered very immobile. Silva et al. (2003) admits Ostrovskiy (1975), refers to a decrease in Th and an increase in K for the alteration environment in variety of ore deposits which suggest that Th was mobilized in hydrothermally altered systems.

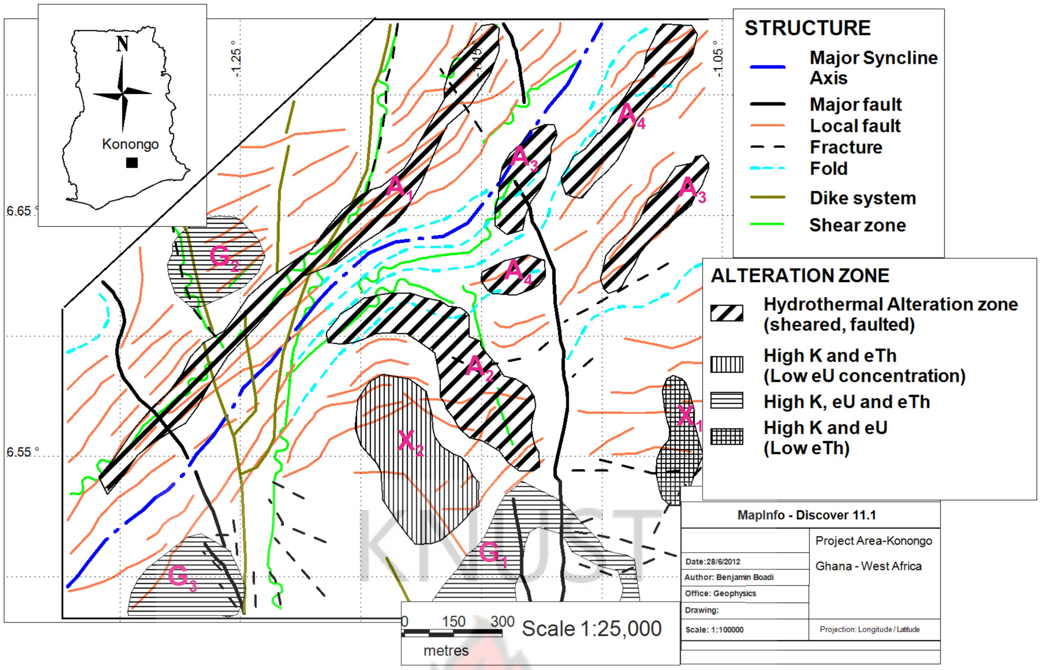

Figure 5.21: Potential alteration zones deduced from the aeromagnetic and radiometric dataset.

The dark regions indicating lower concentration of all three radiometric elements which Silva et al. (2003) indicate are associated with some mafic and ultramafic geological units also coincide with low anomalous magnetic zones of the TMI map (Fig. 5.1). These regions mark the contact zones between the meta-volcanic and meta-sedimentary; meta-volcanic and Tarkwaian Formation; granite batholith and Tarkwaian meta-volcanic. Hydrothermal activities that accompanied the rock deformations and metamorphism thus decreasing magnetization especially within brittle shear zones could possibly be responsible for this observation. High total count radiometric response appearing as white in the ternary image can be attributed to granites (Silva et al., 2003). An evidence of this is the identification of dacitic rocks that were mapped as the Ribeirão Vermelho Formation by geologists of the Rio das Velhas' team (Silva et al., 2003). This formation consists of piroclastic dacitic tuffs and agglomerate horizons with minor lava intercalation.

Graphite, mica, and euhedral to anhedral disseminated Fe sulphides observed in the host rocks in the study area (Cozens, 1989) are interpreted to be hydrothermal alteration products, potentially related to gold mineralization. Evidence of alteration that preceded gold mineralization is best preserved in spatially associated altered mafic dikes S_2, S_3, and S_4 (Fig. 5.4). The isotopic composition of the altered mafic dikes is suggested to be influenced by interaction with fluids generated from Birimian greenschist facies meta-sedimentary rocks (Mumin et al., 1996). Magnetic surveys have identified high magnetic contrast between rock bodies along the contact zone, interpreted as a potential pathway for fluid migration and mineralization.

According to Airo and Karell (2001), sericitisation, biotitisation and carbonate alterations are some processes that tend to destroy magnetite and pyrrhotite in rock alterations. Brabham (1998) made mention that the type of alteration varies in response to the nature of the host rock; abundant silicification and sericite along with widespread pyrite and subordinate pyrrhotite is characteristic of siliclastic host rocks (Banket quartzite).

Sericitic alteration (along with abundant pyrrhotite and minor pyrite) is more conspicuous in the phyllites and the metadolerites feature sericite, carbonate, pyrrhotite and subordinate pyrite. Tourmaline is an accessory mineral in most assemblages, and can be dominant in some; it is also very abundant as a metamorphic mineral in some of the fine-grained meta-sediments (Griffis et al., 2002). The association of this process with the Birimian gold mineralization leads to the destruction of magnetic minerals along the fault zones thereby creating high magnetic contrast between these zones and the host rocks.

The effect of metamorphism and hydrothermal alterations on magnetic properties and radiometric elements (K, Th and U) concentration generally depends on the metamorphic grade, the mineral composition of the host rocks as well as the content of the hydrothermal fluid (Clark, 1997). Understanding the fundamentals effects of rocks alterations is invariably important to the production of a reliable geological and hydrothermal alteration maps and the delineation of geological structures which are sensitive tools that aid the prediction of potential ore zones from airborne geophysical datasets for exploration (Amenyoh et al., 2009).

5.3.4 Mineralization and Mineralization Potentials

In order to predict favourable locations for possible blind ore deposits in the study area, both structural and alteration patterns were taken into consideration. High structural connectivity and areas of intensive alterations reflected as low magnetic anomalous and high K concentration were considered particularly, where the two alteration types coincide and also marked by faults, fault intersections, fractures and shear zones. The features marked A_1, A_2, A_3 and A_4 (Fig. 5.22) are areas with high potential for gold mineralization.

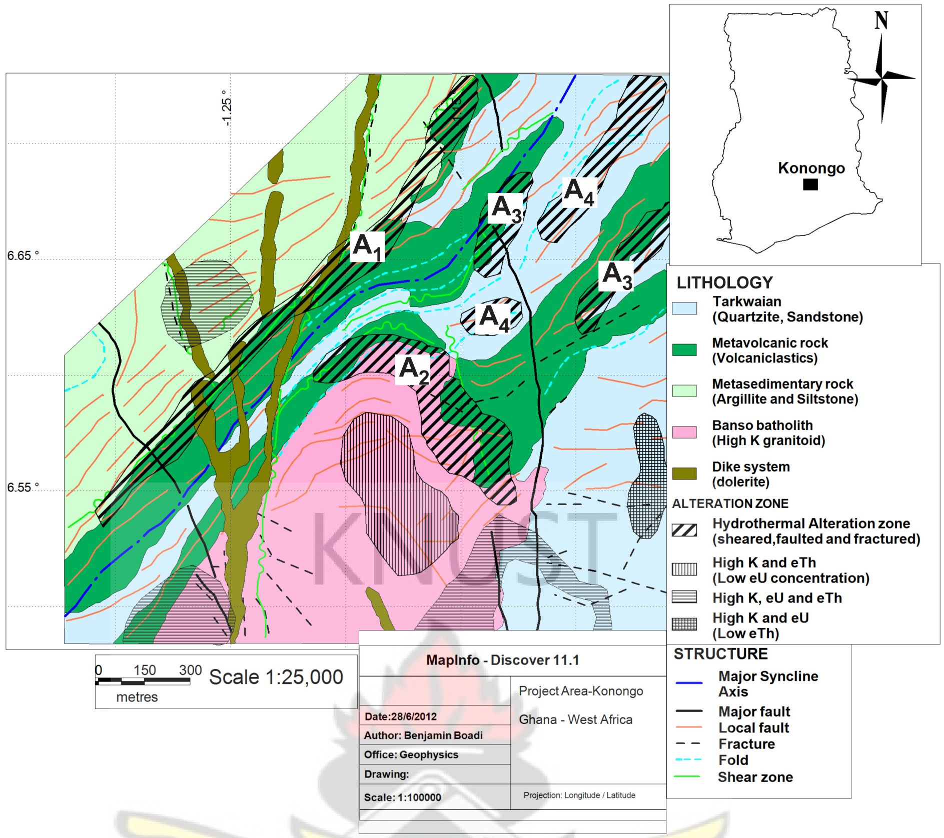

Figure 5.22: Proposed geological map of Konongo area.

The aeromagnetic dataset presents complex structural features (faults, fractures, folds and shear zones) that resulted from three main deformational phases; D_1-NE, D_2-NNW and D_3-NNE. Along the regional syncline axis there are positions where the NE-SW trending faults intersected this fold axis (Fig. 5.22); these intersections are favourable locations for ore-bearing fluid deposition.

The complexity and intensity of faulting and fracturing is registered more in the NE and SW of the area (Fig. 5.22). This is aided by the splay of dolerite dikes and the major fault S_1 leading to the building up of structural corridors striking NE within the Tarkwaian Formation, meta-sedimentary and meta-volcanic rocks. The dike system intersects the contact zones of the Banso Batholith, meta-volcanics M_{V1}, M_{V2}, Tarkwaian Formation and the meta-sedimentary rock unit.

The contact zone between the meta-sedimentary and meta-volcanic (Fig. 5.11) is more faulted and sheared creating hanging walls (S_2 and S_3) and foot walls (F_2 and F_3) as compared to the contact zone between the meta-volcanic and Banso Batholith which is sheared rather than faulted as seen in Fig. 5.6. The dike system (S_2, S_3 and S_4) and the fault S_1 cut across NE trending D_1 structures (faults) thus rendering these contact zones more permeable and fractured for accumulation of hydrothermal fluids. The sheared zone that trends NE-SW along the S_4 dike is of much importance. It cuts across the contact zone of the geological unit and the regional synclinal axis as well as D_1 structures along its path.

Gold mineralization in the Konongo area of Ghana occurs in parallel zones striking north-east within Precambrian rocks. Detailed structural study indicates that sediments of the mineralized zones show distinct phases of fold deformation. These phases and associated shearing play an important part in the mobilization and concentration of the gold deposits (Cozens, 1989). The NE limbs of M_{V1} and M_{V2} experience intense series of shearing and folding compared to M_{V3} which more faulted and fractured. The folding is as a result of the intruding granitoid.

The shearing and thrust faulting of S_2 and S_3 dikes at the contact zones between the meta-volcanic M_{V2} and the meta-sedimentary rock led to developing of hang wall (within the meta-sedimentary rock) and foot wall (within the meta-volcanic rock). This region corresponds to the hydrothermal altered zone marked as A_2 in Fig. 5.21. A typical example is the mining of the Boabedroo mineralization which commenced at the surface in the hanging wall of the main Odumase shear zone (Cozens, 1989).

The Banso Batholith located at south of the study area, host NW-SE and ENE-WSW splay faults that accommodate stress from the major dike system, regional faults F_M and F_N as well as S_5. The F_M fault traverse the contact zone of the Banso Batholith and the Tarkwaian Formation while the fault F_N cuts through the Tarkwaian Formation, the meta-volcanic M_{V3} and the contacts zone between these geological units. From structural view point, this environment is favourable for fluid deposition since the sheared, faulted and fractured contact zone between the Banso Batholith and M_{V3} enhanced alteration features (A_1 in Fig. 5.22), that can be considered for exploration provided it can be proved that mineralization is later than or synchronous with the formation of the fault splays.

The X_1 region in Fig. 5.21 reflects low magnetic anomaly in the magnetic maps and also registered low U and Th but fairly high K in Fig. 5.12. Areas where these two alterations coincide are marked by faults and fractures within the Tarkwaian Formation and noted in the ternary image as a region with high K and U concentration. Arkosic sandstones which contain feldspars, which have significant potassium content, but a low thorium content, thus, low Th/K ratio as shown in Fig. 5.15 is possible to inhabit this X_1 region. Furthermore, in the hydrothermal alteration zones (Fig. 5.21) A_3, (which marks the contact between M_{V3}, M_{V2} and the Tarkwaian Formation) and A_4 (those that lies within the faulted area of the Tarkwaian Formation), are all potential areas for gold mineralization.

CHAPTER 6

SUMMARY AND CONCLUSIONS

6.1 Summary

In order to map the lithology, geological structures and hydrothermal alteration map of the Konongo area, airborne radiometric and magnetic datasets collected over the area was processed and enhanced. The magnetic image enhancing technique applied to the total magnetic intensity (TMI) using Geosoft (Oasis Montaj) and MapInfo-Discover software are reduction to the pole (RTP), analytic signal, first vertical derivative (1VD), first horizontal derivative (1HD) and upward continuation (UC). These filters helped define the lithological boundaries, intersection of geological structures, faults, folds, fractures and dikes.The radiometric data provided geochemical information of potassium (K), thorium (Th) and uranium (U) that proved valuable in delineating bedrock lithology of the area such as the Banso Batholith, Birimian meta-volcanics, Tarkwaian Formation and alteration zones within the lithology and contact zones. The ratio images such as Th/K, U/K and Th/U were also created with the motive to remove lithological differences and effects in the data caused by variations in the soil moisture, non-planar source geometry, and errors associated with altitude correction. U/Th and U/K ratios helped to delineate areas where relative concentrations of uranium are high.

6.2 Conclusions

The analysis of the geophysical features in the study area provides new insights into structural framework and can help geologists target new areas for mineral exploration. Recognizable patterns of geophysical anomalies correspond to geological targets for mineral potential, such as magnetite-rich formations and associated metavolcaniclastic rocks. The interpretation of the high-resolution magnetic dataset has provided both an overview of the regional structure as well as further insight into structural controls of the greenstone-hosted-gold deposits.

The application of integrated airborne geophysical data (magnetic and radiometric) in the study area to predict zones which have the ability to host mineralization have shown that the technique is potent and could be applied in deeply weathered terrains or regolith regions to pick exploration targets for blind ore deposits. The mapped geological structures, lithology and other hydrothermallyaltered zones (playing the role of mineralization indicators) from the aeromagnetic and radiometric datasets have added to the proposal of many authors such as Cozens (1984; 1989) and Griffis et al. (2002) regarding the Konongo district as potential host of commercial deposits.

The airborne magnetic and radiometric data have given a much better idea of the local geology and structures hosting mineralization in the study area. From an exploration point of view, the data was especially useful for interpreting bedrock geology in the area with thick vegetation and very little outcrop. Primary and secondary structures, which are critically important in controlling gold mineralization throughout the extensive metasedimentary and metavolcanic units, were observed directly in the magnetic patterns or inferred through offsets in magnetic and radiometric patterns. In most cases, (Griffis et al., 2002) airborne geophysical data is a useful indirect tool for explorationists but, in some instances, gold mineralization is accompanied by apparent potassic alteration so that some gold prospects have a subtle but discernible expression in the radiometric K data.

An integrated alteration map from radiometric and magnetic datasets established links between lithology, structures and hydrothermal alteration patterns. The relationship shows that the hydrothermal system is structurally controlled and not limited to any specific lithology. Moreover, the area is also marked by a dolerite dike system, concordant with the potential mineralized zones allocated along the contact of the metavolcanic and Tarkwaian Formation, indicating the region of higher fluid pressure and accumulation. The feature of this zone changes in other derivative products and it is possible to define the fault segment and the host association. Another important group of structural elements is represented by the Paleoproterozoic NE structures. They are predominant and cut the other geological units mentioned. In the field, they represent a broad system of fractures and lineaments.

Enhanced structural details which were not captured in the radiometric data were noticeable in the magnetic data. Three structural deformation systems: D_1-NE, D_2-NNW and D_3-NNE were observed from the magnetic data. The major D_2 deformation which produced the regional syncline also produce NE-SW trending shears zones and many faults and fractures that are mainly concentrated along lithological boundaries, especially between the metasedimentary and the metavolcanic rocks. Areas of high strain associated with fault intersections and fracture systems that are accompanied by high K alterations especially when found in mafic host rocks are potential targets for gold mineralization. Circular and sub-circular magnetic shaped bodies which are moderately magnetized and associated with the metavolcanic rocks and Tarkwaian Formation were used as key horizon to locate some prospective zones as possible disseminated sulphide deposits.

Gold occurrences in the Konongo area are small scale deposits but the chances of discovering deposits of economic interest are high (Griffis et al., 2002). The needed evidence of shear zones, faults and fault intersections as well as fracture systems and hydrothermal alteration patterns present in the study area supports the hypothesis of possible commercial ore deposits in the Konongo District. A combined map of lithology, structures and hydrothermal alteration pattern (Fig. 5.22) could serve as a good guide to potential targets in exploration programmes.

The radiometric data is paramount in mapping the lithological units. The integrated interpretation of radiometric and aeromagnetic data provides additional wealthy information on the geology and structures of the study area. From the interpreted geological map, over 60% of the property is mainly underlain by Birimian metamorphosed belt and basin rocks as well as associated Tarkwaian ormation. The increase in K content and decrease in Th/K ratio observed from radiometric interpretation are indicative of hydrothermal alterations.

CHAPTER 7

OUTLOOK AND RECOMMENDATIONS

The geological structures in the area are certainly complex and feature tightly folded and faulted bands of Birimian and Tarkwaian formations; the trends of the major faults as well as the fold planes, strike to the NE and dip steeply to the NW. High structural connectivity regions and areas of intensive alterations reflected as low magnetic anomalous and high K concentration should be considered in further exploration particularly, where the two alteration types coincide and also marked by faults, fault intersections, fractures and shear zones (Fig. 5.22).

The hydrothermal alteration zones that marked the contact between the belt Metavolcanic and the Tarkwaian formation can also be considered as potential target. The interpretation of airborne data is excellent way of mapping lithology, structure and, to some degree, the alteration patterns. However, deposit scale structural and alteration information could only be enhanced by field work to ascertain interpreted formations and geological structure as ground situation.

Further work to progress this interpretation is therefore necessary and recommended. These may include field trace of geology and geological structures, radiometric and magnetic anomalies, soil geochemical sampling as well as the application of any cost effective exploration technique to delineate mineralization.

The Birimian metasediments and metavolcanics (which were truncated at the east and west) in the study area host prominent NE-SW and few NNW-SSE tectonic structures which are extension of the regional gold bearing structures in the popular Ashanti belt. These NNW-SSE and NE-SW regional tectonic structures show evidence of extension beyond this project area. This implies that the structures have not terminated abruptly at the boundaries of the study area. The majority of mineralization occurrences are hosted in Birimian metasediments and metavolcanics (Kesse, 1985). Therefore further geophysical survey will be necessary to investigate the termination point of these lithologies and also to examine whether their continuations are tectonically disturbed by other geological structures that have the potential to host mineralization

Further research should be carried out at the propose potential mineralization zones aimimg at a ground resolution of the details of the regional fold patterns in both the Birimian and Tarkwaian formation sequence. This will help delineate areas in which large scale gold deposits are most likely to exist. This approach to exploration will be cost effective and will allow the more rapid development of the Ghanaian gold mining industry.

Many of the regions in the study area with intensive shearing especially along the contact of the metasediment and metavolcanic which forms the hanging walls (S_2 and S_3 in Fig. 5.11), are often associated with elevated K. These areas are very suitable for further geophysical researches such ground electromagnetic; induce polarization and trenching in order to corroborate the existence of gold or other metal ore mineralization occurrences. This signature may be broad or laterally extensive to provide larger exploration target.

The resolution from the magnetic and radiometric responds for this airborne survey as observed are of regional importance. It is recommended that ground geophysical techniques such as magnetic and radiometric and should be carried out at important areas such as the heavily faulted areas (A_1, A_2, A_3 and A_4) and the region where the dolerite dike system intrudes the Birimian System for a better resolution and details on localized mineralization and rock alteration.

References

1. Adjovu, I. (2006). Nyinahin Concession. Technical report, Mikite Gold Resources Limited.

2. Airo, M. L. and Karell, F. (2001). Interpretation of airborne magnetic and gamma-ray spectrometric data related to Mammaslhti Cu-Zn-Au deposit in eastern Finland. *Special Paper 31*, pages 97–103.

3. Allen, D. G. (2011). The Fahiakoba gold project Ghana, West Africa. Technical report, Asante Gold Corporation.

4. Allibone, A., Teasdale, J., Cameron, G., Etheridge, M., Uttley, P., Soboh, A., Appiah-Kubi, J., Adanu, A., Arthur, R., Mamphey, J., et al. (2002). Timing and structural controls on gold mineralization at the bogoso gold mine, ghana, west africa. *Economic Geology*, 97(5):949–969.

5. Amenyoh, T., Wemegah, D. D., Menyeh, A., and Danuor, S. K. (2009). The use of landsat and aeromagnetic data in the interpretation of geological structures in the Nangodi Belt. Master's thesis, University of Cape Coast.

6. Ansari, A. H. and Alamdar, K. (2009). Reduction to the pole of magnetic anomalies using analytic signal. *World Applied Sciences Journal*, 7(4):405–409.

7. Appiah, H. (1991). Geology and mine exploration trends of Prestea Goldfields, Ghana. *Journal of African Earth Sciences (and the Middle East)*, 13(2):235–241.

8. Asihene, K. A. B. and Barning, K. (1975). *A contribution to the stratigraphy of the Birimian System of Ghana, West Africa*. Ghana Geological Survey.

9. Beard, L. P. and Goitom, B. (2000). Some problems in interpreting low latitude magnetic surveys. *6th EAGE/EEGS Meeting*.

10. Billings, S. D. (1998). *Geophysical aspects of soil mapping using airborne Gamma-Ray Spectrometry*. PhD thesis, Department of Crop Sciences, Faculty of Agriculture, University of Sydney.

11. Boamah, D. (1993). Application of soil geochemistry to gold exploration in the Birimian rocks of Ghana. pages 1–6. Case study from Demoni/ Dankyira area (Unpublished).

12. Boyle, R. (1979). *The geochemistry of gold and its deposits (together with a chapter on geochemical prospecting for the element)*. Geological Survey of Canada.

13. Brabham, G. (1998). The regional geological setting and nature of the Damang stockwork gold deposit - a new type of gold deposit in Ghana. Master's thesis, Dept. of Geology and Geophysics, Univ. of Western Australia, 101pp.

14. Charbonneau, B. (1991). Geochemical evolution and radioactive mineralogy of the Fort Smith radioactive belt, Northwest Territories, Canada. In *Primary Radioactive Minerals (The textural patterns of radioactive mineral paragenetic associations)*, pages 21–48. Theophrastus Publications.

15. Chopin, G. R. (1988). Humics and radionuclide migration. *Radiochima Acta*, 44/45:23–28.

16. Clark, D. A. (1983). Comments on magnetic petrophysics. *Australian Society of Exploration Geophysicists*, Vol. 14:40–62.

17. Clark, D. A. (1997). Magnetic properties of rocks and minerals. *AGSO Journal of Australian Geology and Geophysics*, 17(2).

18. Clark, D. A. and Emerson, D. W. (1991). Notes on rock magnetic characteristics in applied Geophysical studies. *Exploration Geophysics*, Vol. 22:547–555.

19. Cooley, J. W. and Tukey, J. W. (1965). An algorithm for the machine calculation of complex Fourier series. *Math. Comput.*, 19(90):297–301.

20. Cozens, B. (1984). Structural control of the ore system. Konongo Gold Mines, Ghana. Unpublished report.

21. Cozens, B. (1989). The geology and structure of the Konongo gold mine, Ghana, and its implications in exploration. In *Le Maitre R. W. (ed.) Pathways in geology- essays in honour of Edwin Sharbon Hills*, pages 439–456. Blackwell, Melbourne.

22. Darnley, A. G. (1996). Uranium exploration data and global geochemical baselines: The need for coordinated action. In *Uranium Exploration Data and Techniques Applied to the Preparation of Radioelement Maps*. IAEA-TECDOC-980.

23. Davis, D. W., Hirdes, W., Schaltegger, U., and Nunoo, E. A. (1994). U-Pb age constraints on deposition and provenance of Birimian and gold bearing Tarkwaian sediments in Ghana, West Africa. *Precambrian Research*, 67:89–107.

24. Dickson, B. L. and Scott, K. M. (1997). Interpretation of aerial gamma ray surveys-adding the geochemical factors. *AGSO Journal of Australian Geology and Geophysics*, 17(2):187–200.

25. Dobrin, M. B. (1952). *Introduction to Geophysical Prospecting*. Mcgraw Hill Book Co., New York.

26. Eisenlohr, B. N. and Hirdes, W. (1992). The structural development of early Proterozoic Birimian and Tarkwaian rocks in southwest Ghana, West Africa. *Journal of African Earth Science*, 14(3):313–325.

27. El-awady, M. M., El-etr, H., and Bakrah, A. (1984). Aeromagnetic geophysical investigation in El-Faiyum district, western desert, Egypt. *Qatar Univ. Sci. Bull*, 5:335–356.

28. Etheridge, M., Rutland, R., and Wyborn, L. (1987). Orogenesis and tectonic process in the early to middle proterozoic of northern australia. *Proterozoic lithospheric evolution*, 17:131–147.

29. Evans, M. E. (1993). An archaeointensity investigation of a Kiln at Pompeii. *Journal of Geomagnetism and Geoelectricity.*, 43:357–361.

30. Fertl, W. H. (1983). Gamma-ray spectral logging: a new evaluation frontier. *World Oil*, pages 79–91.

31. Grant, F. S. (1985). Aeromagnetic, geology of an ore environment, Magnetite in igneous, sedimentary and metamorphic rocks. *An overvie of Geoexploration*, Vol. 23:303–33.

32. Gregory, A. F. and Horwood, J. L. (1961). *A laboratory study of gamma-ray spectra at the surface of rocks*. Department of Energy, Mines and Resources, Ottowa. Mines Branch Research Report R85.

33. Griffis, R. J. (1998). Explanatory Notes - Geological interpretation of geophysical data from Southwestern Ghana. *Minerals Commission, Accra*, page 51.

34. Griffis, R. J., Barning, K., Agezo, F. L., and Akosah, F. K. (2002). Gold deposits of Ghana. *Minerals Commission Report*, pages 7–12, 19–37, 163–169.

35. Gunn, P. J. (1975). Linear transformations of gravity and magnetic fields. *Geophysical Prospecting*, 23:300–312.

36. Gunn, P. J., Minty, B. R. S., and Milligan, P. (1997). The airborne gamma-ray spectrometric response over arid australian terranes. *Exploration*, 97:733–740.

37. Hall, J. M. and Fisher, B. E. (1987). The characteristics and significance of secondary magnetite in a profile through the dike component of the Troodos, Cyprus, ophiolite. *Canadian Journal of Earth Science*, Vol. 24:2141–2159.

38. Herndon, J. M. (1996). Substructure of the inner core of the Earth. pages 646–648.

39. Hirdes, W. and Nunoo, B. (1994). The Proterozoic paleoplacers at the Tarkwa gold mine, SW - Ghana -sedimentology, mineralogy, and precise age dating of the main reef and west reef, and bearing of the investigations on source area aspects. In *Oberthür, T. (ed.), Metallogenesis of Selected Gold Deposits in Africa*, pages 247–298. Geologische Jahrbuch, Reihe D, Heft 100, Hannover.

40. Hirdes, W., Saager, R., and Leube, A. (1988). New structural, radiometric and mineralogical aspects of the Au–bearing Tarkwaian Group of Ghana. *Bicentennial Gold 88, Melbourne, Abstr.*, pages 146–148.

41. Hirdes, W., Senger, R., Adjei, J., Efa, E., Loh, G., and Tetty, A. (1993). Explanatory notes for the geological map of southwest Ghana 1:100,000, sheet Wiawso (0603d), Asafo (0603c), Kukuom (0603b), Goaso (0603a), Sunyani (0703d) and Berekum (0703c). page 139. Geologisches Jahrbuch, Reine B, Heft 83, Hannover, Germany.

42. Hirst, T. (1942). The geology of the Konongo goldfield and surrounding country. *Gold Coast Geol. Surv. Bull. 14, Accra.*

43. Hoover, D. B. and Pierce, H. A. (1990). Annotated bibliography of gamma-ray methods applied to gold exploration. *U.S. Geological Survey Open-file Report 90-203*, page 23.

44. ICRU (1994). *Gamma ray Spectrometry in the Environment, ICRU Report 53.* International Commission On Radiation Units And Measurements, Bethesda, USA.

45. John, T., Reiner, K., Geoffrey, L., and Wolfgang, H. (1999). The metamorphic evolution of the Paleoproterozoic (Birimian) volcanic Ashanti belt (Ghana, West Africa). *Precambrian Research*, Vol. 98(1-2).

46. Junner, N. R. (1940). Geology of the Gold Coast and Western Togoland. *Geological Survey Bulletin No.1*.

47. Keating, P. B. (1995). A simple technique to identify magnetic anomalies due to kimberlite pipes. *Exploration and Mining Geology*, 4(2):121–125.

48. Kesse, G. O. (1985). *The Mineral and Rock Resources of Ghana*.

49. Kiessling, R. (1997). Sedimentation and structure in the Tarkwaian group of the Bui Basin in West-Ghana;. In *A. Zitzmann (ed.), Geological, Geophysical and Geochemical Investigations in the Bui Belt Area in Ghana. Geol. Jb. Reihe B*, volume 88, page 269.

50. Killeen, P. G. (1979). Gamma ray spectrometric methods in uranium exploration–application and interpretation. In *Geophysics and Geochemistry in the Search for Metallic Ores, edited by P.J. Hood*, pages 163–230.

51. Krishnaswami, S. (1999). Thorium. *Encyclopedia of Geochemistry*, page 712. Kluwer Academic Publishers, London.

52. Langmuir, D. and Hermans, J. S. (1980). The mobility of thorium in natural waters at low temperatures. *Geochimica et Cosmochimica Acta*, 44:1753–1766.

53. Ledru, P., Vera, J., Milesi, J. P., and Tegyey, M. (1994). Markers of the last stages of the Paleoproterozoic collision: evidence for a 2Ga continent involving circum-South Atlantic provinces. *Prec. Res.*, 69:169–191.

54. Leube, A., Hirdes, W., Mauer, R., and Kesse, G. (1990). The early proterozoic birimian supergroup of ghana and some aspects of its associated gold mineralization. *Precambrian Research*, 46:139–165.

55. Li, X. (2008). Magnetic reduction-to-the-pole at low latitudes. *The Meter Reader*, pages 990–1002. Fugro Gravity and Magnetic Services, Houston, USA.

56. Lo, B. H. and Pitcher, D. H. (1996). A case history on the use of regional aeromagnetic and radiometric data sets for lode gold exploration in ghana. *Annual Meeting Expanded Abstracts, Society of Exploration Geophysicists*, pages 592–595.

57. Loh, G. and Hirdes, W. (1996). Explanatory notes for the geological map of southwest Ghana - 1:100,000 scale (Axim and Takoradi sheets). *Ghana Geol. Surv. Bull. 49, Accra.*, page 63.

58. Manu, J. (1993). Gold deposits of Birimian greenstone belts in Ghana: Hydrothermal alteration and thermodynamics. Verlag Mainz, Wissenchaftsverlag, Aachen Herstellung: Fotodruck Mainz GmbH Susterfeldstr. 83. 52072 Aachen.

59. Mauer, R. (1986). Granitoids. In *Leube, A., and Hirdes, W., 1986, The Birimian Supergroup of Ghana, Depositional environment, structural development and conceptual model of an early Proterozoic suite*, page 259.

60. Mendonça, C. A. and Silva, J. B. C. (1993). A stable truncated series approximation of the reduction-to-the-pole operator. *Geophysics*, Vol. 58(No. 8).

61. Milesi, J. P., Ledru, P., Feybesse, J. L., Dommanget, A., and Marcoux, E. (1992). Early proterozoic ore deposits and tectonics of the Birimian orogenic belt, West Africa. *Prec. Res.*, 58:305–344.

62. Milligan, P. R. and Gunn, P. J. (1997). Enhancement and presentation of airborne geophysical data. *AGSO Journal of Australian Geology and Geophysics*, 17(2):64–774.

63. Milsom, J. (2003). *Field Geophysics, the geological field guide series*. John Wiley and Sons Ltd, The Atrium, Southern Gate, Chichester, West Sussex PO19 8SQ, England, third edition.

64. Minty, B. R. S. (1996). The fundamentals of airborne gamma-ray spectrometry. *AGSO Journal of Australian Geology and Geophysics*, 17(2):39–50.

65. Moon, P. A. and Mason, D. (1971). The geology of Field Sheets 129 and 131, Bompata S.W and N.W. *Geological Survey Bulletin*, No. 31.

66. Moxham, R. M., Foote, R. S., and Bunker, C. M. (1965). Gamma-ray spectrometer studies of hydrothermally altered rocks. *Economic Geology*, 6:653–71.

67. Mumin, A. H., Fleet, M. E., and Longstaffe, F. J. (1996). Evolution of hydrothermal fluids in the ashanti gold belt, ghana; stable isotope geochemistry of carbonates, graphite, and quartz. *Economic Geology*, 91(1):135–148.

68. Murphy, B. S. R. (2007). Airborne geophysics and the indian scenario. *J. Ind. Geophysics Union*, 11(1):1–28.

69. Nabighian, M. N. (1972). The analytical signal of two-dimensional magnetic bodies with polygonal cross-section: its properties and use for automated anomaly interpretation. *Geophysics*, 37(3):507–517.

70. Nagata, T. (1961). *Rock Magnetism*. Tokyo: Maruzen, 2nd edition.

71. Nicolet, J. P. and Erdi-Krausz, G. (2003). *Guidelines for radioelement mapping using gamma ray spectrometry data*. IAEA-TECDOC-1363. IAEA.

72. Ntiamoah-Agyakwa, Y. (1979). Relationship between gold and manganese mineralizations in the Birimian of Ghana, West Africa. *Geol. Mag.*, 116(5):345–352.

73. Oliver, B. (2009). *Million Ounce Gold Project Optioned*. Signature Metals Limited, Level 1 / 33 Richardson Street, WEST PERTH-Australia.

74. Ostrovskiy, E. A. (1975). Antagonism of radioactive elements in wellrock alteration fields and its use in aerogamma spectrometric prospecting. *International Geological Review*, 17:461–8.

75. Perrouty, S., Jessell, M., Aillères, L., Baratoux, L., and Bourassa, Y. (2009). Structural analysis of the southern ashanti belt, ghana, using airborne geophysical data. *ASEG Extended Abstracts*, 2010(1):1–4.

76. Petersen, N. (1990). Curie temperature. In *James, D. E. (ed.), The Encyclopedia of solid Earth Geophysics*, pages 166–173. New York: Van Nostrand Reinhold.

77. Phillips, D. J. (1997). Potential-field geophysical software for the PC, version 2.2. *U.S.G.S. Open-File Report 97-725*, page 34.

78. Plumlee, G. S., Smith, K. S., Ficklin, W. H., and Briggs, P. H. (1992). Geological and geochemical controls on the composition of mine drainages and natural drainages in

mineralized areas. Proceedings, 7th International Water-Rock Interaction Conference, pages 419–422. Park City, Utah, July, 1992.

79. Plummer, C. C., McGeary, D., and Carlson, D. H. (2001). *Physical Geology*. New York: McGraw Hill, 8th edition.

80. Rajagopalan, S. (2003). *Exploration Geophysics*, Vol. 34(No. 4):257–262.

81. Reeves, C. V. (1989). Aeromagnetic interpretation and rock magnetism. *First Break*, Vol. 7:275–286.

82. Reynolds, J. M. (1997). *An Introduction to Applied and Environmental Geophysics*. John Wiley and Sons Ltd, Baffins Lane, Chichester, West Sussex PO19 1UD, England.

83. Roest, W. R. and Pilkington, M. (1993). Identifying remanent magnetiza- tion effects in magnetic data. *Geophysics*, 58:653–659.

84. Sawyer, L. M. and Gunn, P. (2008). *Bulman Project EL 23814, MLN 726, MLN 727, Airborne Geophysics Data Interpretation*. Geos Mining project 2141 -1.

85. Sharma, P. V. (1986). *Geophysical Methods in Geology*. New York: Elsevier Science, 2nd edition.

86. Shives, R., Charbonneau, B., and Ford, K. (2000). The detection of potassic alteration by gamma-ray spectrometry-recognition of alteration related to mineralization. *Geophysics-Wisconsin The Tulsa-Society Of Exploration Geophysicists*, 65(6):2001–2011.

87. Sillitoe, R. H. (1979). Some thoughts on gold-rich porphyry copper deposits. *mineralium deposita*, Vol. 14:161–1744.

88. Silva, A. M., Pires, A. C. B., McCafferty, A., Moraes, R. A. V., and Xia, H. (2003). Application of airborne geophysical data to mineral exploration in the uneven exposed terrains of the Rio Das Velhas greenstone belt. *Revista Brasileira de Geociências*, 33(2):17–28.

89. Strangway, D. W. (1970). *History of the Earth's Magnetic Field*. New York: McGraw Hill.

90. Strogen, P. (1991). The sedimentology, stratigraphy and structure of the Tarkwaian, Western Region, and its relevance to gold exploration and development. *Proceedings of the International Conference on the Geology of Ghana, 1988, Accra*, 3:R1–39.

91. Studemeister, P. A. (1983). The redox state of iron: a powerful indicator of hydrothermal alteration. *Geoscience Canada*, Vol. 10:189–194.

92. Tay, C. and Momade, F. (2009). Trace metal contamination in water from abandoned mining and non-mining areas in the northern parts of the Ashanti gold belt, Ghana. *West African Journal of Applied Ecology*, 10(1).

93. Telford, W. M., Geldart, L. P., and Sheriff, R. E. (1990). *Applied Geophysics*. Cambridge University Press, second edition.

94. Wemegah, D. D., Menyeh, B. A., and Danuor, S. K. (2009). Magnetic Susceptibility Characterization of mineralized and non mineralized rocks of the Subenso Concession of Newmont Ghana Gold Limited. In *Ghana Science Association Biennial Conference*.

95. Whitham, K. (1960). Measurement of the geomagnetic elements. In *Methods and techniques in Geophysics*, volume Vol. 1, pages 134–48. S. K. Runcorn.

96. Wilford, J. R., Bierwirth, P. N., and Craig, M. A. (1997). Application of airborne gamma-ray

spectrometry in soil/regolith mapping and applied geomorphology. *AGSO Journal of Australian Geology and Geophysics*, 17(2):201–216.

97. Wright, J. B. (1985). *Geology and Mineral Deposits of West Africa*. Allen and Unwin, London, 189 pp.

98. Zitzmann, A., Kiessling, R., and Loh., G. (1997). Geology of the Bui Belt area in Ghana. In *A. Zitzmann (ed), Geological, Geophysical and Geochemical Investigation in the Bui Belt Area in Ghana.*, page 269. Geol. Jb. Reihe B, Heft 88.

Appendix A

Aeromagnetic and Radiometric Images of Konongo Area

A.1 TDR and 1VD Images in Pseudocolor

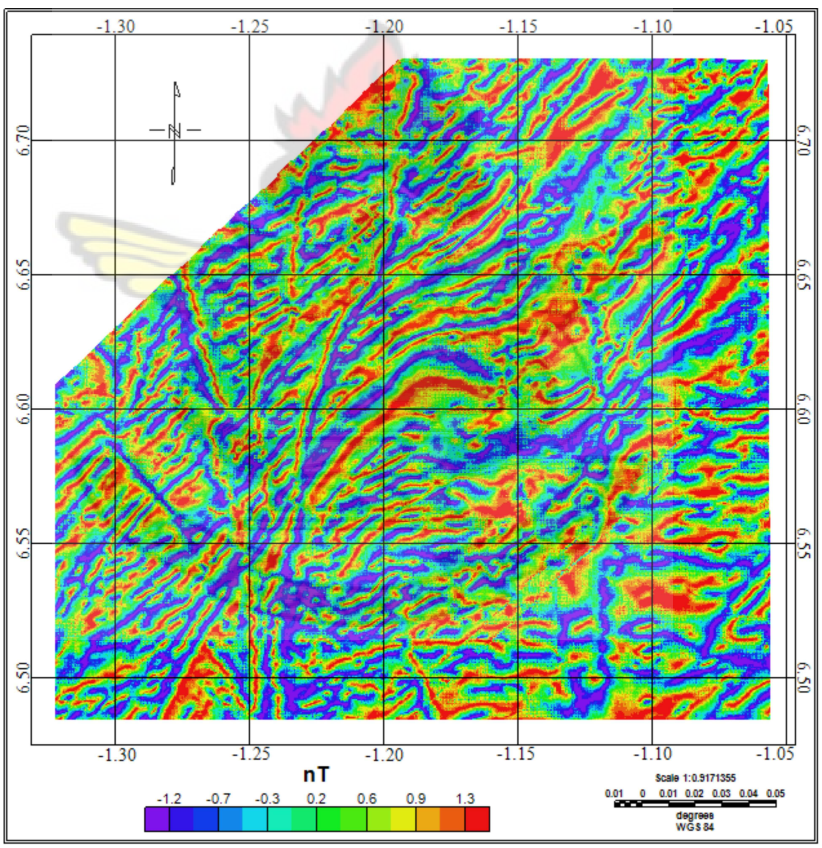

Figure A.1: A magnetic TDR map

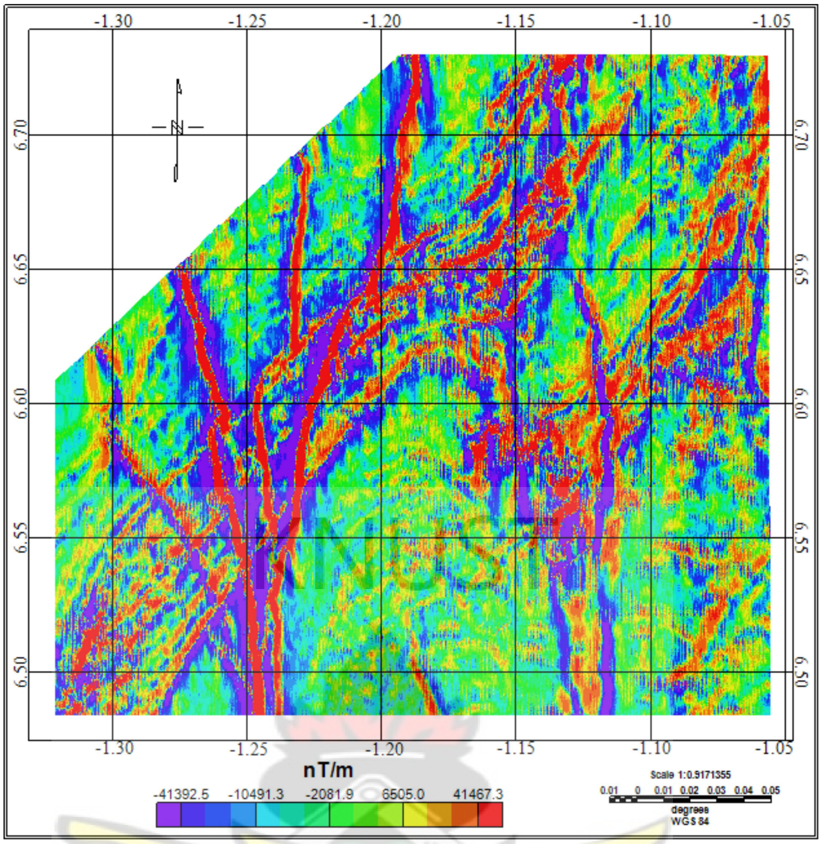

Figure A.2: First order vertical derivative map and upward continued to 100 m showing magnetic structures

A.2 Potassium Uranium and Thorium Ratio Maps

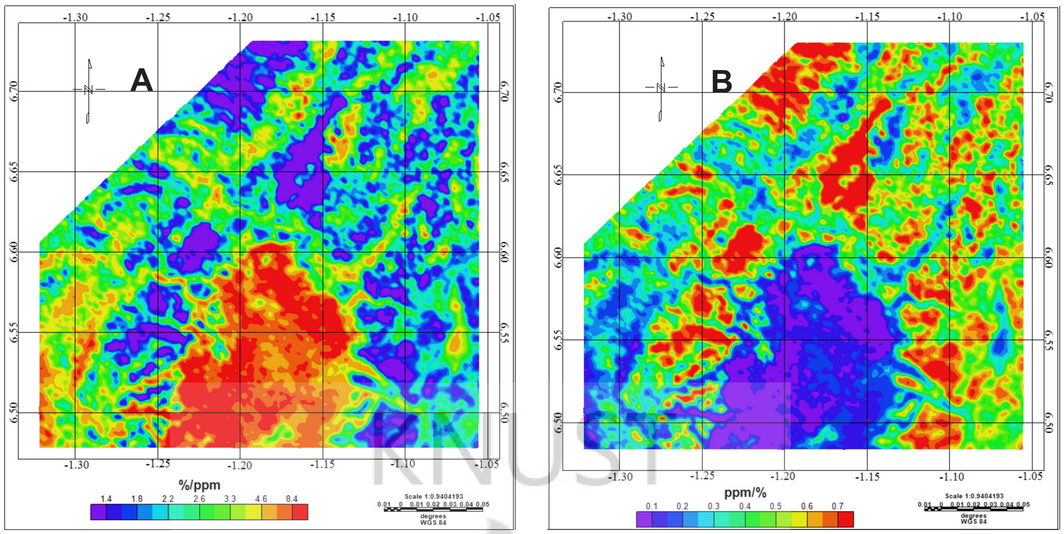

Figure A.3: Gamma spectrometric images of the Konongo project area. A) K/Th; B) Th/K

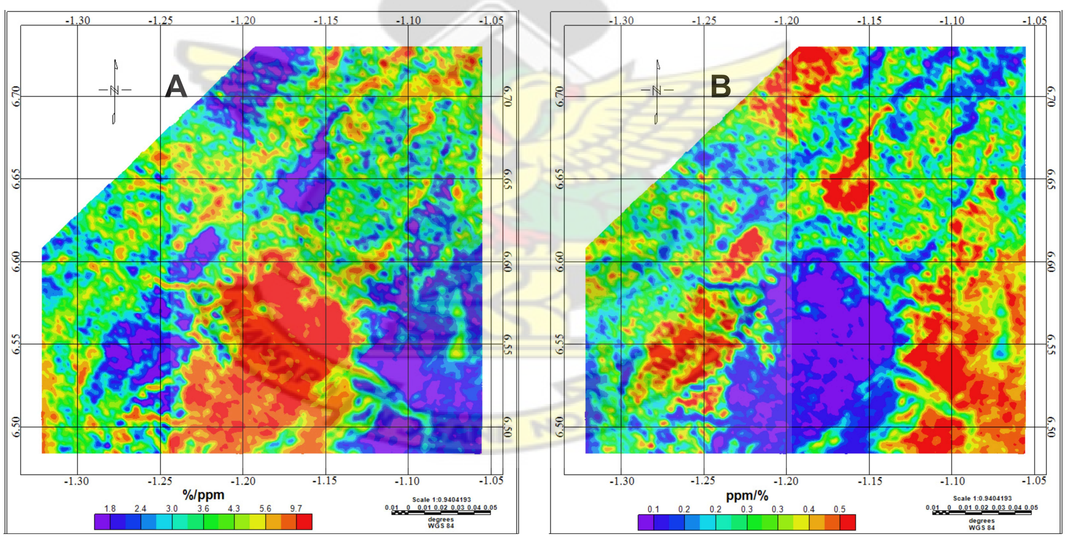

Figure A.4: Gamma spectrometric images of the Konongo project area. A) K/U; B) U/K

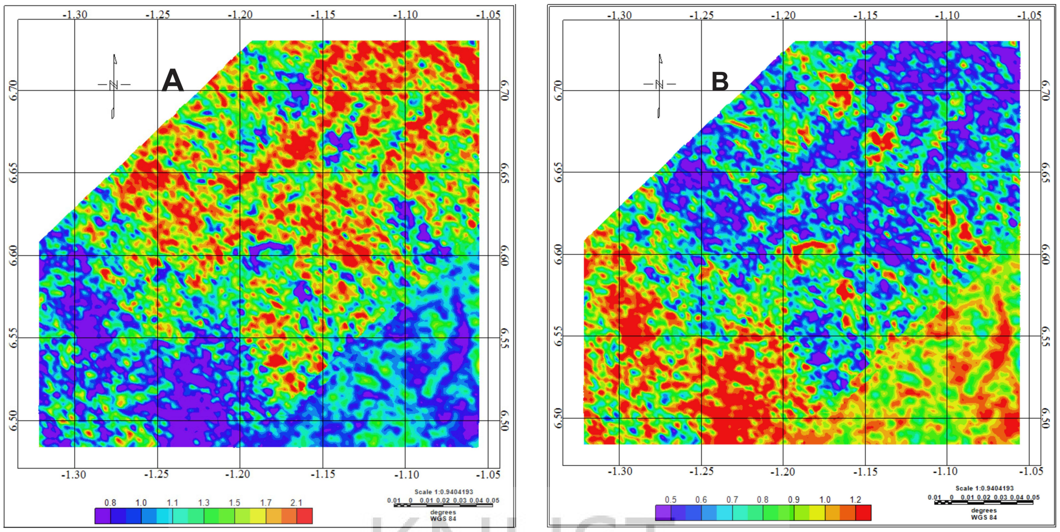

Figure A.5: Gamma spectrometric images of the Konongo project area. A) Th/U; B) U/Th

m

Appendix B

B.1 Used Softwares

- LaTeX : typesetting and layout
- Coral Draw X5 : graphics
- Oasis Montaj (Geosoft): data processing and enhancing
- MapInfo 10.5-Discover 11.1: data processing and enhancing
- Golden Software Surfer 10 : plots
- Model Vision Professional 8 : data processing